



TECHNISCHE
UNIVERSITÄT
WIEN

DIPLOMARBEIT

DETERMINATION OF THE FREEZE/THAW SURFACE STATE FROM ERS-2 BACKSCATTER DATA

Ausgeführt am Institut für Photogrammetrie und Fernerkundung
zum Zwecke der Erlangung des akademischen Grades eines Diplom-Ingenieur

unter der Leitung von
Univ.Prof. Dipl.-Ing. Dr.techn. Wolfgang Wagner

und der Betreuung durch
Dipl.-Ing. Christoph Reimer

eingereicht an der Technischen Universität Wien
Fakultät für Mathematik und Geoinformation
von

ISABELLA MARIA PFEIL

Matrikelnummer 1026550
Niedergleinkerstr. 22
4407 Dietach

Wien, am 10. Mai 2016

.....

Abstract

The freeze/thaw cycle of the Earth's surface determines the timing and the length of the vegetation growing season and has a high impact on the land-atmosphere carbon dioxide exchange. For applications like permafrost monitoring and climate studies, information on the freeze/thaw state of the surface is highly valuable.

The Remote Sensing research group at TU Wien has developed methods to retrieve global freeze/thaw states of the Earth's surface from backscatter measurements obtained from microwave scatterometers. The algorithm for the retrieval of the surface state was originally developed for data from the Advanced Scatterometer (ASCAT), covering the period from 2007 until present. Since geoscientific studies require data from different periods, it's desirable to have long time series available.

The aim of this thesis was to investigate if the ASCAT surface state algorithm can also be applied on data from the scatterometer (ESCAT) on-board the European Remote Sensing (ERS) satellites in order to obtain prolonged freeze/thaw time series, despite the lower amount of available observations because of limitations in the observation geometry and technical problems during the mission. The algorithm requires a certain amount of observations under different conditions in order to derive a surface state, which made the data availability the largest factor of uncertainty when starting the work on the algorithm adaptation.

Different climate and land cover regions were selected to compare the ESCAT surface state flags with those retrieved from ASCAT backscatter data. The overall outcome shows very satisfying results, contradicting the expectation that the low data availability might prevent a successful determination of the surface state from ESCAT data.

Furthermore, the ESCAT surface state flags were validated against soil and surface temperature data from the Global Land Data Assimilation System (GLDAS) and in-situ networks, as well as against arctic freeze/thaw soil state from the National Snow and Ice Data Center (NSIDC). All validations show very good coherence between the datasets.

Kurzfassung

Etwa zwei Drittel der globalen Landmassen erleben einen jährlichen Frost/Tau-Zyklus. Dieser bestimmt nicht nur den Beginn und die Dauer der Vegetations- und Anbauperiode, sondern hat auch eine große Wirkung auf den CO_2 -Austausch zwischen Land und Atmosphäre. Zahlreiche Anwendungen wie Klimastudien und Permafrostüberwachungen könnten ohne Kenntnis des Frost/Tau-Zyklus nicht durchgeführt werden.

In der Forschungsgruppe Fernerkundung der TU Wien werden Methoden entwickelt, den Frost/Tau-Zyklus aus Satellitenbeobachtungen des Rückstreuerverhaltens der Erdoberfläche abzuleiten. Der Algorithmus, der ursprünglich für Messungen des Advanced Scatterometer (ASCAT) entwickelt wurde, liefert Ergebnisse von 2007 bis heute. Allerdings sind für geowissenschaftliche Studien möglichst lange Zeitserien wünschenswert.

Ziel dieser Arbeit war die Adaptierung des Algorithmus für Daten der Scatterometer (ESCAT) der European Remote Sensing (ERS) Satelliten, um die Verfügbarkeit der Frost/Tau-Zeitserien in die Vergangenheit zu verlängern. Um plausible Ergebnisse zu liefern, benötigt der Algorithmus ausreichend Messungen auf der ganzen kontinentalen Erdoberfläche unter möglichst vielen verschiedenen Frost/Tau-Zuständen. Der größte Unsicherheitsfaktor hierbei war deshalb die verglichen mit ASCAT geringere Anzahl an Beobachtungen, bedingt durch die Geometrie der ESCAT-Scatterometer und technische Probleme während der Mission.

Für den Vergleich der Ergebnisse der Frost/Tau-Zustandsbestimmung von ESCAT- mit jenen von ASCAT-Daten wurden verschiedene Klima- und Vegetationsregionen ausgewählt. Der Vergleich liefert sehr positive Ergebnisse.

Zur weiteren Beurteilung der Ergebnisse wurden die Frost/Tau-Zeitserien mit Boden- und Oberflächentemperaturmodellen des Global Land Data Assimilation System (GLDAS), Temperaturmessungen an Beobachtungsstationen des International Soil Moisture Network (ISMN) sowie dem Frost/Tau-Datensatz des National Snow and Ice Data Center (NSIDC) validiert. Die Ergebnisse zeigen eine hohe Übereinstimmung der ESCAT Zeitserien mit allen Datensätzen.

Danksagung

Diese Diplomarbeit entstand am Department für Geodäsie und Geoinformation der TU Wien. Ich möchte mich bei allen meinen Kollegen bedanken, allen voran bei meinen Betreuern Wolfgang Wagner und Christoph Reimer, die jederzeit ein offenes Ohr für meine Fragen hatten und mir mit ihrer Fachkenntnis und vielen wertvollen Ratschlägen immer wieder weitergeholfen haben. Besonders die Diskussionen mit Christoph, aber auch anderen Kollegen im Department waren für mich entscheidend für die Fertigstellung der Arbeit.

Außerdem möchte ich mich bei meinen Eltern, meinen Geschwistern und meinem Freund bedanken. Jeder hat auf seine Weise einen Teil dazu beigetragen, dass ich soweit kommen durfte – nicht nur während des Schreibens der Diplomarbeit, sondern während des gesamten Studiums.

Contents

List of Acronyms	viii
List of Figures	ix
List of Tables	xi
1 Introduction	1
2 Microwave Remote Sensing of the Freeze/Thaw State	3
2.1 Scattering Mechanisms	3
2.2 Radar Equation and Backscattering Coefficient	4
2.3 Backscatter at the Freezing Point	6
2.4 Backscatter from Dry Snow	7
2.5 Backscatter during Snowmelt	7
3 Data Description	8
3.1 ESCAT Backscatter Data	8
3.2 ASCAT Backscatter Data	11
3.3 ERA-Interim Data	11
4 Determination of the Surface State Flag	12
4.1 Grid Definition	12
4.2 Calculation of the Freeze/Thaw Parameters	12
4.3 Surface State Flag	22
4.4 Adaptation of the SSF Algorithm	26
4.5 Processing Flags	26
5 Results of the SSF determination	29
5.1 Climate and Land Cover	30
5.2 Surface state flags from ASCAT and ESCAT	31

5.2.1	SSF determination in cold climate	32
5.2.2	SSF determination of permanent wetlands in cold climate	34
5.2.3	SSF determination in cold continental climate	34
5.2.4	SSF determination in polar Tundra climate	34
5.2.5	SSF determination in heterogenous land cover (cold climate)	38
5.2.6	SSF determination in heterogenous land cover (temperate climate)	38
6	Validation of the Surface State Flag	41
6.1	Validation Against In-Situ Temperature Data	41
6.2	Validation Against F/T State Data from the NSIDC	46
6.3	Validation Against Temperature Data from GLDAS	48
6.3.1	Validation of Seasonal Results	52
7	Conclusion	56
A	Additional Figures	58
A.1	Freeze/Thaw Parameters	58
A.2	Surface State Flags in Different Climatic Regions	64
A.2.1	SSF determination in cold climate (mixed land cover)	64
A.2.2	SSF determination in cold climate (woody savannas)	64
A.2.3	SSF determination in cold climate (shrublands)	64
A.2.4	SSF determination in polar Tundra climate climate (shrublands)	64
	Bibliography	69

List of Acronyms

ASCAT	Advanced Scatterometer
ECMWF	European Centre for Medium-Range Weather Forecasts
ERA	ECMWF Re-Analysis
ERS	European Remote Sensing Satellite
ESCAT	Scatterometer on-board the European Remote Sensing Satellites ERS-1/2
FT	Freeze/Thaw
GLDAS	Global Land Data Assimilation System
ISMN	International Soil Moisture Network
MOHC	Met Office Hadley Centre
NASA	National Aeronautics and Space Administration
NSIDC	National Snow and Ice Data Center
SAR	Synthetic Aperture Radar
SSF	Surface State Flag
TU WIEN	Technical University of Vienna
WARP	Water Retrieval Package
WMO	World Meteorological Organization

List of Figures

2.1	NASA Earth Observation – Electromagnetic spectrum	4
3.1	<i>Bartalis (2009)</i> – ESCAT and ASCAT scatterometer geometry	9
3.2	<i>De Chiara et al. (2007)</i> – ERS-2 global mission scenario	10
3.3	<i>De Chiara et al. (2007)</i> – ERS-2 regional mission scenario	10
4.1	Backscatter-Temperature behaviour Alaska, Happy Valley	13
4.2	Backscatter-Temperature behaviour Russia, Apuka	14
4.3	Backscatter-Temperature behaviour Russia, Buyaga	15
4.4	Backscatter-Temperature behaviour China, Mazong Shan	16
4.5	Backscatter-Temperature behaviour Russia, Solnechnaya Bay	16
4.6	Mean backscatter in summer	18
4.7	Mean backscatter in winter	19
4.8	Transition day 1 (winter – summer)	20
4.9	Transition day 2 (summer – winter)	21
4.10	<i>Naeimi et al. (2012)</i> – SSF regions	22
4.11	<i>Naeimi et al. (2012)</i> – Examples for thresholds in two regions	24
4.12	<i>Naeimi et al. (2012)</i> – Decision tree 1	25
4.13	<i>Naeimi et al. (2012)</i> – Decision tree 2	25
4.14	SSF processing flags from ASCAT and ESCAT data	28
5.1	SSF time series from ASCAT and ESCAT data	29
5.2	<i>Peel et al. (2007)</i> – Koeppen-Geiger climate map	30
5.3	SSF – cold climate (cell 2154)	33
5.4	SSF – permanent wetlands in cold climate (cell 1830)	35
5.5	SSF – cold continental climate (cell 1576)	36
5.6	SSF – polar Tundra climate (cell 500)	37
5.7	SSF – cold climate, heterogenous land cover (cell 1362)	39
5.8	SSF – temperate climate, heterogenous land cover (cell 1360)	40

6.1	Validation: SSF – BNZ-LTER station UP ₃ A	42
6.2	Validation: SSF – SNOTEL station Coldfoot	44
6.3	Validation: SSF – SNOTEL station Harts Pass	44
6.4	Validation: SSF – SNOTEL station Happy Jack	45
6.5	Validation: SSF – SNOTEL station Laprele Creek	45
6.6	Validation: SSF – BNZ-LTER station CRREL-Met	46
6.7	Validation: SSF – NSIDC (cell 500)	47
6.8	Validation: SSF – NSIDC (cell 2154)	47
6.9	Validation: SSF – GLDAS (cell 500)	50
6.10	Validation: SSF – GLDAS (cell 1360)	51
6.11	Validation: SSF – GLDAS, divided into seasons (cell 2154)	53
6.12	Validation: SSF – GLDAS, divided into seasons (cell 1830)	53
6.13	Validation: SSF – GLDAS, divided into seasons (cell 1576)	54
6.14	Validation: SSF – GLDAS, divided into seasons (cell 500)	54
6.15	Validation: SSF – GLDAS, divided into seasons (cell 1362)	55
6.16	Validation: SSF – GLDAS, divided into seasons (cell 1360)	55
A.1	Freeze/thaw threshold	59
A.2	Snowmelt/water level	60
A.3	Standard deviation during frozen period	61
A.4	Steepness of linear regression during frozen period	62
A.5	Permanent ice flag	63
A.6	SSF – cold climate, mixed land cover (cell 1398)	65
A.7	SSF – cold climate, woody savannas (cell 1507)	66
A.8	SSF – cold climate, shrublands (cell 1903)	67
A.9	SSF – polar Tundra climate, shrublands (cell 1904)	68

List of Tables

5.1	<i>Peel et al. (2007)</i> – Koeppen-Geiger climate classes	31
5.2	<i>Channan et al. (2014)</i> – MODIS land cover classes	32
6.1	SNOTEL and BNZ-LTER station overview	43
6.2	Possible validation outcomes	48
6.3	Possible validation outcomes (seasonal)	52

Chapter 1

Introduction

About 50 million km² of the terrestrial northern hemisphere experience seasonal surface freezing and thawing processes. Globally, about two thirds of the Earth's landmasses are subject to this phenomenon. The freeze/thaw cycle determines the timing and the length of the vegetation growing season and has a high impact on the land-atmosphere carbon dioxide exchange. It affects seasonal snowmelt and associated soil thaw, runoff generation and flooding, ice break up in large rivers and lakes, and trace gas dynamics [Kimball *et al.*, 2001].

It is therefore important to monitor the changes between the surface states. Conventional methods such as using temperature records from in-situ stations are often severely hampered by the low density of weather stations, especially in Canada and Sibiria. In order to obtain a global dataset of the freeze/thaw cycle, optical satellite remote sensing methods provide a good mean since their observations of albedo, temperature and snow coverage can be used to infer surface freeze/thaw state. The drawback of optical methods is however their generally coarse temporal resolution (revisit times of 8-16 days for boreal and arctic regions, [Kimball *et al.*, 2001]) because of the fact that they cannot gather information without solar illumination or during cloud coverage and aerosol contamination. Especially in the transition time from winter to spring, when a high temporal coverage is particular important, these problems are most likely to occur.

Remote sensing satellites that operate in a microwave frequency region do not face these problems: as a consequence of the used frequency, which lies in the range of 1-100 GHz, microwave instruments are not dependent on solar illumination and can penetrate cloud cover. This makes them a perfect means for observing the Earth's freeze/thaw cycle.

The two sensors used for this work are the ESCAT scatterometer on-board the ERS-2 and the ASCAT (Advanced Scatterometer) onboard the MetOp-A satellite. ERS-2 was launched by ESA in April 1995 and switched off in September 2011. MetOp-A carrying the ASCAT sensor was

launched by the National Aeronautics and Space Administration (NASA) in October 2006 and is still active.

The Remote Sensing research group at the department for Geodesy and Geoinformation at TU Wien develops methods for the retrieval of soil moisture from radar backscatter data. The developed processor, the WAter Retrieval Package (WARP), includes a method for determining the freeze/thaw state of the surface. Since this method was originally developed for ASCAT data, the goal of this thesis is to investigate if this method can also be applied on ESCAT data in order to obtain prolonged freeze/thaw time series. Due to technical problems of the gyroscopes and a tape recorder failure on-board ERS-2, the available amount of data is limited from 2003 onwards (see Section 3.1). Since the algorithm requires a certain amount of observations under different surface state conditions in order to derive a surface state, the data availability was the largest factor of uncertainty when starting the work on the algorithm adaptation.

Chapter 2 gives an overview of the fundamentals of microwave remote sensing, including the definition of microwaves, their advantage compared to other electromagnetic waves, and the quantities used in remote sensing. Furthermore, basic aspects of remote sensing over snow covered and frozen surfaces are explained.

The sensors used in this work are the ESCAT scatterometer on-board ERS-2 and the Advanced Scatterometer (ASCAT) on-board MetOp. Information on these instruments is provided in Chapter 3, along with the description of the temperature dataset used for the determination of the surface state.

In Chapter 4, the surface state flag algorithm is presented. Challenges in view of the adaptation of the algorithm for ESCAT data are explained.

Chapter 5 provides the results of the SSF process for different climatic regions. It is shown that despite the previously mentioned challenges, the algorithm produces more than acceptable results for ESCAT backscatter data.

A validation of the obtained results against different datasets (e.g. air and surface temperature, Freeze/Thaw soil state) is done in chapter 6.

Chapter 7 sums up and discusses the findings of the previously carried out analyses and concludes the successful adaption of the SSF algorithm for ESCAT backscatter data.

Chapter 2

Microwave Remote Sensing of the Freeze/Thaw State

Microwaves are electromagnetic waves of approximately 1 m to 1 mm wavelength (0.3 to 300 GHz frequency) with characteristics that make them very suitable for Earth Observation. The majority of particularly lower microwave frequencies are transmitted through the atmosphere. Microwaves with frequencies up to 20 GHz even penetrate clouds and rain to some extent.

Microwaves are capable to penetrate more deeply into vegetation and ground than optical waves, dependent on the microwave frequency, the moisture content and the density of the vegetation [Ulaby *et al.*, 1981].

Additionally, microwave instruments don't require the sun as illumination source – therefore, they can be operated not only during the day but also at night.

Because of these characteristics, microwaves are a very suitable means for Earth observation, and complement the information gained from sensors working in the optical electromagnetic range.

Figure 2.1 shows the frequency range of microwaves in the electromagnetic spectrum. Microwaves have longer wavelengths than electromagnetic waves in the visible and infrared range.

2.1 Scattering Mechanisms

An incident electromagnetic wave interacts with the media it impinges on in different ways. If the surface acts as a boundary between two homogenous media (i.e. air and soil), a portion of the wave is scattered and reflected back into the upper medium, and the rest is transmitted to the lower

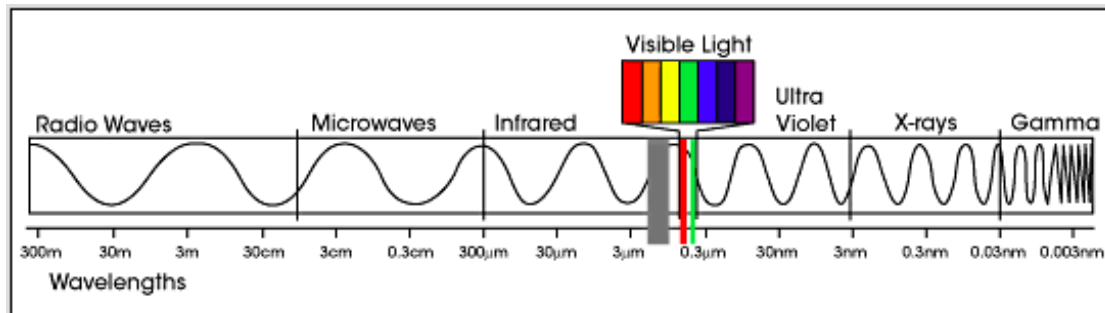


Figure 2.1: Microwaves in the electromagnetic spectrum. [from the NASA Earth Observation webpage]

medium. This process is called **surface scattering**. Depending on the surface roughness, the wave will be either reflected specularly or diffusely. The rougher the surface, the larger the diffusely scattered portion. A calm water body acts like a smooth plane and causes specular reflection.

Trees with their leafs and twigs or snow packs containing grains and air bubbles are heterogenous media. The process that applies to such media is called **volume scattering**. Unlike in the previous case, there is no sharp boundary between two homogenous media but rather a heterogenous boundary layer. Scattering happens inside the boundary layer, dependent on the physical and dielectric properties of the layer.

If both surface and volume scattering occur in a medium, the effects are summarized.

2.2 Radar Equation and Backscattering Coefficient

If a microwave is transmitted by an antenna, it will impinge on the ground with a certain power. Depending on the target that the wave impinges on, a certain amount of the wave's initial power is scattered towards the receiver, which collects the incident wave again.

This fundamental relation between the transmitter, the scatterer and the receiver is expressed by the radar equation, which is given here for the monostatic case (transmitter and receiver location are identical) [Ulaby et al., 1982]:

$$P_r = \frac{P_t G^2 \lambda^2}{(4\pi)^3 R^4} \sigma = \frac{P_t A^2}{4\pi \lambda^2 R^4} \sigma$$

P_r ... received power
 P_t ... transmitted power
 G ... antenna gain
 λ ... wavelength
 $\frac{1}{4\pi R^2}$... spreading loss
 A ... effective area of the antenna

The physical quantity that is commonly used in remote sensing is the **normalized backscattering coefficient**. It describes the electromagnetic energy that is intercepted and reradiated at the same wavelength by an object, normalized by the object's area. The backscattering coefficient depends on multiple factors like the size, shape, material, edges of the object and the wavelength and polarization of the incident wave. Complex objects can be a combination of multiple scattering sources with different characteristics. In that case, the backscattering coefficient contains amplitude and phase information from each scattering source.

If the radar cross section σ is defined as

$$\sigma = \lim_{R \rightarrow \infty} \frac{4\pi R^2 |E_s|^2}{|E_i|^2}$$

E_s ... electric field scattered by an object
 E_i ... incident electric field,

it can be used to calculate the normalized backscattering coefficient σ^0 as follows:

$$\sigma^0 = \frac{d\sigma}{dA}$$

dA ... differential unit area

However, determining the radar cross section requires solving Maxwell's equations, which has not been very successful. Instead, computer programs have been developed that break down complex targets into many simple objects and are able to compute the overall radar cross section. The radar cross section of simple objects can be determined more easily considering different wavelength-dependent scattering regions [Toomay and Hannen, 2004].

Under the assumption that no single scatterer dominates the signal, the backscattering coefficient σ^0 is used as the most important quantity in microwave remote sensing.

2.3 Backscatter at the Freezing Point

If a microwave impinges on a scatterer on the Earth's surface, the interaction with the surface and the finally reflected part of the wave's energy depend on the following parameters:

- Geometric properties
 - shape of the scatter point
 - size of the scatter point
 - spatial arrangement of the components in the footprint
- Dielectric properties of the surface
- Frequency of the incident signal

The geometric properties determined by the surface roughness play an important role in the reflection process. If an observed surface is smooth (e.g. surface of a calm water body), specular reflection dominates and no backscatter will be measured by the sensor. The rougher the surface, the larger the part of the signal that is diffusely scattered, which increases the backscatter value that is finally measured by the sensor.

Water is the element that dominates microwave measurements because of its abundance in nature and its characteristic dielectric properties. The two positively charged hydrogen atoms and the negatively charged oxygen atom that form the water molecule are arranged in a way that they form a dipole. Water has therefore a high dielectric constant, which increases the backscatter values measured over surfaces that contain water. However, the presence of water decreases the penetration depth. Backscatter measurements are therefore only representative for the upper two to five centimeters of the soil.

If soil freezes, the water molecules get bound in a crystalline lattice, which causes the dielectric constant and consequently the backscatter observed with for example a C-band microwave sensor to decrease substantially. This behavior is the reason why a differentiation between unfrozen and frozen soils can be made based on backscatter values.

The idea of the surface state algorithm is to find a threshold below/above which all backscatter values are flagged as frozen/unfrozen. In order to find that threshold, all backscatter observations of one point are plotted over the corresponding temperature measurements of the same point at the same time. More information on this approach is provided in Section 4.3.

2.4 Backscatter from Dry Snow

The backscatter signal from dry snow depends on numerous snow properties such as the density and average size of the grains, the snow depth, the temperature and the age of the snowpack. A snowpack is characterized by volume rather than surface scattering, which causes the backscatter signal to increase as soon as snow accumulates over the surface. This effect makes it difficult to distinguish a signal reflected from snow and a signal reflected from moisture-rich soil (see Section 4.2, Figure 4.3).

If the temperature decreases further, volume scattering can increase even more in very deep and dry snowpacks due to snow metamorphism. Snow metamorphism is influenced by snow and air temperatures and vapor pressures, snowpack energy balance, liquid water content and impurities on the snow surface [Rango, 1993].

In addition to that, the backscatter from fresh and dry snow is completely different to that of old snow.

2.5 Backscatter during Snowmelt

When temperature increases, surface-covering snow and ice melt and form numerous shallow water ponds. Those cause the signal to be scattered specularly – the backscatter drops substantially. This can be seen in Section 4.2, Figure 4.5. If snow is still present, increasing wetness in the snow pack also causes the backscatter to decrease.

Moreover, additional structures such as ice lenses can be formed by the freeze and thaw cycles which affect the backscatter behavior and make the characterization of snow more complex [Rango, 1993].

Chapter 3

Data Description

3.1 ESCAT Backscatter Data

The European Remote Sensing Satellite 2 (ERS-2) was launched on April 21, 1995 as the follow-on mission to ERS-1.

The satellite had six different instruments on board: a Ku-Band radar altimeter (working at 13.8 GHz), an along-track scanning radiometer (operating in the infrared and microwave region), the global ozone monitoring experiment (ultraviolet and visible spectrometer), a microwave radiometer (working at 23.8 and 36.5 GHz) and an active microwave instrument (AMI), acquiring in C-band at 5.3 GHz.

The AMI could be operated in SAR mode, which produced 100 km-wide stripes of high resolution imagery, in SAR wave mode, providing 5 km x 5 km images at intervals of 200 km along track, or in scatterometer mode, producing radar backscatter measurements of the Earth's surface. For this work, the dataset acquired in scatterometer mode is made use of.

The geometry of the ERS-2 scatterometer (ESCAT) is shown in Figure 3.1. It consisted of three antennas, one orientated orthogonal to the satellite track, one looking 45° forward, and one looking 45° afterward (commonly referred to as mid-beam, fore-beam and aft-beam). The resulting 500 km wide swath was centered 450 km right of the satellite's nadir. The nominal spatial resolution of the scatterometer data is 50 km [*Crapolicchio et al., 2012*]).

The ESCAT data processing had to be adapted because of a few important changes during the ERS-2 mission. In January 2000, three of the six on-board gyroscopes failed (gyro 1, 2 (both x -direction), and 5, corresponding to the z -direction). The operation mode was changed from nominal to the mono-gyro configuration, which meant a degradation of the accuracy of the satellite attitude, mainly for the yaw angle. Due to the degradation, the data distribution and assimilation

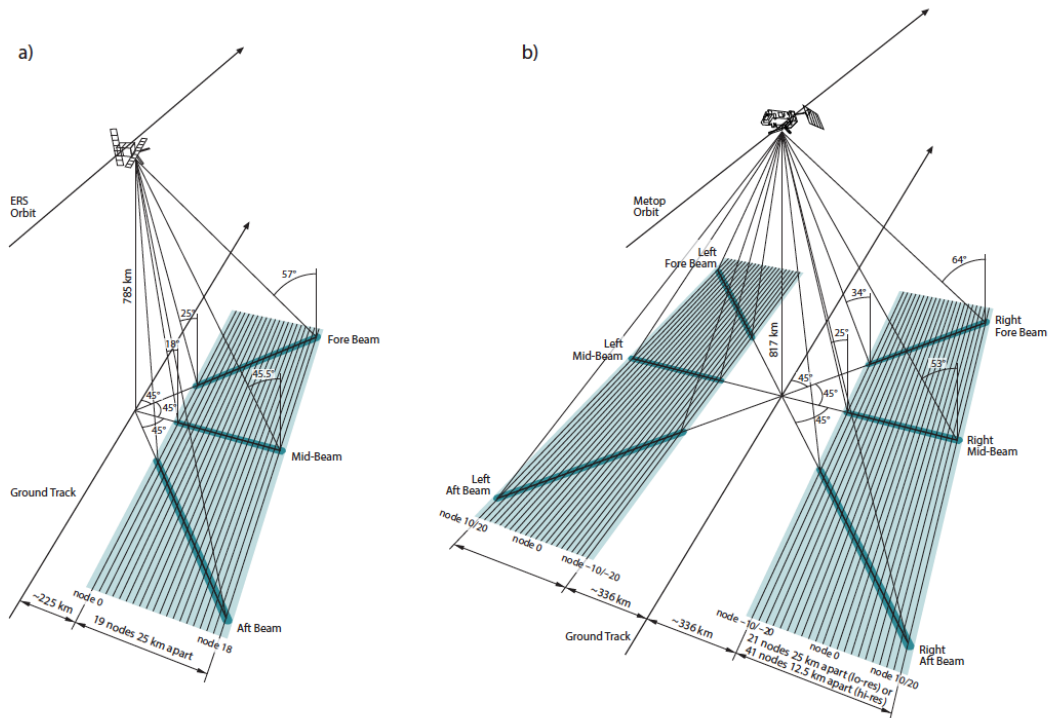


Figure 3.1: Geometry of the ESCAT (a) and ASCAT (b) scatterometers. [Bartalis, 2009]

was discontinuous and finally interrupted. The scatterometer processor was reviewed in order to compensate for the degraded attitude and to recover the scatterometer mission.

One year later, in January 2001, gyroscopes 3 and 6 failed (corresponding to the y - and z -direction), which lead to the so-called zero-gyro mode. The remaining gyroscope was only used for orbital maneuvers.

In July 2003, the on-board tape recorder failed and the mission passed from global to regional coverage – from that time on, data was only available when the satellite was within the visibility of a ground station. One month later, the scatterometer processor was adapted to the gyroscopes failure by including the successful ESACA algorithm. The number of ground stations was increased during the following years in order to better cope with the coverage of the regional mission scenario, which lead to the following operative stations at the end of the ERS-2 mission: Beijing (CN), Chetumal (MX), Cuiaba (BR), Gatineau (CDN), Hobart (AUS), Kiruna (S), Maspalomas (E), Matera (I), McMurdo (Antarctica), Miami (U.S.), Singapore, and West Freugh (U.K.). The data coverage of the global and regional scenario is shown in Figure 3.2 and Figure 3.3, respectively.

The mission ended in July 2011, when the ERS-2 started to be decommissioned and de-orbited.

The ERS-2 backscatter data used in this work is available from May 1997 to February 2003 with a spatial resolution of 25 km. Data for one grid point is available approximately every 1-5 days. Starting in 2001, the dataset contains gaps due to the introduction of the zero-gyro mode and the regional scenario.

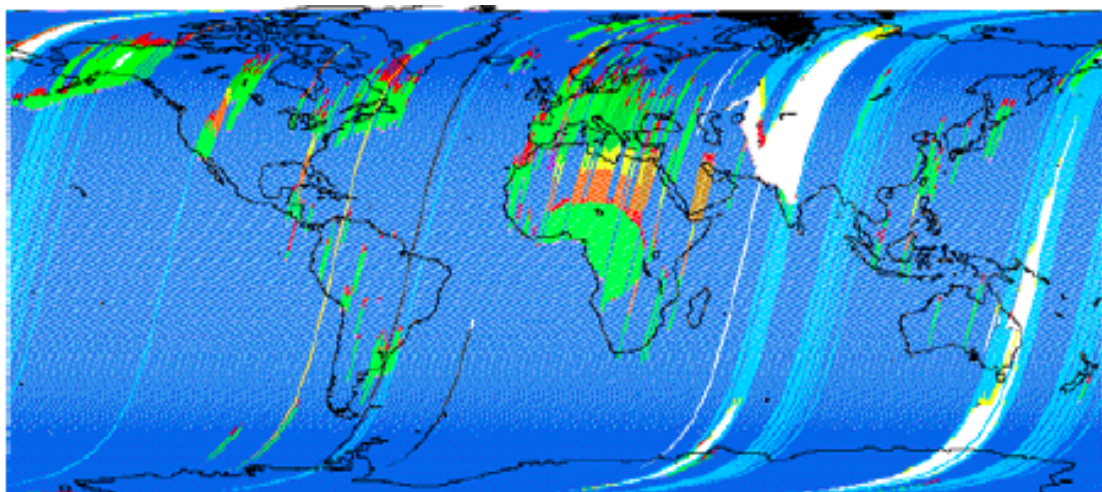


Figure 3.2: ERS-2 global mission scenario 1991-2003. [De Chiara et al., 2007]

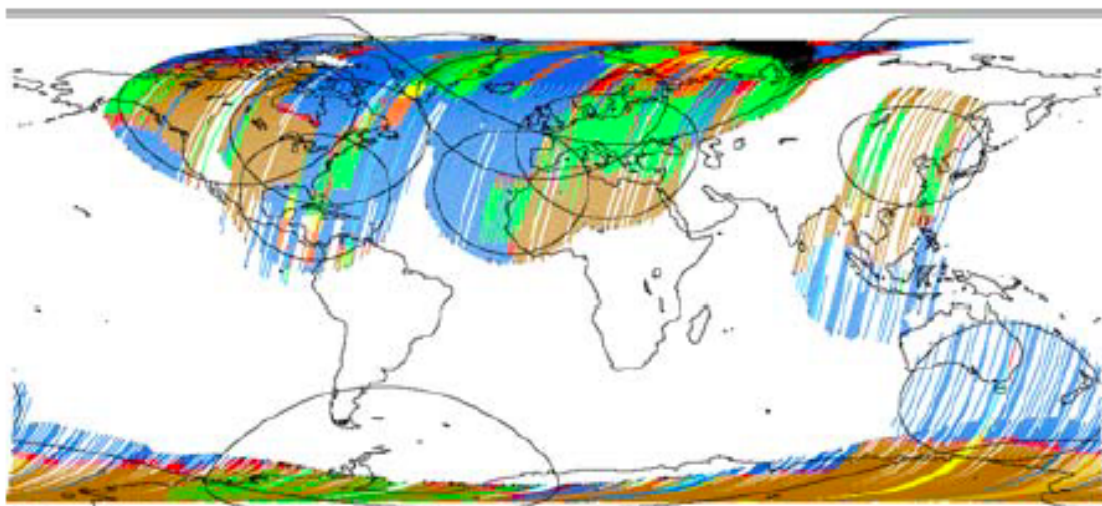


Figure 3.3: ERS-2 regional mission scenario 2003-2007. [De Chiara et al., 2007]

3.2 ASCAT Backscatter Data

The ASCAT is the Advanced SCATterometer carried on-board the MetOp-A Satellite amongst other European sensors (IASI, GOME-2, GRAS [from the [ESA webpage](#)]). The satellite was launched in October 2006 by EUMETSAT as the first of a series of three polar orbiting meteorological satellites [Naeimi *et al.*, 2012]. ASCAT is a microwave sensor operated at 5.255 GHz (C-band) with a similar geometry like its predecessor ERS-2. An important difference between the two scatterometers is that ASCAT consists of six antennas instead of three. Three antennas illuminate two 550 km swaths left and right of the satellite respectively (see Figure 3.1). The incidence angles range from 25-65°. [Figa-Saldaña *et al.*, 2002].

The TU Wien WARP processor uses backscatter data from ASCAT to derive soil moisture. One step within the soil moisture retrieval is the determination of the surface state during the observation time. ASCAT data from 2007 to 2013 were used in this work, with a spatial resolution of 25 km and a revisit time of approximately one day per grid point.

3.3 ERA-Interim Data

The surface state flag processor requires external temperature data for the calculation of the static freeze/thaw thresholds (see Section 4.2). Naeimi *et al.* (2012) chose the ERA-Interim dataset for this purpose, which covers a time period of more than 20 years (from 1979 to present). The database is freely available for research and education purposes. More than 25 different instruments on-board 45 different satellites collect the data that is then assimilated into the dataset [Poli *et al.*, 2010].

Chapter 4

Determination of the Surface State Flag

The calculation of the surface state flag is done using a threshold-analysis method. As a first step, backscatter measurements normalized to a common incidence angle and temperature data are collocated. Based on this collocation, static freeze/thaw parameters are calculated, which are then combined to the required thresholds. A decision tree is defined which returns the surface state flag for a corresponding backscatter value.

4.1 Grid Definition

All datasets used within the surface state processor are resampled to a discrete global grid (DGG) with 12.5 km grid point spacing. For reasons of data storage but also easier data analysis, grid points are put together in $5^\circ \times 5^\circ$ cells. The grid point numbering starts with grid point 0 at 0° latitude and 0° longitude and continues in a clockwise manner around this first grid point.

The numbering of the cells starts at -90° latitude and -180° longitude, continues in vertical direction and ends at 90° latitude and 180° longitude.

4.2 Calculation of the Freeze/Thaw Parameters

In the first step of the calculation of the freeze/thaw parameters, backscatter values normalized to a common incidence angle are compared to the ERA Interim surface temperature dataset. In most cases, the relationship between the two datasets follows a certain trend: In winter, when the soil moisture is lower and the soil is frozen, backscatter values are lower than in summer, where a high soil moisture dominates most landscapes. However, this behaviour varies depending on climatic conditions and land cover. If possible, a logistic function is fit to all observations between

-10°C and +10°C, from which the freeze/thaw parameters can be derived. The logistic curves are displayed in black in Figure 4.1-Figure 4.5.

A typical example for the backscatter-temperature relationship at higher latitudes is shown in Figure 4.1. The chosen grid point is located in the Happy Valley, Alaska, at 69.16° northern latitude and 148.84° western longitude. This area shows low backscatter values in winter due to frozen soil, and high backscatter values due to vegetation growth and high soil moisture in summer. The two images show all ASCAT backscatter measurements from 2007-2013 and all ESCAT measurements from 1997-2003, respectively. The difference in the amount of observations is clearly visible.

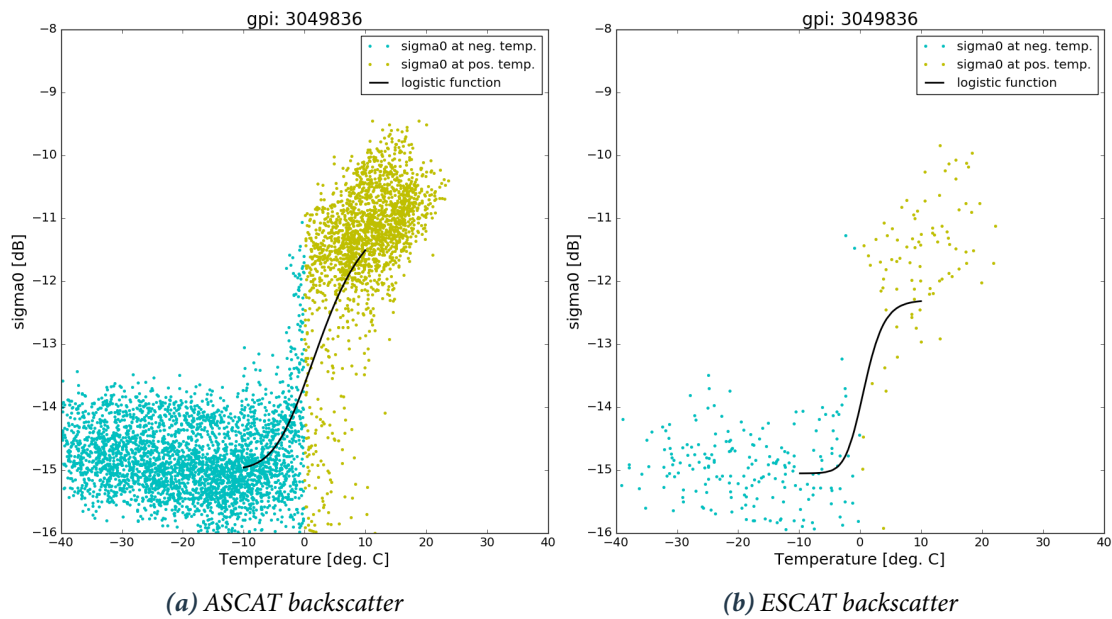


Figure 4.1: Behaviour of normalized backscatter against ERA Interim surface temperature for a grid point in Alaska, Happy Valley.

Another example for the backscatter-temperature behaviour is shown in Figure 4.2 for a grid point in Apuka (Russia, 60.97° northern latitude, 168.27° eastern longitude). The relationship between temperature and backscatter is similar to the grid point in Alaska, however, the grid point in Apuka faces a melting period which is depicted by very low backscatter values around the freezing point. During snow melt, water collects on the surface which leads to specular reflection; thus, very little to no backscatter at all is measured.

Figure 4.3 shows another grid point in Russia (Buyaga, 60.08° northern latitude, 126.19° eastern longitude). The backscatter-temperature behaviour is again similar, but the backscatter shows an increasing trend at very low temperatures. This behaviour is caused by snow metamorphism,

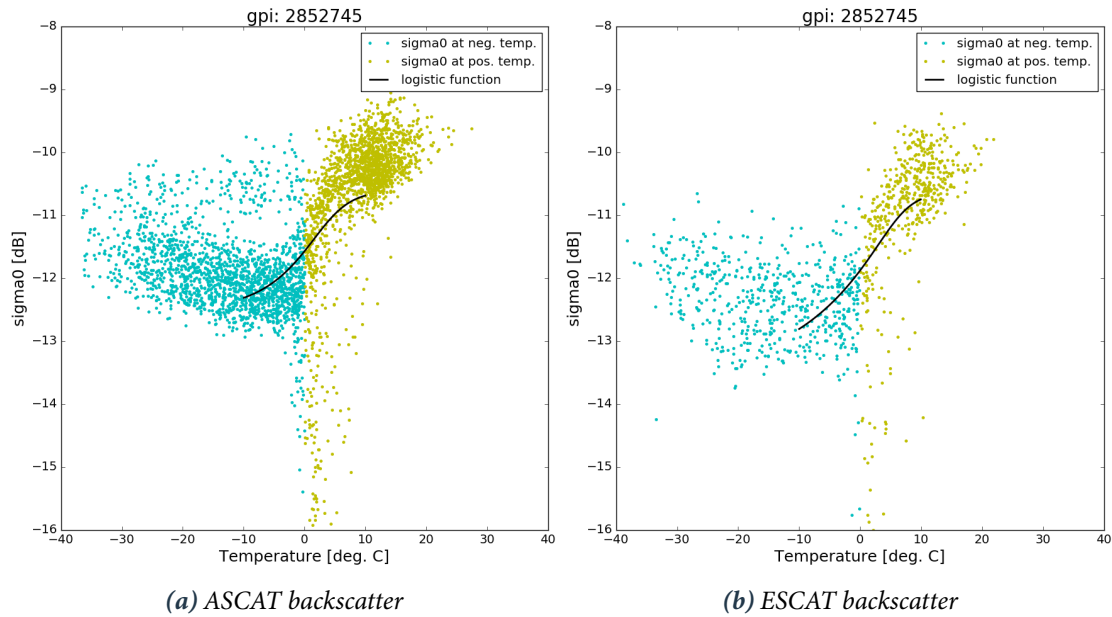


Figure 4.2: Behaviour of normalized backscatter against ERA Interim surface temperature for a grid point in Russia, Apuka.

volume scattering from dry snow and possibly also from frozen soil. In such cases, the discrimination of frozen and unfrozen conditions is difficult since the backscatter values at low temperatures can reach to the level of backscatter from wet soil.

Another example where the discrimination of frozen and unfrozen soil is almost impossible is a grid point in Mazong Shan, in the Gobi desert (41.76° northern latitude, 97.25° eastern longitude, see Figure 4.4). This area is characterized by an extreme climate with very cold winters and very hot summers, with temperatures ranging from -40°C to $+40^\circ\text{C}$. The soil is extremely dry and there is no vegetation cover due to very low precipitation. Since the backscatter values from dry and frozen soil are about the same level, surface state changes are not clearly observable in this region.

Finally, Figure 4.5 shows the typical backscatter-temperature behaviour of a grid point covered by permanent ice (Solnechnaya Bay in Russia, 78.45° northern latitude, 104.02° eastern longitude). Most of the time, the temperatures are beneath 0°C . In summer, the upper surface layer melts, which leads to very low backscatter values. The curve fitted to the measurements shows a negative behaviour, which is used in the SSF processor for characterizing permanent ice.

From each logistic curve, the following parameters can be derived:

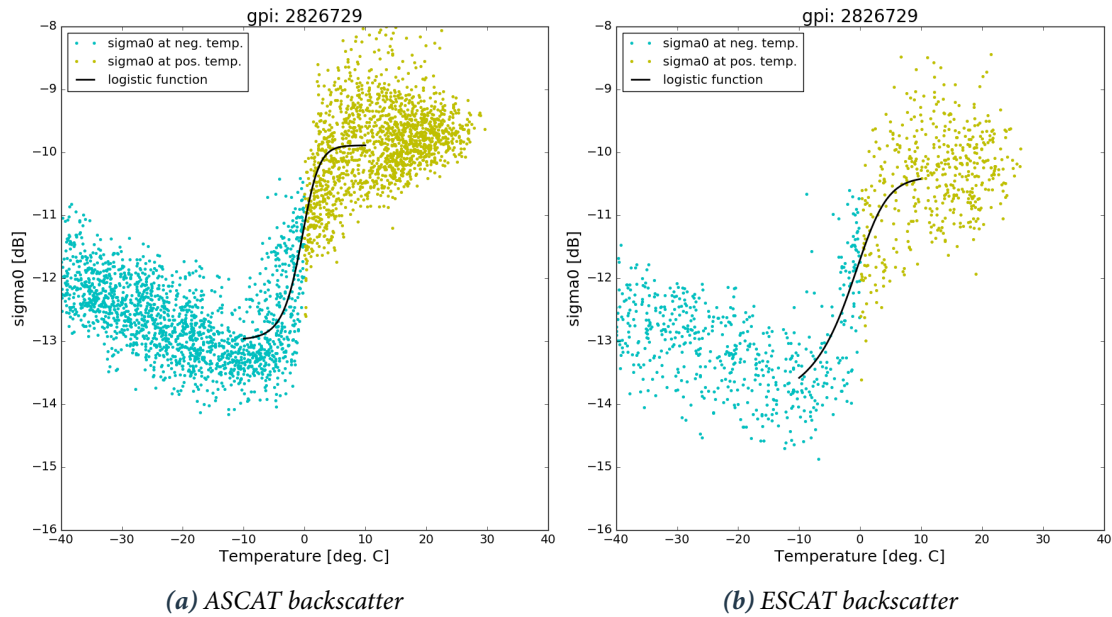


Figure 4.3: Behaviour of normalized backscatter against ERA Interim surface temperature for a grid point in Russia, Buyaga.

- **Freeze/thaw threshold:** Backscatter values below this threshold indicate a frozen condition. The threshold is found by calculating the inflection point of the logistic function between $\pm 10^{\circ}\text{C}$.
- **Snowmelt/water level:** Backscatter value below that level designate snowmelt/water on the surface. It is found via a statistical outlier method: The outlier with the highest backscatter value is used for the snowmelt threshold. If no outlier is detected, the lowest backscatter measurement is used as threshold.
- **Mean backscatter in summer/winter:** Mean normalized backscatter value in summer/winter
- **Transition point 1 and 2:** The day of year when the transition between winter and summer (1) and summer and winter (2) happens. The transition days are found using a step filter on the temperature and backscatter time series.
- **Steepness of linear regression during frozen period:** The frozen period is defined between -35°C and -5°C . This parameter indicates volume scattering.
- **Standard deviation during frozen period:** The standard deviation of the normalized backscatter during frozen period
- **Permanent ice flag:** True if the logistic function has a negative behavior

Such a set of freeze/thaw (FT) parameters is calculated for each grid point. These parameters are

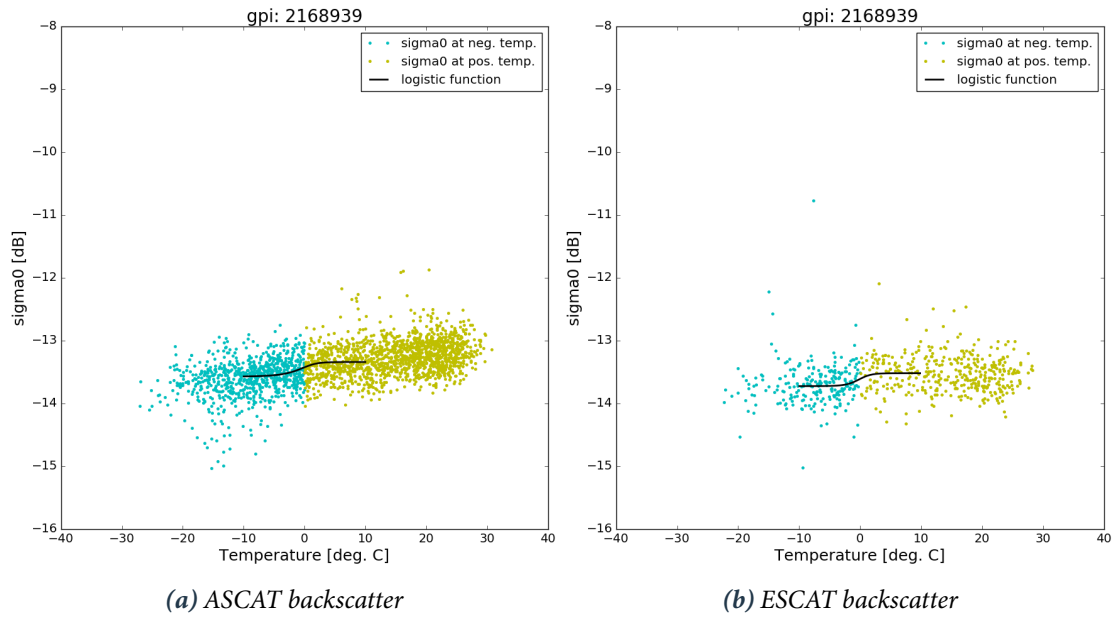


Figure 4.4: Behaviour of normalized backscatter against ERA Interim surface temperature for a grid point in China, Mazong Shan.

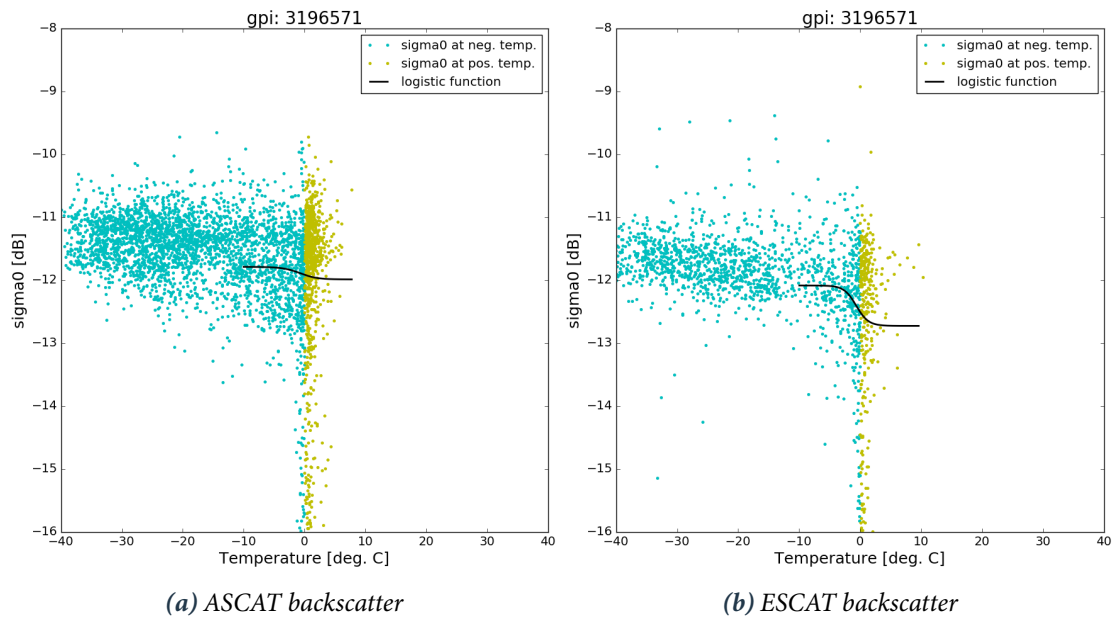
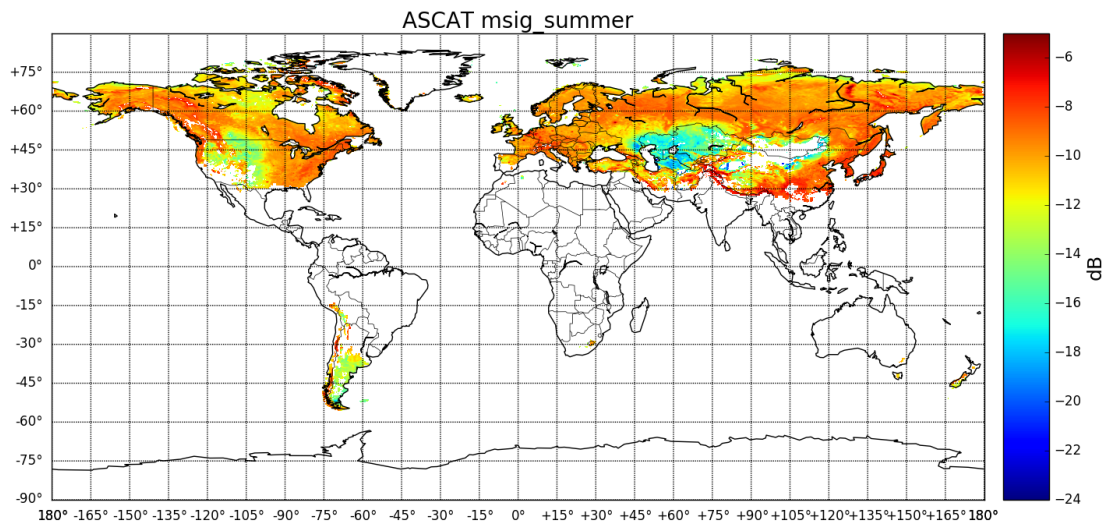


Figure 4.5: Behaviour of normalized backscatter against ERA Interim surface temperature for a grid point in Russia, Solnechnaya Bay.

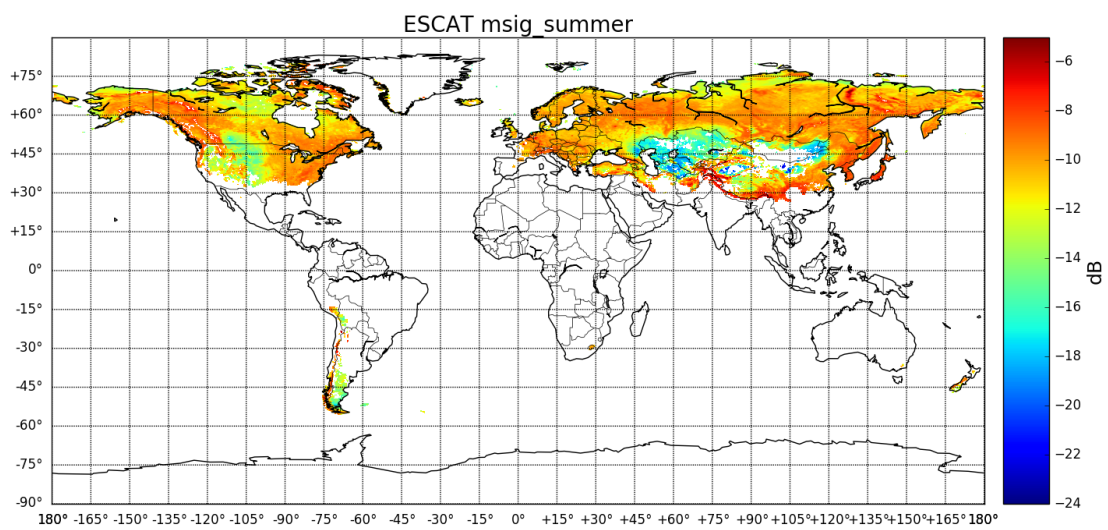
static, which means that they are calculated once and are assumed not to change over time. The derivation of the FT parameters depends strongly on the quality of the fit of the logistic curve. Generally, the quality of the fit is better, the more observations are available around the freezing point – therefore, the logistic curve obtained from observations of the ESCAT scatterometer on-board the ERS-2 satellite is usually not as well controlled as the fit to ASCAT data. The quality of the fit also depends on how well the backscatter-temperature relationship follows the form of a logistic curve [Naeimi *et al.*, 2012].

Figure 4.6-Figure 4.9 show the global values of four FT parameters derived from ASCAT and ESCAT data, respectively. More images of the FT parameters can be found in Appendix A.1, Figure A.1-Figure A.5. When comparing the results, it must be considered that the underlying datasets cover different time periods (ASCAT: 2007-2013, ESCAT: 1997-2003). Another reason for differences in the derived parameters results from the number of available observations, which is considerably higher for ASCAT than for ESCAT in certain regions.

Some of the parameters show a dependency on climatic factors, topography and land cover, whereas some depend more on parameters like surface roughness. A dependency on the climate and elevation is clearly visible in the images of the transition days, which show a latitude-dependent trend and a pattern reflecting the Earth's topography. The transition from winter to summer happens later in the year for grid points at high latitudes and high altitudes, whereas the transition from summer to winter happens earlier for these grid points.

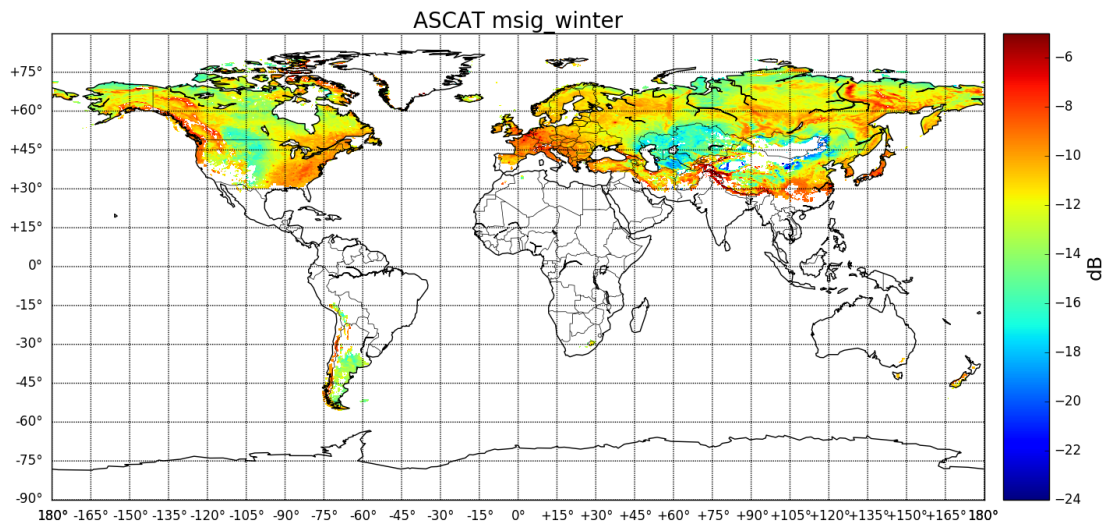


(a) ASCAT — Mean backscatter in summer

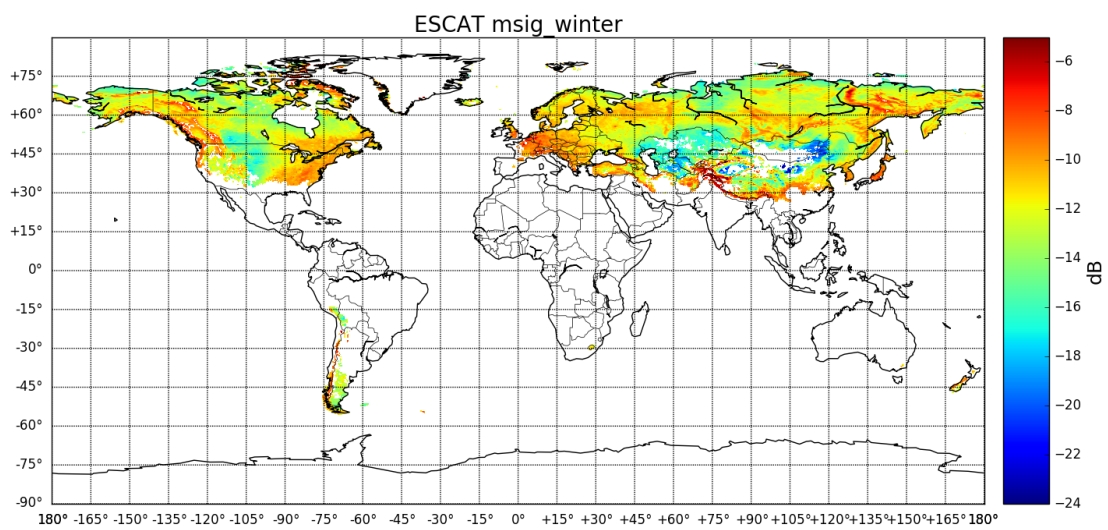


(b) ESCAT — Mean backscatter in summer

Figure 4.6: Mean backscatter in summer derived from ASCAT and ESCAT backscatter data.

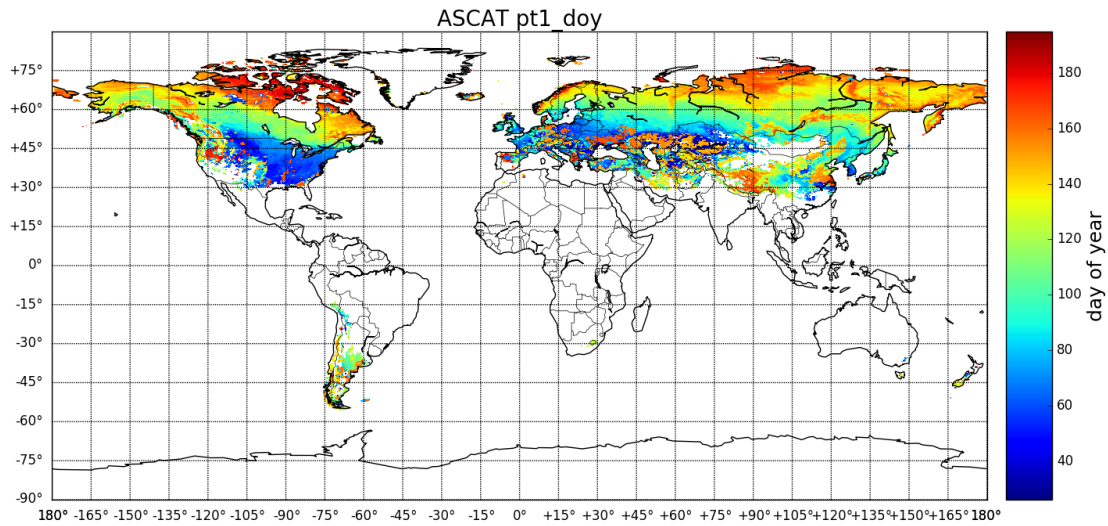


(a) ASCAT — Mean backscatter in winter

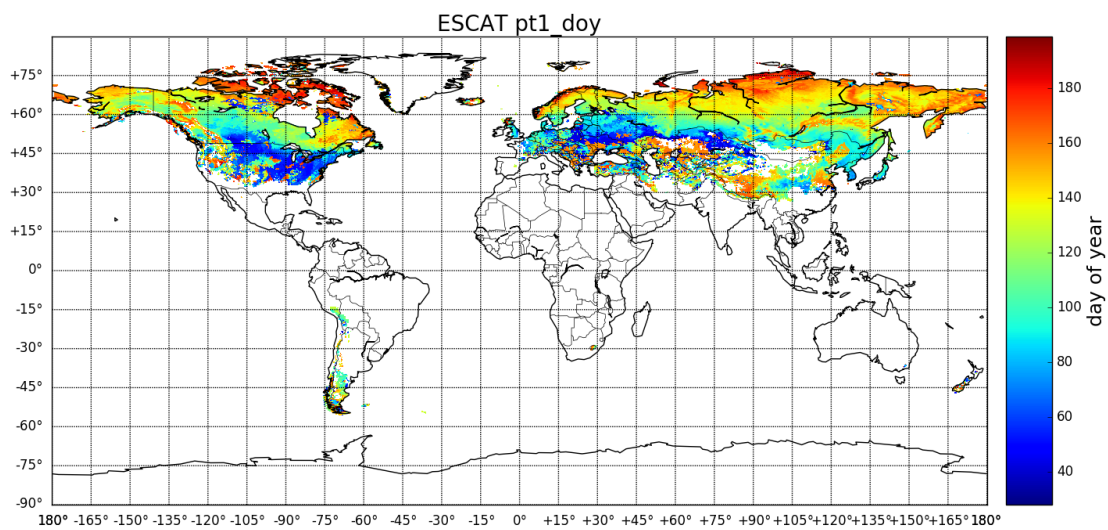


(b) ESCAT — Mean backscatter in winter

Figure 4.7: Mean backscatter in winter derived from ASCAT and ESCAT backscatter data.

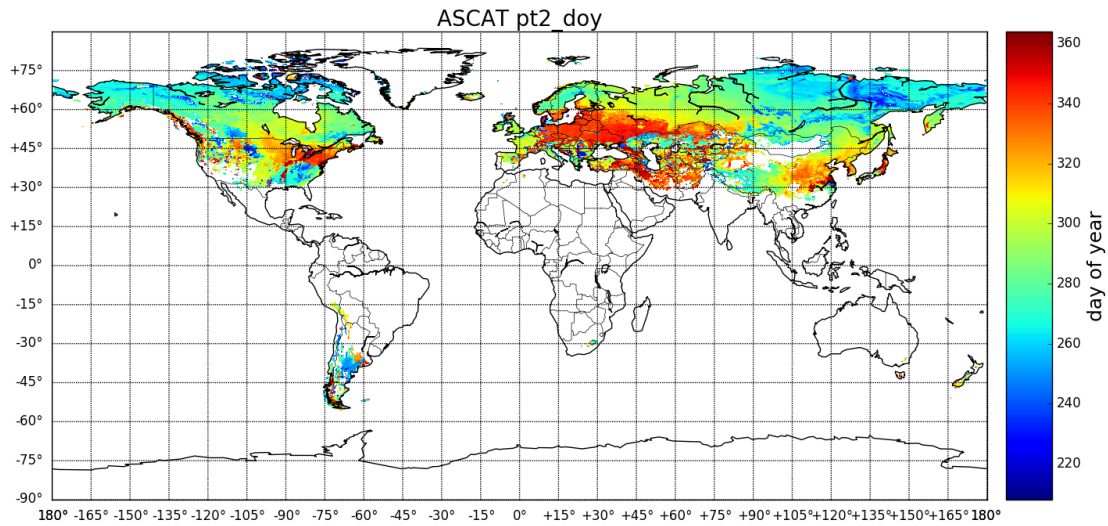


(a) ASCAT — Transition day 1 (winter – summer)

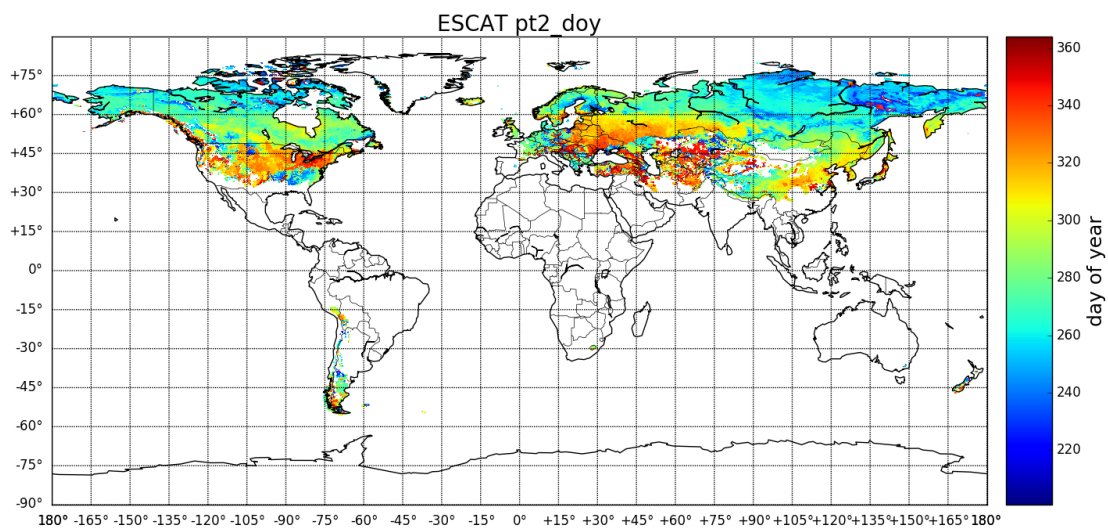


(b) ESCAT — Transition day 1 (winter – summer)

Figure 4.8: Transition day 1 (winter – summer) derived from ASCAT and ESCAT backscatter data.



(a) ASCAT — Transition day 2 (summer – winter)



(b) ESCAT — Transition day 2 (summer – winter)

Figure 4.9: Transition day 2 (summer – winter) derived from ASCAT and ESCAT backscatter data.

4.3 Surface State Flag

The freeze/thaw parameters introduced and described in Section 4.2 are then used to set up decision trees for the determination of the surface state flag (SSF). The SSF can take on the following values:

- unfrozen
- frozen
- snowmelt/water on surface
- permanent ice
- unknown

As mentioned before, "normal" conditions are that backscatter is higher in summer than in winter. However, there are regions where the opposite is true, i.e. backscatter is higher in winter than in summer. Such conditions can be due to more precipitation and less evaporation in winter than in summer (hereafter referred to as region 2; e.g. Central Europe) and fewer freezing events than in regions with "normal" conditions (hereafter referred to as region 1) [Naeimi *et al.*, 2012]. The regional classification that is used in the decision trees is depicted in Figure 4.10.

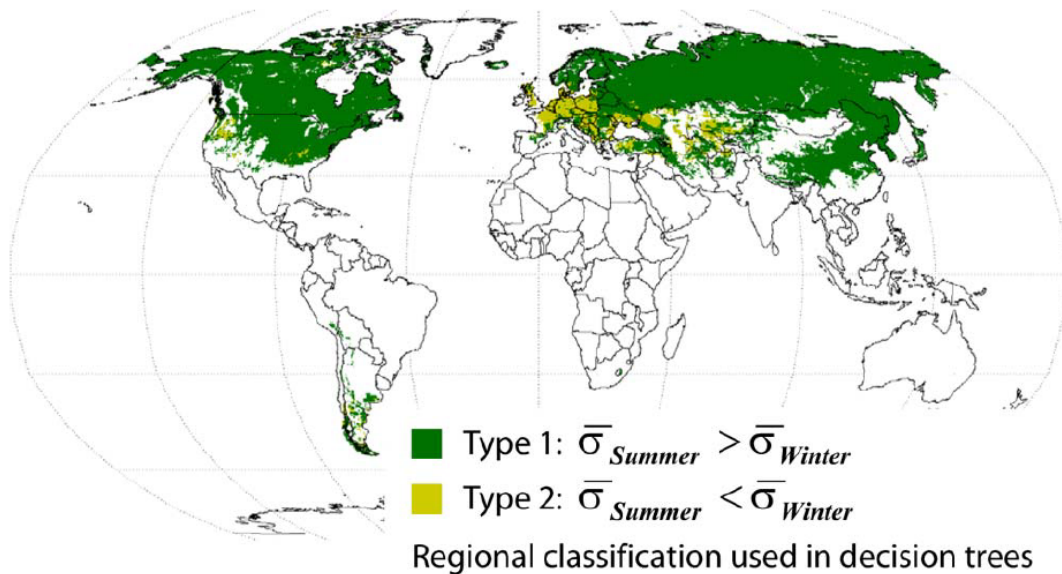


Figure 4.10: Distinction between region 1 (higher backscatter in winter than in summer) and region 2 (higher backscatter in summer than in winter). 96% of all grid points are classified into region 1. [Naeimi *et al.*, 2012]

Two different decision trees were developed to distinguish between region 1 and region 2.

For the setup of the decision trees, six thresholds are defined from the previously calculated FT parameters [Naeimi et al., 2012]:

$$Thr1 = (\sigma_{FTL} + \bar{\sigma}_{Summer})/2$$

$$Thr2 = \sigma_{FTL} + 2 \times \xi_{\sigma_{40}}$$

$$Thr3 = \sigma_{FTL} - 2 \times \xi_{\sigma_{40}}$$

$$Thr4 = (\sigma_{FTL} + \sigma_{SML})/2$$

$$Thr5 = \sigma_{SML} + 2 \times \xi_{\sigma_{40}}$$

$$Thr6 = \sigma_{SML} - 2 \times \xi_{\sigma_{40}}$$

with σ_{FTL} and σ_{SML} as the normalized backscatter at freeze/thaw and snowmelt levels, and $\bar{\sigma}_{Summer}$ as the mean of normalized backscatter in summer. $Thr1$ defines the upper extreme level of freezing; measurements above $Thr1$ are expected to be unfrozen. $Thr2$ and $Thr3$ are the upper and lower levels of σ_{FTL} , $Thr5$ and $Thr6$ are the upper and lower uncertainty range of σ_{SML} . $Thr4$, the midpoint between σ_{FTL} and σ_{SML} , is the maximum value for snowmelt or water on the surface. Figure 4.11 shows examples for the thresholds.

Additionally, the decision trees require the definition of the following parameters:

- $\xi_{\sigma_{40}}$, noise of the incidence angle normalized backscatter. The parameter is the result of error propagation through the TU Wien normalization algorithm [Naeimi, 2009] and gives the uncertainty of the normalized backscatter.
- $\Delta_{\sigma_{40}} = \sigma_{40} - \hat{\sigma}_{40}$, the deviation of the normalized backscatter from an exponentially weighted average of the backscatter values from the last n days. n has been set to 5 days in the SSF algorithm.
- $Stdev(\sigma_{40}^{frozen})$, the standard deviation of the normalized backscatter during the frozen period, which is calculated from normalized backscatter measurements corresponding to temperature values between $-20^{\circ}C$ and $-5^{\circ}C$
- Deep snow flag, which shows areas in which volume scattering from dry snow must be considered. For all grid points where $-30^{\circ}C \times d\sigma_{40}/dT > 2 \times Stdev(\sigma_{40}^{frozen})$, the deep snow flag is set as *True*.

Figure 4.11 shows the backscatter-temperature relationships of two grid points in the first- and second-type region, respectively. The thresholds are depicted as dashed lines. For the grid point

in region 2 located in Itzehoe, Germany, only *Thr2*, *Thr3* and *Thr6* can be defined because of the special backscatter-temperature relationship, visible in Figure 4.11b. There is no clear threshold between Winter and Summer backscatter observations – similar values appear in both seasons, which requires a different approach than the grid points that show a "normal" behaviour.

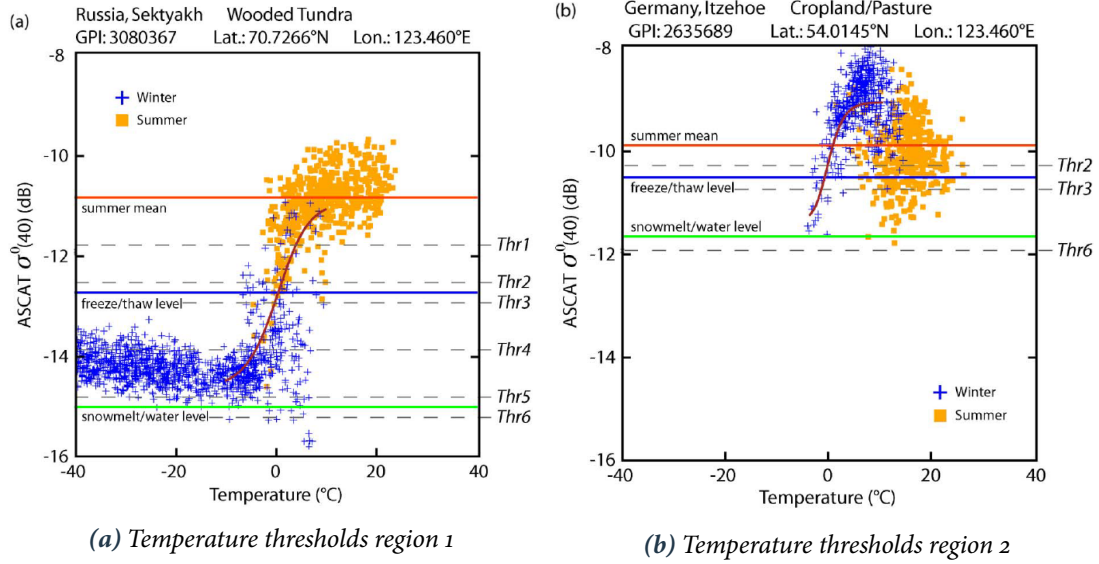


Figure 4.11: The backscatter-temperature relationships of two grid points in the (a) first- and (b) second-type region. The thresholds are depicted as dashed lines. [Naeimi et al., 2012]

One year is separated into different seasons in the SSF processor: Winter (W), transition from winter to summer 1 (TWS₁), transition from winter to summer 2 (TWS₂), summer (S), transition from summer to winter 1 (TSW₁) and transition from summer to winter 2 (TSW₂). The two transition zones in spring (TWS₁ and TWS₂) and in fall (TSW₁ and TSW₂) are combined to TWS and TSW in decision tree 1. They are defined as the period ± 30 days around the transition days 1 and 2, which are two of the previously calculated FT parameters.

In both decision trees, the evaluation of the normalized backscatter measurements (σ_{40}) happens in a step-wise approach, depending on the timestamp of the measurement. Based on the previously calculated thresholds, a surface state flag is determined for each σ_{40} observation, with different levels of complexity depending on the timestamp and the location of the measurement (region 1 or 2). Generally, the second decision tree includes more straightforward conditions for the surface state flagging because no transition zones are assumed – TWS₂, summer, and TSW₁ are combined to the "warm season", TSW₂, winter and TWS₁ and combined to the "cold season". The frozen flag is only set by the anomaly detection modules since freezing events are not frequent in region 2. Figure 4.12 and Figure 4.13 show the two decision trees as flowcharts.

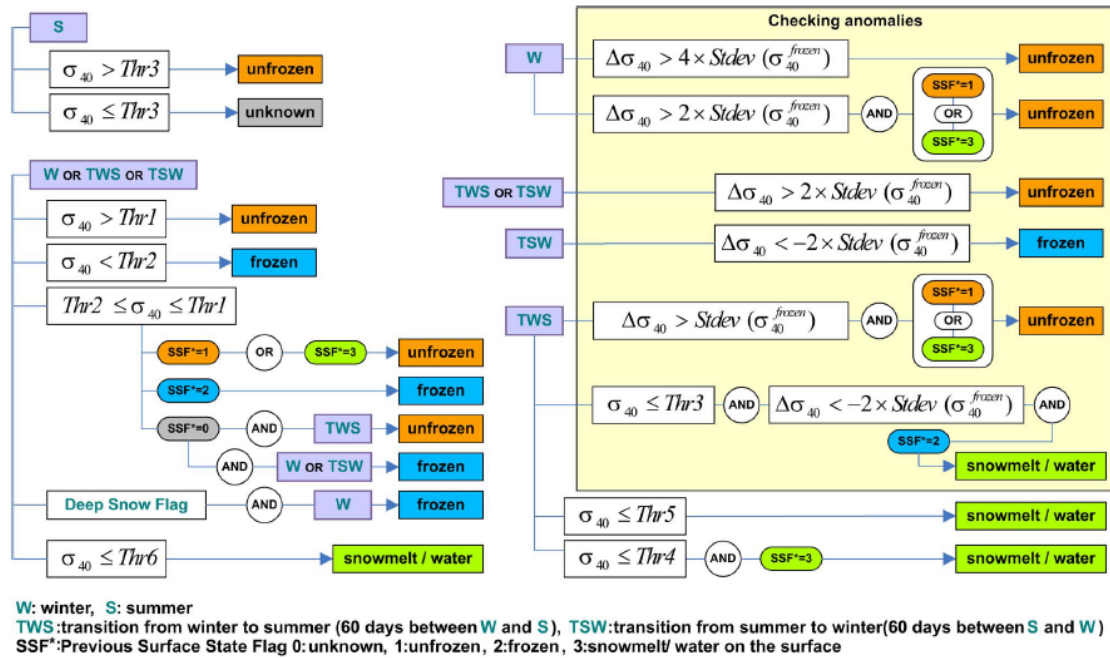


Figure 4.12: Decision tree for region 1 (backscatter higher in summer than in winter). [Naeimi et al., 2012]

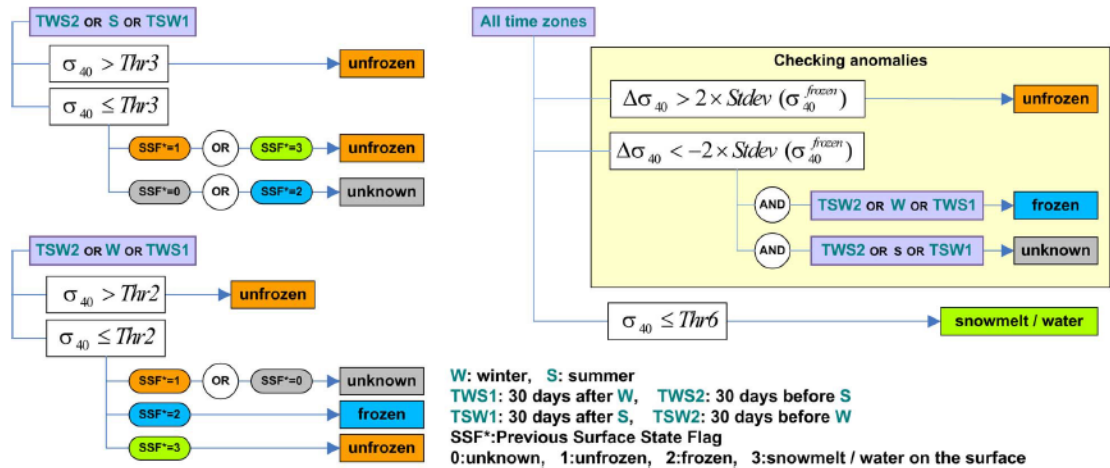


Figure 4.13: Decision tree for region 2 (backscatter higher in winter than in summer). [Naeimi et al., 2012]

4.4 Adaptation of the SSF Algorithm

The first run of the SSF algorithm with ESCAT backscatter data produced incorrect results. The main reason for these results were differences between the ASCAT and ESCAT input data format. After some adaptation of the code that does the data handling, the output for ESCAT SSF time series looked promising and the analysis and validation of the results was started.

The region for which SSF can be determined from ESCAT data is a bit smaller than for ASCAT data due to the lower data availability. Especially in regions that do not face frequent freezing periods, the availability of backscatter measurements under frozen conditions is limited. Therefore, the fitting of a logistic curve is not possible, which leads to no freeze/thaw parameters and finally to no SSF determination. However, the overall performance of the algorithm is still satisfyingly high despite the lower ESCAT data availability.

4.5 Processing Flags

In order to get a better feeling for the performance of the SSF determination, processing flags were calculated during the SSF process (see Figure 4.14a and Figure 4.14b). The value of the processing flag provides information on whether the determination of a surface state flag was successful or failed, and if it failed, why it did so. Valid observations are defined as observations between $\pm 10^{\circ}\text{C}$. Frozen observations are all observations below 0°C . Surface state flags can only be derived for dark blue areas.

- dark blue: processing okay
- light blue: not enough frozen observations
- cyan: not enough valid observations (frozen and unfrozen)
- red: logistic curve too flat, no reliable thresholds can be derived

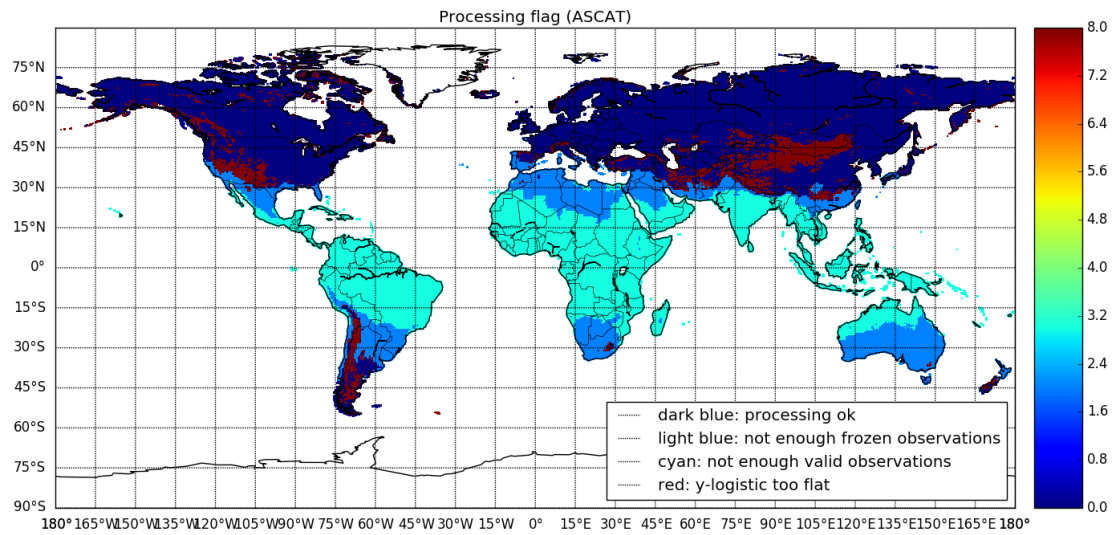
The threshold for "enough valid/frozen observations" is 10, respectively. If less than 10 valid observations are available, the processing is stopped. For light blue and cyan areas, no surface state flag can therefore be calculated.

Red areas show too little difference between frozen and unfrozen backscatter measurements, which leads to a flat logistic curve. It's therefore impossible to derive a trustworthy classification based on the logistic curve that is fitted to the data.

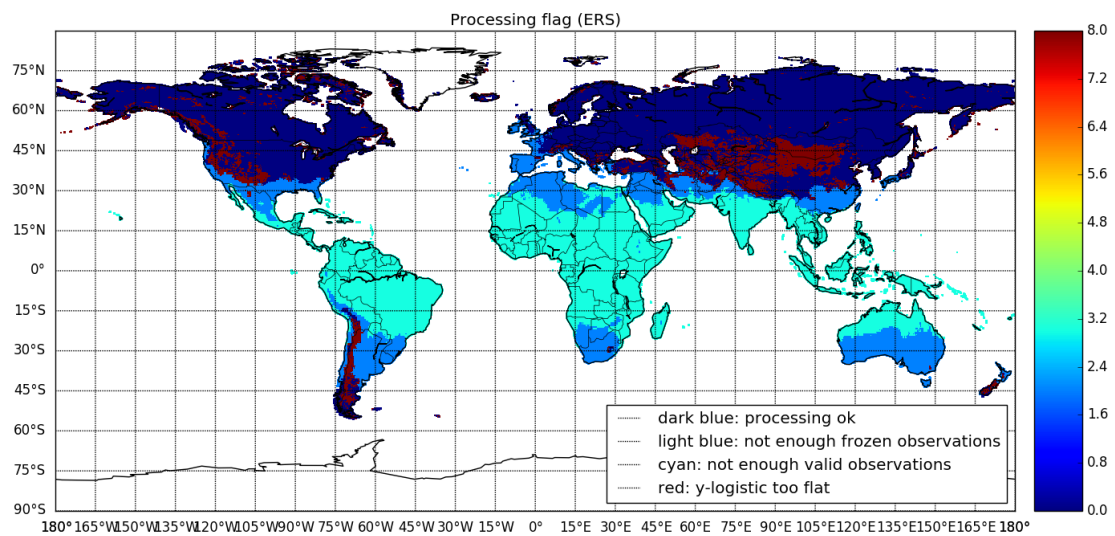
Approximately $\pm 15 - 20^{\circ}$ north and south of the equator, no SSF can be determined due to too few frozen observations or no frozen observations at all. At higher latitudes, the determination of

the SSF usually works well: for about 75% of the landmasses above 30° northern latitude, reliable results can be derived. Problematic areas are most of all mountain ranges (e.g. the Himalayas, the Alps, the Rocky Mountains, the Andes), but also very dry regions like the Gobi desert.

The processing flag map from ESCAT data (Figure 4.14b) shows more light blue areas than the map from ASCAT data, due to the lower number of available data (e.g. in western Europe).



(a) SSF Processing flags (ASCAT)



(b) SSF Processing flags (ERSAT)

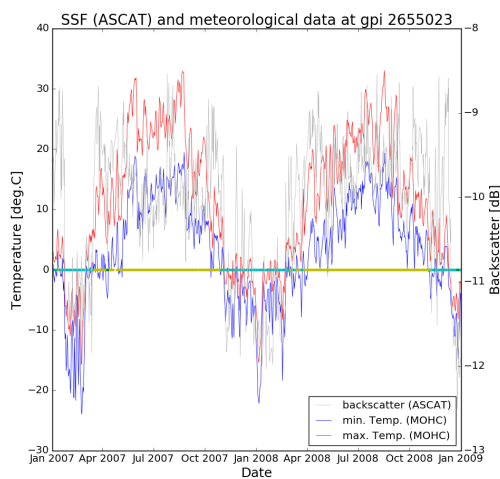
Figure 4.14: Surface state flags can only be determined for dark blue areas. For light blue and cyan areas, no SSF can be determined due to too few available observations. In red areas, enough observations are available, but the difference between backscatter in summer and backscatter in winter is too small to derive a surface state flag.

Chapter 5

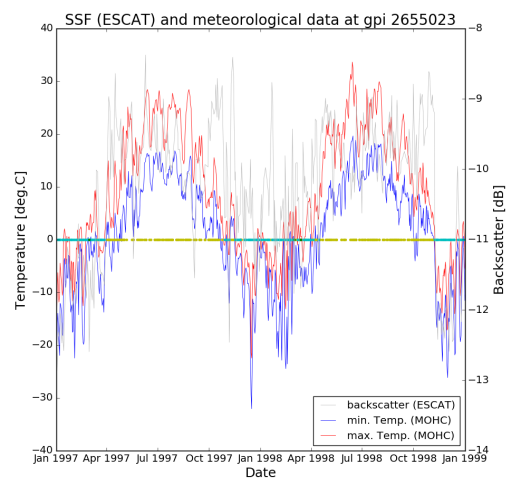
Results of the SSF determination

The following figures show the determined surface state flag time series for different grid points. Possible values are

- unfrozen (yellow)
- frozen (cyan)
- snowmelt/water on surface (green)
- permanent ice (purple)
- unknown (grey)



(a) SSF derived from ASCAT backscatter data



(b) SSF derived from ESCAT backscatter data

Figure 5.1: SSF time series from ASCAT and ESCAT data compared to the corresponding backscatter data from ASCAT and ESCAT and minimum/maximum temperature data from the Met Office Hadley Centre.

Figure 5.1a and Figure 5.1b show example time series of surface states for a grid point in Russia, derived from ASCAT and ESCAT, respectively. The grid point is located at 54.58° northern latitude and 36.73° eastern longitude in an area dominated by cold continental climate without a dry season, covered mostly with croplands.

The SSF time series show very good agreement with the corresponding backscatter time series and the minimum and maximum temperature curves from the Met Office Hadley Centre [Caesar et al., 2006]. The dataset has been created using daily temperature observations from over 27000 stations, interpolated to a regular grid. For the periods when the surface state is determined to be "snowmelt" (depicted in green in the images), the temperature curves show a corresponding behavior (e.g. in April 2007).

5.1 Climate and Land Cover

On the following pages, 5° × 5° regions are classified according to the Koeppen-Geiger climate classification (see Figure 5.2, [Peel et al., 2007]) and the MODIS land cover map [Channan et al., 2014].

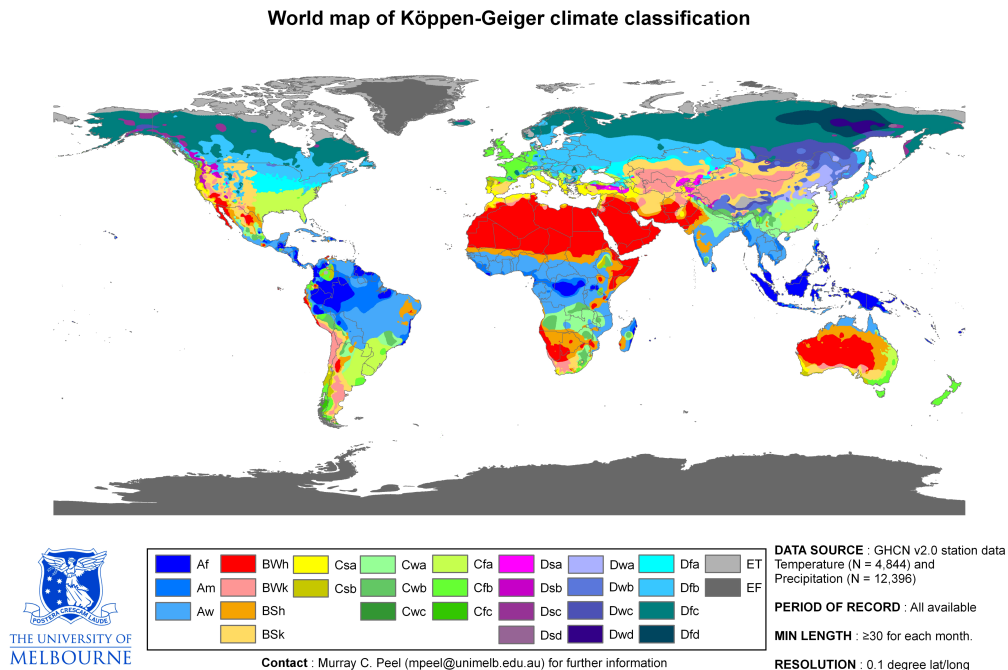


Figure 5.2: Koeppen-Geiger climate map. Detailed information on the classes is provided in Table 5.1 [Peel et al., 2007].

1st	2nd	3rd	Description
A			Tropical
	f		- Rainforest
	m		- Monsoon
	w		- Savannah
B			Arid
	W		- Desert
	S		- Steppe
		h	- Hot
		k	- Cold
C			Temperate
	s		- Dry Summer
	w		- Dry Winter
	f		- Without dry season
		a	- Hot Summer
		b	- Warm Summer
		c	- Cold Summer
D			Cold
	s		- Dry Summer
	w		- Dry Winter
	f		- Without dry season
		a	- Hot Summer
		b	- Warm Summer
		c	- Cold Summer
		d	- Very Cold Winter
E			Polar
	T		- Tundra
	F		- Frost

Table 5.1: Koeppen-Geiger climate classes [Peel et al., 2007]

The Koeppen-Geiger classification consists of five main categories, which are divided further into different amounts of subcategories. All categories are listed in Table 5.1.

Table 5.2 shows the land cover classes used by the MODIS land cover maps.

5.2 Surface state flags from ASCAT and ESCAT

In order to obtain an impression not only for one grid point at a time but for a larger area, the SSF time series were plotted region-wise, meaning that the SSF time series of all grid points of one $5^\circ \times 5^\circ$ region are plotted above each other (see Figure 5.3-Figure 5.8). The date range is plotted on

Land cover classes	
Water	Woody savannas
Evergreen needleleaf forest	Savannas
Evergreen broadleaf forest	Grasslands
Deciduous needleleaf forest	Permanent wetlands
Deciduous broadleaf forest	Croplands
Mixed forest	Urban and built-up
Closed shrublands	Cropland/natural vegetation mosaic
Open shrublands	Barren or sparsely vegetated
Snow and ice	

Table 5.2: MODIS land cover classes [Channan et al., 2014]

the x-axis, while the values of the y-axis refer to the numbers of the grid points in the respective area. The grid points are sorted by their index, which is determined as follows: grid point index 0 is located at 0° latitude and 0° longitude. The grid points are sorted from South to North and from West to East on the Northern Hemisphere east of the Prime Meridian, and from East to West on the Northern Hemisphere west of the Prime Meridian.

Each of the regions has a certain cell number depending on its latitude and longitude, which is used for identification and referencing hereafter.

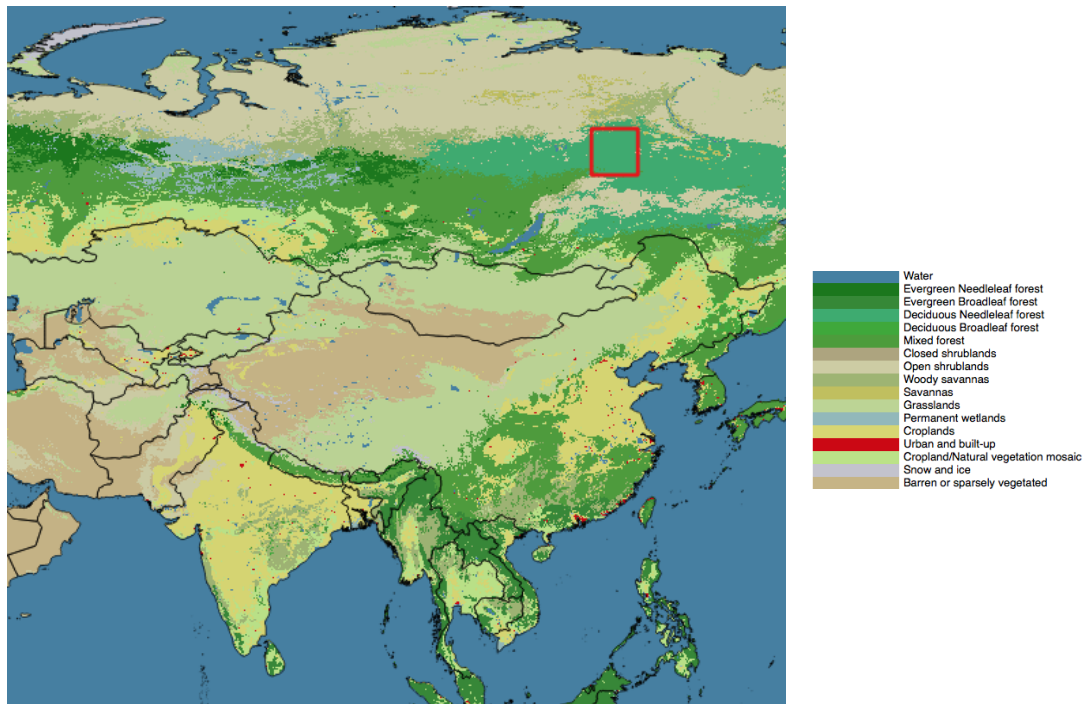
When comparing the results for ASCAT and ESCAT backscatter, it has to be noted that the respective date ranges are different (ASCAT: 2007-2013, ESCAT: 1997-2003). Also, due to the lower data availability, there can be gaps in the time series in the ESCAT SSF plots.

5.2.1 SSF determination in cold climate

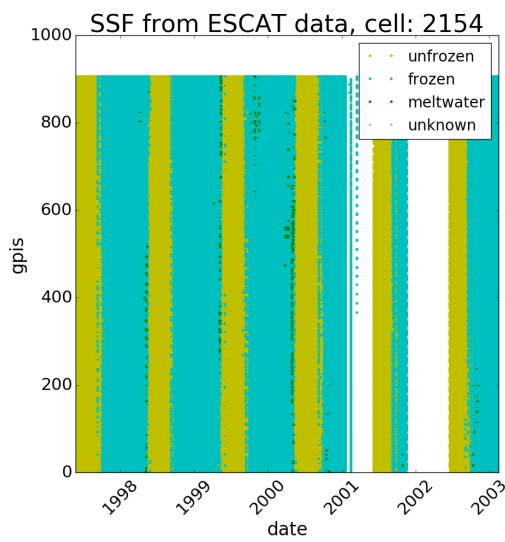
The selected area is located in central Russia (60-65° northern latitude, 115-120° eastern longitude; cell 2154). The climate there is cold, without a dry season and with cold summers. The area is dominated by deciduous needleleaf forest as displayed in Figure 5.3a. The determined surface state flags reflect the homogeneity of the land cover; there is almost no variation in the classification of the different grid points.

The fact that the region is predominantly covered by deciduous needleleaf trees plays a role in the scattering behavior of the area: since deciduous trees lose their leaves in winter, there is less volume scattering due to leaves, which makes the retrieval of the soil moisture and soil state in winter easier. The frozen period lasts about 6-8 months per year.

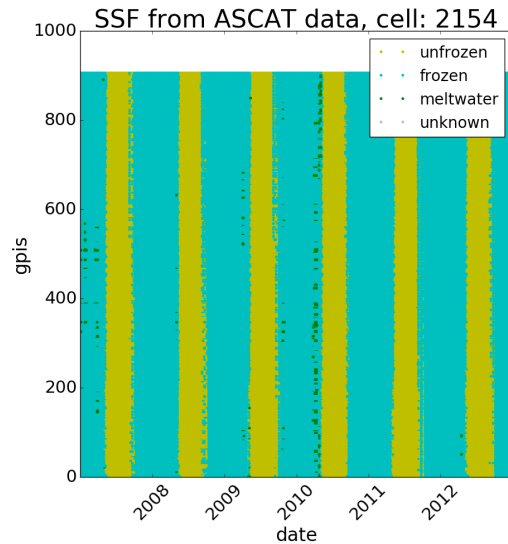
In the ESCAT image (Figure 6.8a), the data gap due to the gyroscopes' failure in 2001 is clearly visible.



(a) Location of cell 2154



(b) SSF from ESCAT data



(c) SSF from ASCAT data

Figure 5.3: SSF time series plot for cell 2154, determined from ESCAT (b) and ASCAT (c) backscatter values. The cell is located in cold climate, dominated by deciduous needleleaf forest.

5.2.2 SSF determination of permanent wetlands in cold climate

Figure 5.4a shows the selected area, which is located in central Russia (60-65° northern latitude, 70-75° eastern longitude; cell 1830) and dominated by permanent wetlands. Its climate is cold without a dry season.

The winters last longer than the summers, but shorter than the winters in the region mentioned in Section 5.2.1, which is located at the same geographical latitude. This might be due to the different land cover types that dominate the regions and the fact that the region mentioned in Section 5.2.1 is situated further to the interior of the continent.

5.2.3 SSF determination in cold continental climate

The selected region is situated in south-west Russia at the border to Ukraine (50-55° northern latitude, 35-40° eastern longitude; cell 1576), so, 10° south of the previously analyzed regions. It is located in cold climate with warm summers but no dry season; the land cover is dominated by croplands (Figure 5.5a).

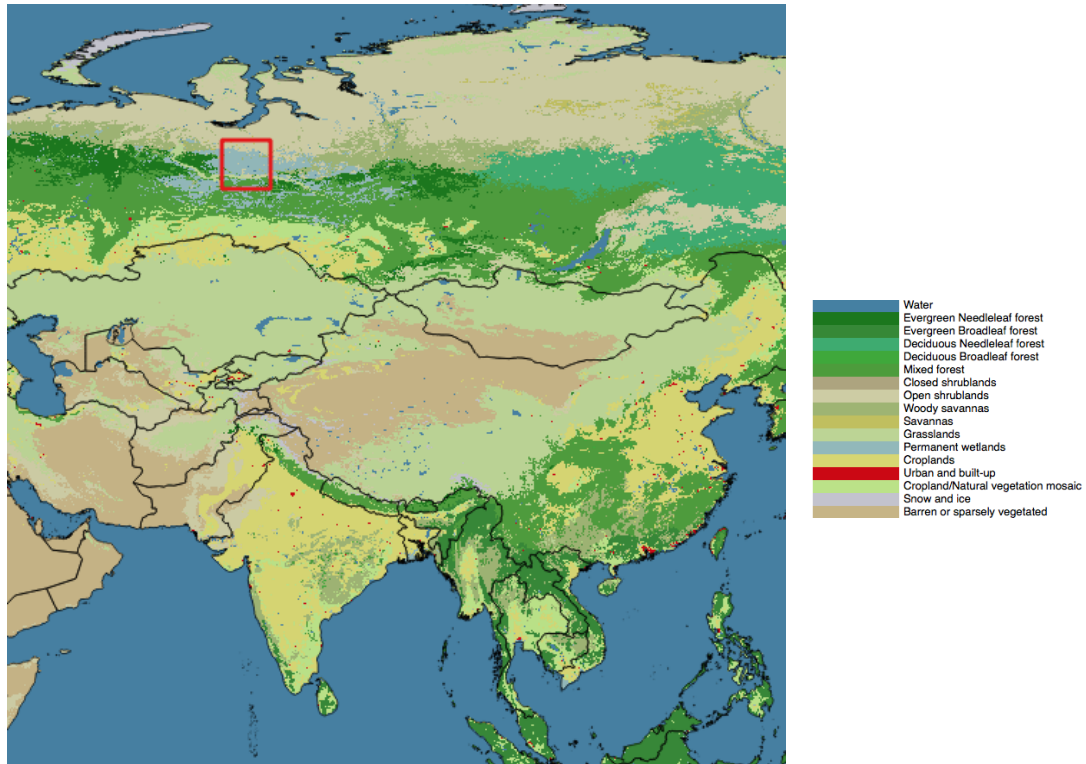
The frozen period usually starts in November and lasts until March/April of the following year. It is interrupted by short-term melting periods at some grid points. Both Figure 5.5b and Figure 5.5c show a very similar pattern.

5.2.4 SSF determination in polar Tundra climate

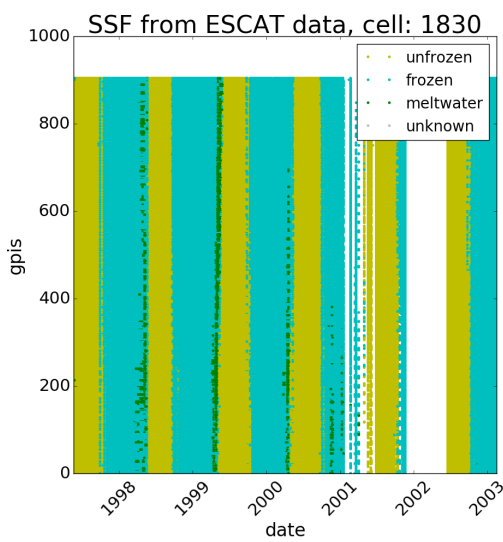
Figure 5.6a shows an area in northern Canada (70-75° northern latitude, 110-115° western longitude; cell 500). The land cover in this area mainly consists of grasslands, only some smaller areas show barren or sparsely vegetated land. According to the Koeppen-Geiger climate map, the region is dominated by polar Tundra climate.

The surface is frozen for most time of the year, only during summer there is an unfrozen period of about two-three months. A few grid points show only frozen conditions throughout the year. Before every unfrozen period, most of the grid points show a melting period of about two weeks. In some parts of the area, the frozen period is interrupted by short-term melting events.

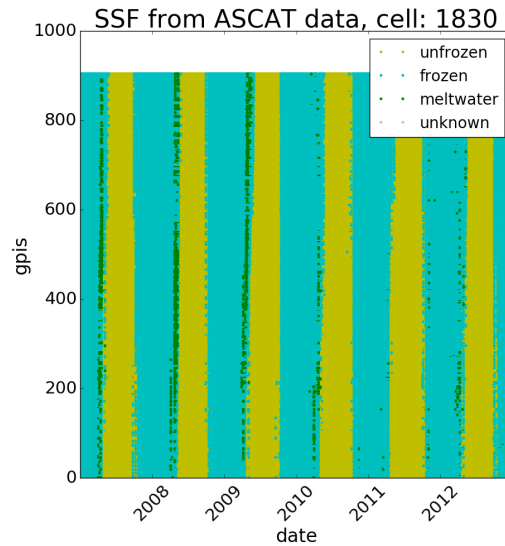
The Surfaces State Flags derived from ASCAT and ESCAT data show very similar patterns. In the ESCAT results (Figure 6.7a), the data gap due to the failure of the gyroscopes is visible from 2001 onwards.



(a) Location of cell 1830

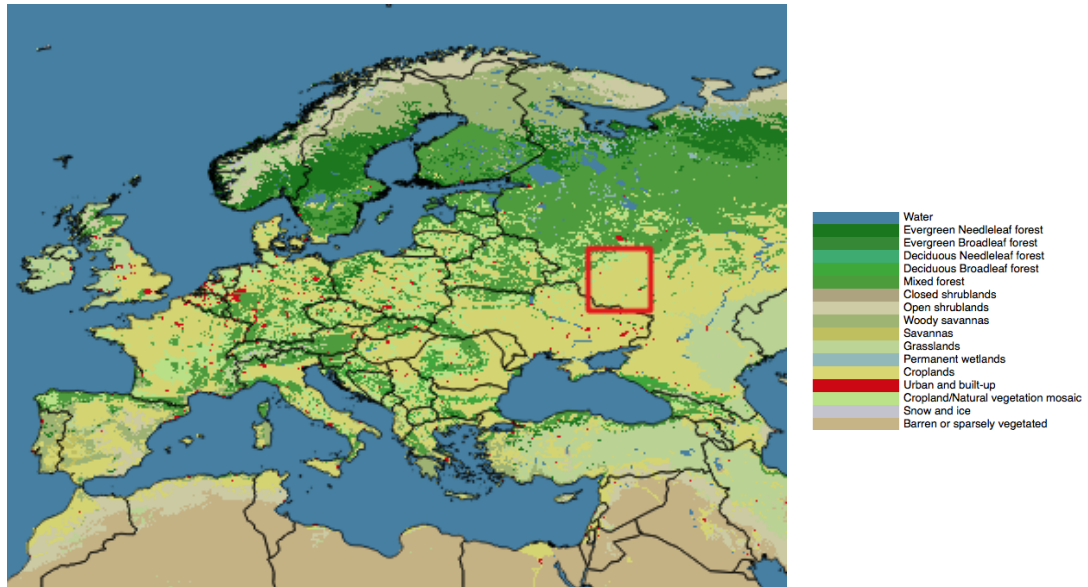


(b) SSF from ESCAT data

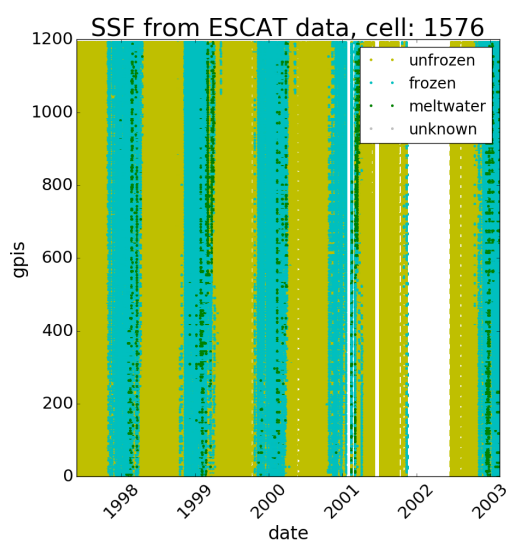


(c) SSF from ASCAT data

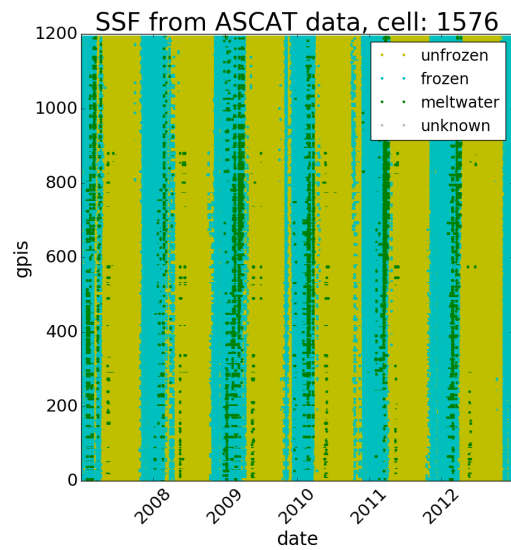
Figure 5.4: SSF time series plot for cell 1830, determined from ESCAT (b) and ASCAT (c) backscatter values. The cell is dominated by permanent wetlands and located in cold climate.



(a) Location of cell 1576

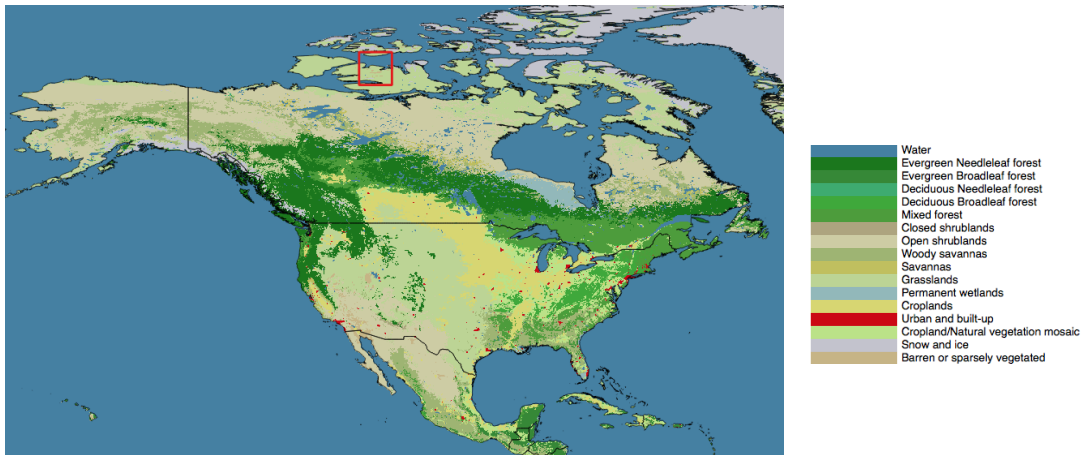


(b) SSF from ESCAT data

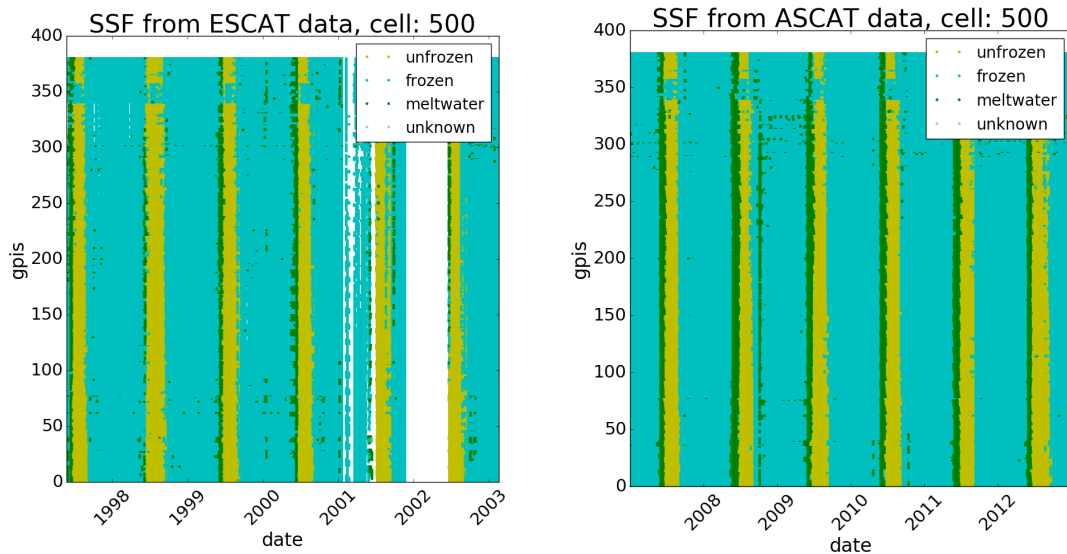


(c) SSF from ASCAT data

Figure 5.5: SSF time series plot for cell 1576, determined from ESCAT (b) and ASCAT (c) backscatter values. The cell is located in cold continental climate in a region dominated by croplands.



(a) Location of cell 500



(b) SSF from ESCAT data

(c) SSF from ASCAT data

Figure 5.6: SSF time series plot for cell 500, determined from ESCAT (b) and ASCAT (c) backscatter values. This cell is located in polar Tundra climate in an area dominated by grasslands.

5.2.5 SSF determination in heterogenous land cover (cold climate)

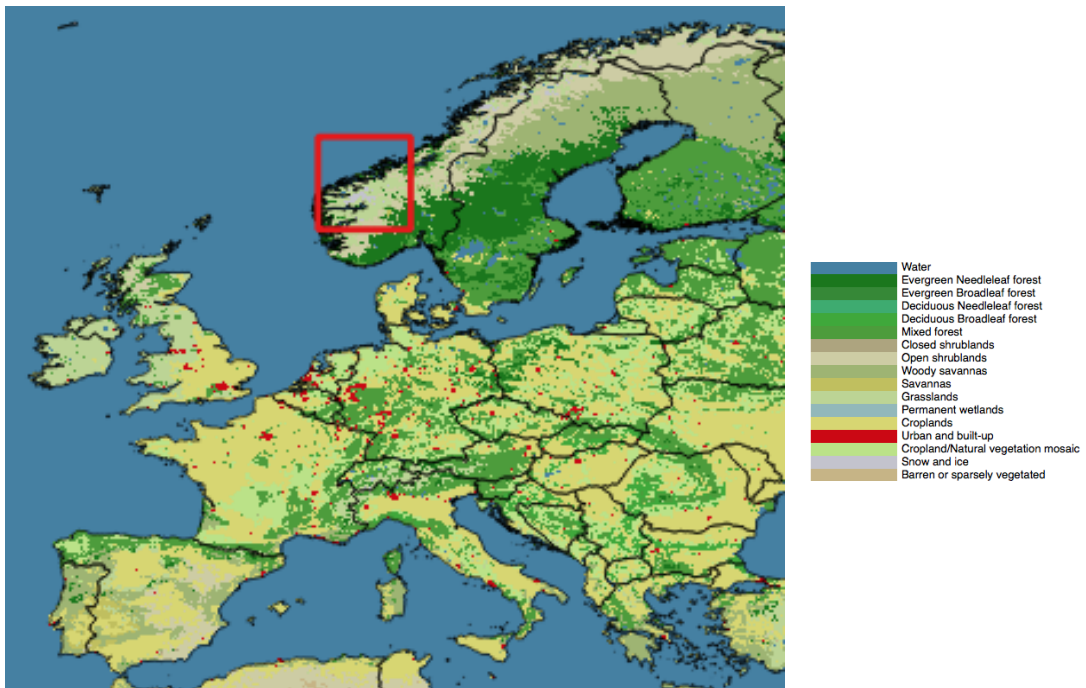
The selected area is located in the southern part of Norway (60-65° northern latitude, 5-10° eastern longitude, cell 1362; see Figure 5.7a). The region is dominated by cold climate, parts of it are classified as polar Tundra climate areas. The land cover type is dominated by grasslands and snow and ice in the higher-elevated parts of the cell.

The frozen period lasts longer than the unfrozen period in this region. There are differences between certain grid points due to the rather heterogenous land cover – some grid points experience a longer unfrozen period than others, and at some grid points, the surface never freezes. As in the regions analyzed earlier, both images (ASCAT and ESCAT) show a similar pattern.

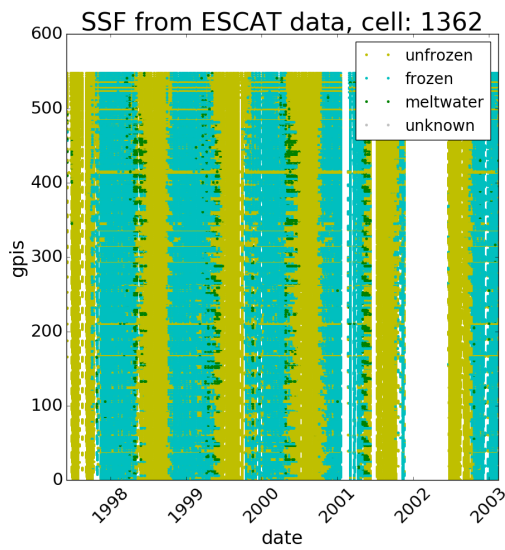
5.2.6 SSF determination in heterogenous land cover (temperate climate)

The selected region covers parts of northwestern Germany, the Netherlands and Belgium (50-55° northern latitude, 5-10° eastern longitude; cell 1360). It is located in temperate climate with warm summers and without a dry season. The region is covered by heterogenous land, including mixed forest, croplands, natural vegetation mosaics, and urban/built-up areas (Figure 5.8a).

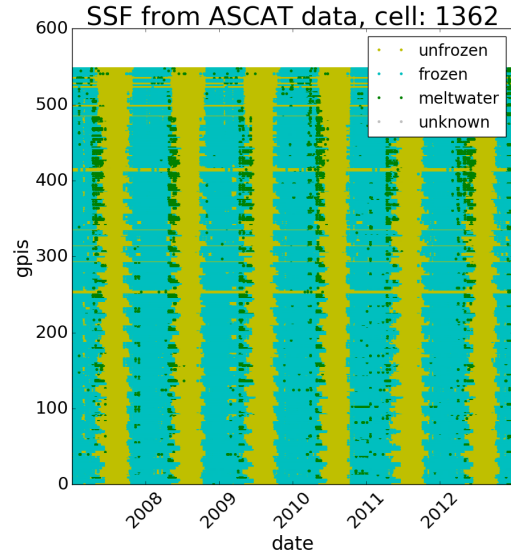
The heterogenous land cover reflects as vertical changes in Figure 5.8b and Figure 5.8c, that means that there are visible differences in the surface state between the different grid points. The frozen period lasts about two months in this region. This long duration is unexpected due to the influence of the Gulf Stream on the climate of the area surrounding the North Sea. However, the SSF algorithm is designed to flag untrusted soil moisture values, which are retrieved from backscatter values that might have been measured over frozen soils. The risk of flagging too many values is accepted in order to provide a reliable soil moisture product.



(a) Location of cell 1362

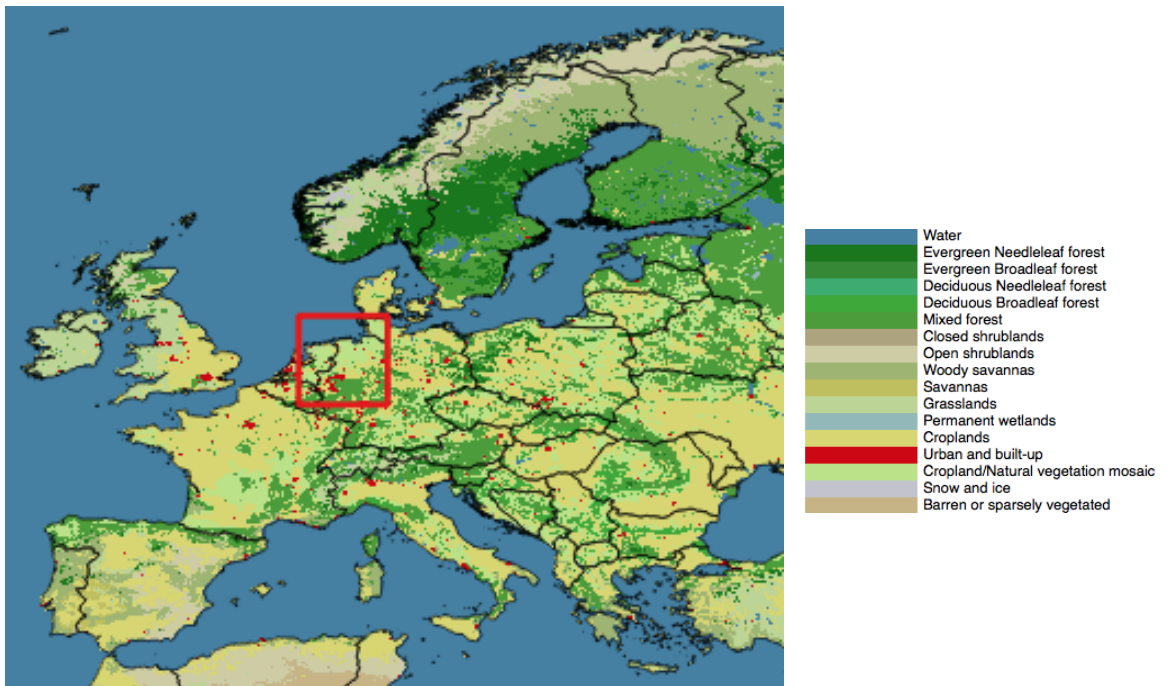


(b) SSF from ESCAT data

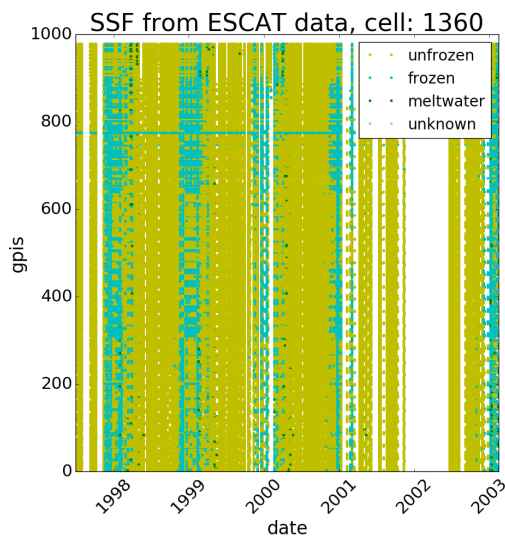


(c) SSF from ASCAT data

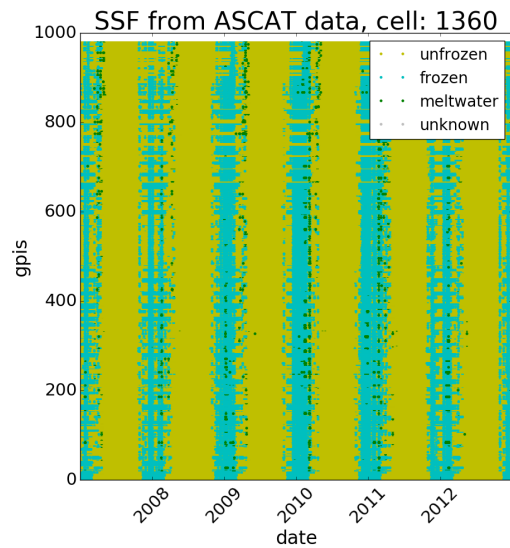
Figure 5.7: SSF time series plot for cell 1362, determined from ESCAT (b) and ASCAT (c) backscatter values. The cell is located in cold climate and covered by heterogenous land types.



(a) Location of cell 1360



(b) SSF from ESCAT data



(c) SSF from ASCAT data

Figure 5.8: SSF time series plot for cell 1360, determined from ESCAT (b) and ASCAT (c) backscatter values. This cell is located in temperate climate, in an area with very heterogenous land cover.

Chapter 6

Validation of the Surface State Flag

In the previous section, the results of the SSF determination from ESCAT backscatter data have been compared to SSF time series determined from ASCAT backscatter data. In order to get a better understanding of the performance, a validation is done against different types of datasets in the following section. The validation datasets include temperature data from in-situ station networks, Freeze/Thaw state time series from the National Snow and Ice Data Center (NSIDC), and model temperature data from the Global Land Data Assimilation System (GLDAS).

6.1 Validation Against In-Situ Temperature Data

The International Soil Moisture Network (ISMN) collects soil moisture and various additional geophysical variables from global networks and makes the database available for geoscientific users. In this work, temperature data from in-situ stations from the SNOTEL and BNZ-LTER networks in the USA were used to validate the surface state flag.

After the first assessment of the ESCAT SSF results, the dataset was reprocessed, leading to an SSF time series availability until 2011. During the validation with ISMN data, these prolonged time series were made use of.

Figure 6.1 shows the validation of surface state time series determined from ESCAT backscatter data against temperature data from the BNZ-LTER station UP3A. This station is located in central Alaska, at 64.8° latitude and -148.3° longitude. On the large scale, the surface state and the temperature time series show very good agreement. However, the temperature dataset alone is not enough to validate the SSF performance during time periods with complex surface state changes (spring snowmelt, freezing in fall). An example is the classified "snowmelt" in April 2002, which is not documented by the temperature dataset.

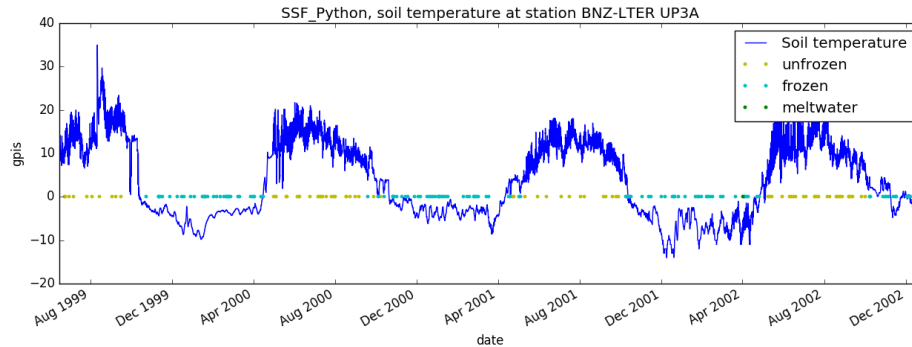


Figure 6.1: Validation of SSF from ESCAT backscatter data against temperature data from the BNZ-LTER station UP_{3A}.

The SNOTEL network covers the western states of the USA, including Alaska. At most of the stations, meteorological data such as air temperature, precipitation and snow depth is measured in addition to the soil moisture. Figure 6.2-Figure 6.6 show the validation of the ESCAT surface state flag with four selected SNOTEL stations and one BNZ-LTER station, namely Coldfoot, Harts Pass, Happy Jack, Laprele Creek and CRREL-Met. An overview of the stations is given in Table 6.1. In this table, the Koeppen-Geiger climate and MODIS land cover classes are again used.

The station Coldfoot in Alaska (Figure 6.2) shows generally very good correspondance between the SSF and the meteorological datasets. The station experiences a melting period of a few weeks in April/May 2006, depicted by green SSF values during that time. By the end of the melting period, the snow has gone. The SSF and the snow cover data show this relationship really well.

At the station Harts Pass (Washington State, Figure 6.3), temperatures rise above 0°C in April/May. Despite the duration of this season of several weeks, no snowmelt or unfrozen soil is classified by the SSF. This might be due to the deep snow cover that is still present until the early summer months (approximately mid-June), which prevents the microwave signal from reaching the surface.

Figure 6.4 shows the surface state flag and meteorological data from the station Happy Jack (Arizona). This station is situated in temperate climate and experiences dry and hot summers. The land cover is dominated by evergreen needleleaf forests and woody savannas. A frozen period of about 2-4 months is depicted by the SSF, although the soil temperature almost never gets below 0°C. The air temperature curve indicates negative temperatures during the frozen period, however, the temperatures are above 0°C most of the time. No melting period is indicated by the SSF.

Station	Location	Climate	Land Cover
Coldfoot (Alaska)	67.25 N 150.18 W	Cold, no dry season, cold summer	Open shrublands
Harts Pass (Washington)	48.72 N 120.66 W	Cold, dry and cold summer	Evergreen needleleaf forest
Happy Jack (Arizona)	34.75 N 111.41 W	Temperate, dry and hot summer	Evergreen needleleaf forest, woody savannas
Laprele Creek (Wyoming)	42.44 N 105.86 W	Arid Steppe, cold	Evergreen Needleleaf forest
CRREL-Met (Alaska)	65.15 N 147.49 W	Cold, no dry season, cold summer	Woody savannas

Table 6.1: Location, Koeppen-Geiger climate zone and MODIS land cover type of the selected SNOTEL and BNZ-LTER stations.

The station Laprele Creek (Wyoming, see Figure 6.5) is located in cold and arid Steppe climate. The land cover is dominated by evergreen needleleaf forests. In Figure 6.5, the SSF is displayed – unlike before – slightly below 0°C in order not to overlap with the soil temperature dataset. The frozen period indicated by the SSF time series shows good correspondence with the air temperature curve. As before, the soil temperature seems not to affect the surface state as much as the air temperature. The deep snow cover in the winter months might prevent the microwave signal from reaching the soil.

Figure 6.6 shows the BNZ-LTER station CRREL-Met in Alaska, situated in cold climate. The land cover is dominated by woody savannas. In addition to the air temperature dataset, precipitation and snow depth data are available for CRREL-Met. A short melting period is indicated by the SSF in spring and fall. In November/December 2007, the melting period lasts a few weeks and is also indicated by the temperature dataset.

In general, the meteorological data from all selected stations corresponds very well with the ESCAT surface state time series. At some stations, a more detailed analysis is necessary in order to explain all occurring effects, e.g. the frozen period at station Happy Jack, where the temperature datasets indicate an unfrozen surface state.

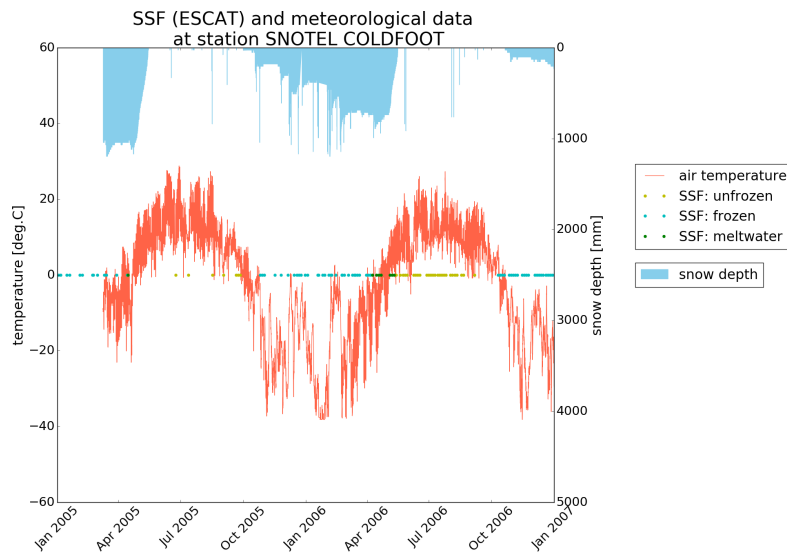


Figure 6.2: Validation of SSF from ESCAT backscatter data against meteorological data from the SNOTEL station Coldfoot. Coldfoot is located in cold climate without a dry season; the land cover in this area is dominated by open shrubland.

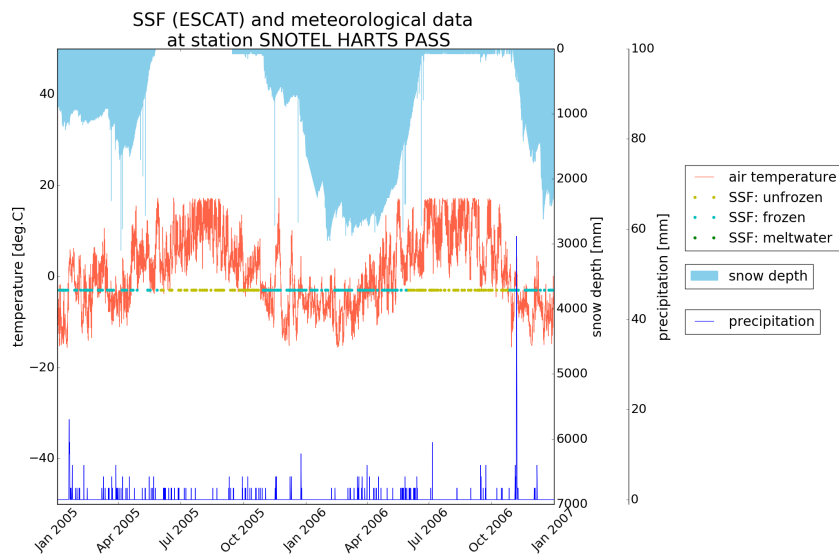


Figure 6.3: Validation of SSF from ESCAT backscatter data against meteorological data from the SNOTEL station Harts Pass. Harts Pass is situated in an area dominated by evergreen needleleaf forests, in cold climate with cold, dry summers.

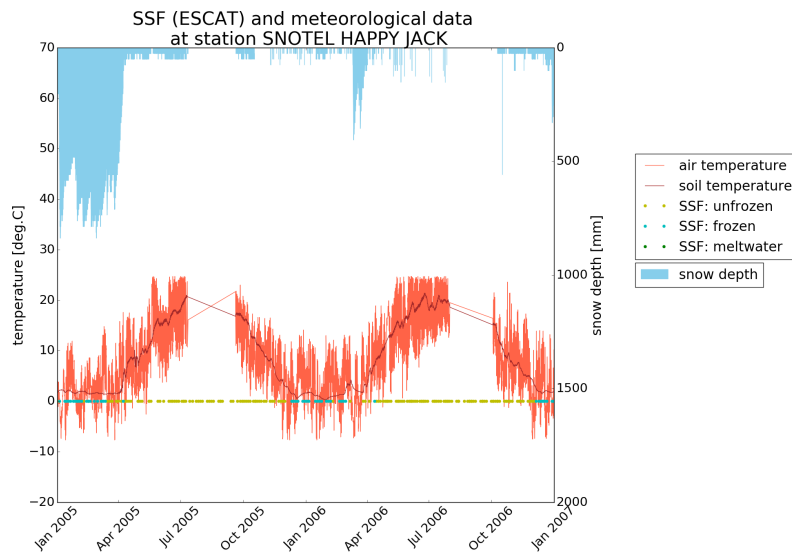


Figure 6.4: Validation of SSF from ESCAT backscatter data against meteorological data from the SNOTEL station Happy Jack. The station is situated in an area dominated by woody savannas and evergreen needleleaf forests, in temperate climate with dry, hot summers.

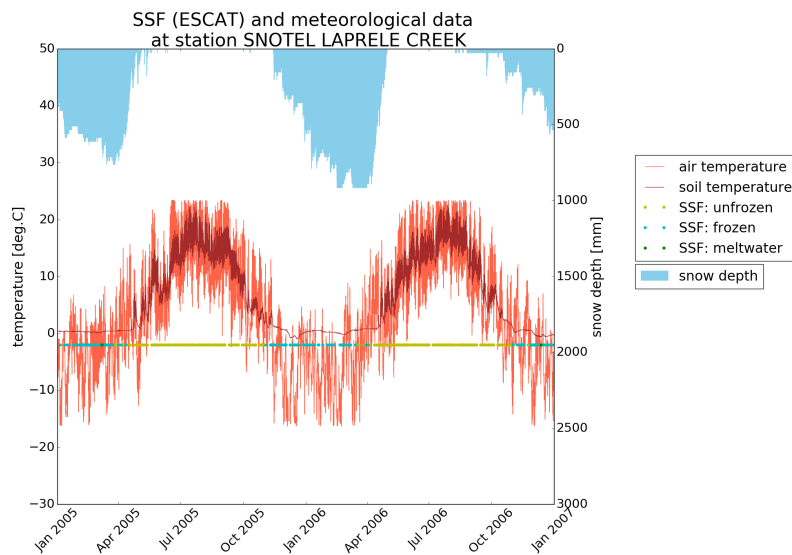


Figure 6.5: Validation of SSF from ESCAT backscatter data against meteorological data from the SNOTEL station Laprele Creek. Laprele Creek is situated in an area dominated by evergreen needleleaf forests, in arid, cold Steppe climate.

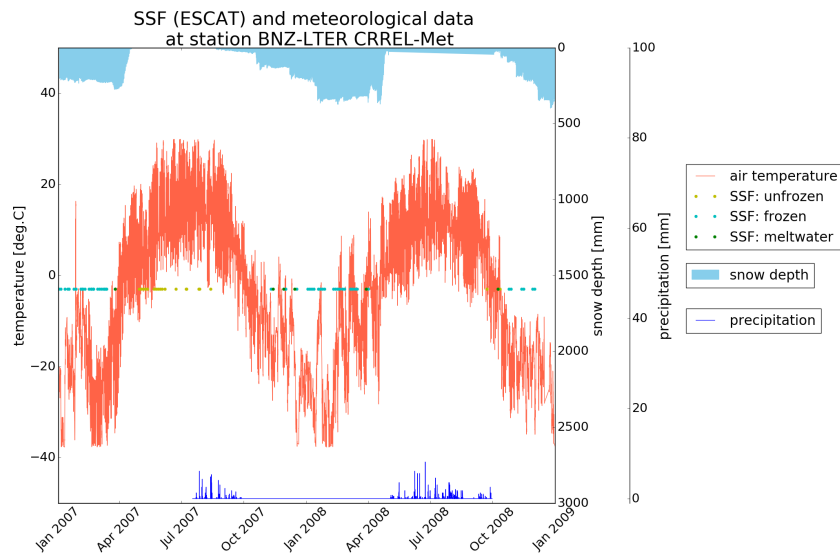


Figure 6.6: Validation of SSF from ESCAT backscatter data against meteorological data from the BNZ-LTER station CRREL-Met. This station is situated in an area dominated by woody savannas, in cold climate with cold summers.

6.2 Validation Against F/T State Data from the NSIDC

Passive microwave remote sensing data from SMMR and SSM/I as well as a numerical model are used to determine the near-surface (< 5 cm) soil freeze/thaw status on snow-free and snow-covered land, respectively. Daily values are available from October 1978 until June 2004 with a spatial resolution of 25 km x 25 km, covering land surfaces over the Arctic terrestrial drainage basin [Zhang and Armstrong, 2003 updated 2005].

In Figure 6.7, NSIDC freeze/thaw soil states are shown next to the SSF derived from ESCAT data for 1997-2003. The NSIDC dataset tends to estimate a shorter unfrozen period than the surface state flag. Also, many grid points are flagged by the NSIDC dataset due to their location close to the sea.

Figure 6.8 shows the SSF and NSIDC F/T state for a region in eastern Russia. Apart from the ESCAT data gap between 2001 and 2003 and the fact that the NSIDC does not classify snow-melt periods, the two images look almost identical. The NSIDC tends to classify slightly longer unfrozen periods than the SSF algorithm.

In Figure 6.7 and Figure 6.8, only grid points that are covered by both NSIDC and ESCAT are displayed.

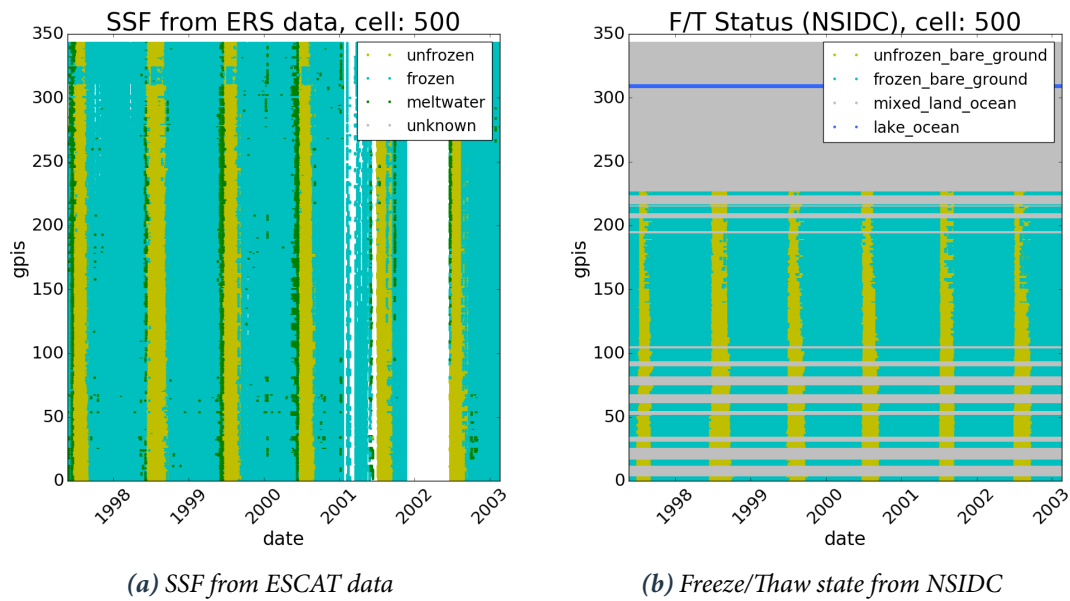


Figure 6.7: Validation of SSF against Freeze/Thaw state from the NSIDC for a region in polar Tundra climate (northern Canada; cell 500).

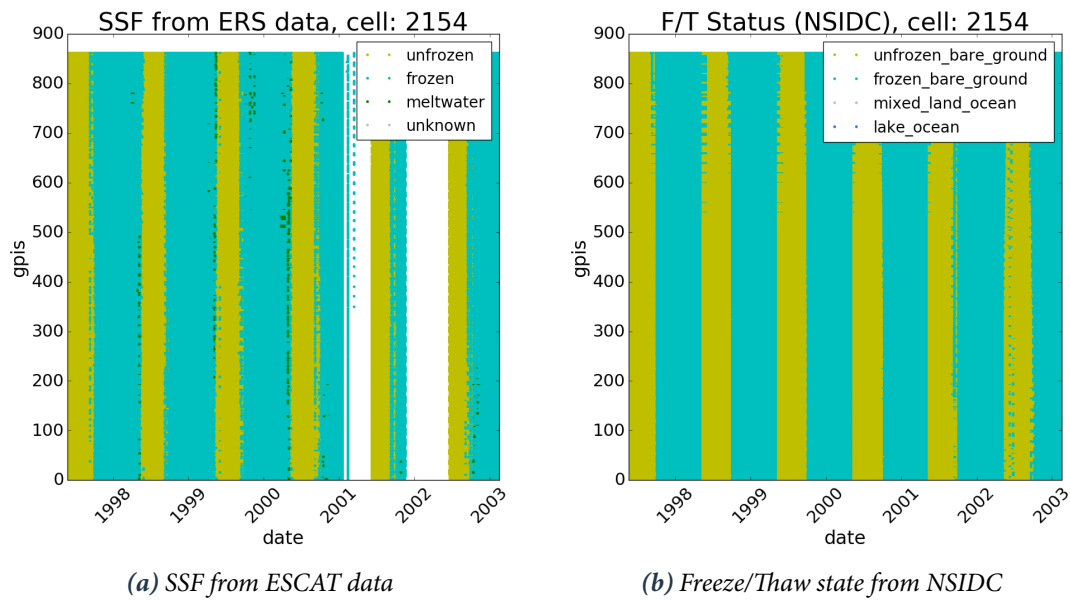


Figure 6.8: Validation of SSF against Freeze/Thaw state from the NSIDC for a region in cold climate covered with deciduous needleleaf forests (Russia; cell 2154).

6.3 Validation Against Temperature Data from GLDAS

For this validation, both surface and soil temperature (0.00-0.10 m) from the Global Land Data Assimilation System (GLDAS) are used. GLDAS has been developed to generate fields of land-surface states (e.g. temperature, soil moisture, or snow) using both satellite and ground-based data products. It is a joint development by scientists at the National Aeronautics and Space Administration (NASA) Goddard Space Flight Center and the National Oceanic and Atmospheric Administration (NOAA) National Centers for Environmental Prediction. The GLDAS temperature dataset is available from February 2000 until present with values provided every 3 hours on a 0.25° regular global grid [Rodell *et al.*, 2004].

In the validation process, surface state time series are compared to the corresponding temperatures of the GLDAS. If both the SSF and the GLDAS temperature classify a certain measurement as the same state (i.e. frozen state: SSF = 1, temperature < 0°C, unfrozen state: SSF = 0, temperature > 0°C), the classification of the SSF is considered correct. If the SSF and GLDAS temperature contradict each other (e.g. SSF: frozen, but temperature > 0°C), the classification is considered incorrect.

Additional to the four outcome options of frozen/frozen, frozen/unfrozen, unfrozen/frozen and unfrozen/unfrozen, the number of correctly classified observations – ignoring their values, so, the sum of correctly classified frozen and unfrozen observations – is calculated.

SSF	GLDAS	Color
Frozen	Frozen	Blue
Frozen	Unfrozen	Green
Unfrozen	Unfrozen	Cyan
Unfrozen	Frozen	Red

Table 6.2: Possible validation outcomes and the colors used in Figure 6.9 and Figure 6.10

For the validation, soil temperature as well as surface temperature data were used. The ESCAT backscatter measurements represent the upper few centimeters of the soil, which would suggest using soil temperature. However, the upper soil layer reacts very quickly to changes in the air temperature – it's therefore interesting to compare if the surface temperature is maybe better suited for the SSF validation, or if the choice of the temperature dataset doesn't affect the validation results much.

Figure 6.9 and Figure 6.10 show the results of the validation. Table 6.2 shows an overview of the

possible validation results and how they are displayed in the figures. A fifth validation result is shown: the number of correctly classified observations, thus the sum of correctly classified frozen and unfrozen observations. These values are displayed in purple in the figures.

The x-axis shows all grid points of the selected $5^\circ \times 5^\circ$ region, the validation results are plotted on the y-axis. Periodic fluctuations in the curves are due to the sorting of the grid points from East to West and South to North (Northern Hemisphere, west of the Prime Meridian) and from West to East and South to North (Northern Hemisphere, east of the Prime Meridian). The curves show the percentage of classified observations for the following classes: frozen/frozen (blue), unfrozen/unfrozen (cyan), frozen/unfrozen (green), unfrozen/frozen (red), and correctly classified observations (frozen/frozen and unfrozen/unfrozen; purple). The higher the values of the purple curve, the better the validation.

Cell 500, a region located in polar Tundra climate covered mostly with grasslands, shows very good validation results, with the percentage of correctly classified observations above 90 (see Figure 6.9). There are a few grid points that show sudden drops in the purple curve; those are most likely grid points situated close to the Sea, which makes the SSF determination difficult.

Figure 6.10 shows the validation results of the region covering parts of northern Germany, the Netherlands and Belgium, situated in temperate climate, influenced by the Gulf Stream and consisting of multiple different land cover types. This region faces freezing very rarely, causing the blue curve (frozen/frozen classification) to be very low. The cyan (unfrozen/unfrozen) and purple (correctly classified observations) curves are lower than in Figure 6.9, but still above 70%.

In both images, there is no visible difference between the two used temperature datasets (surface and soil).

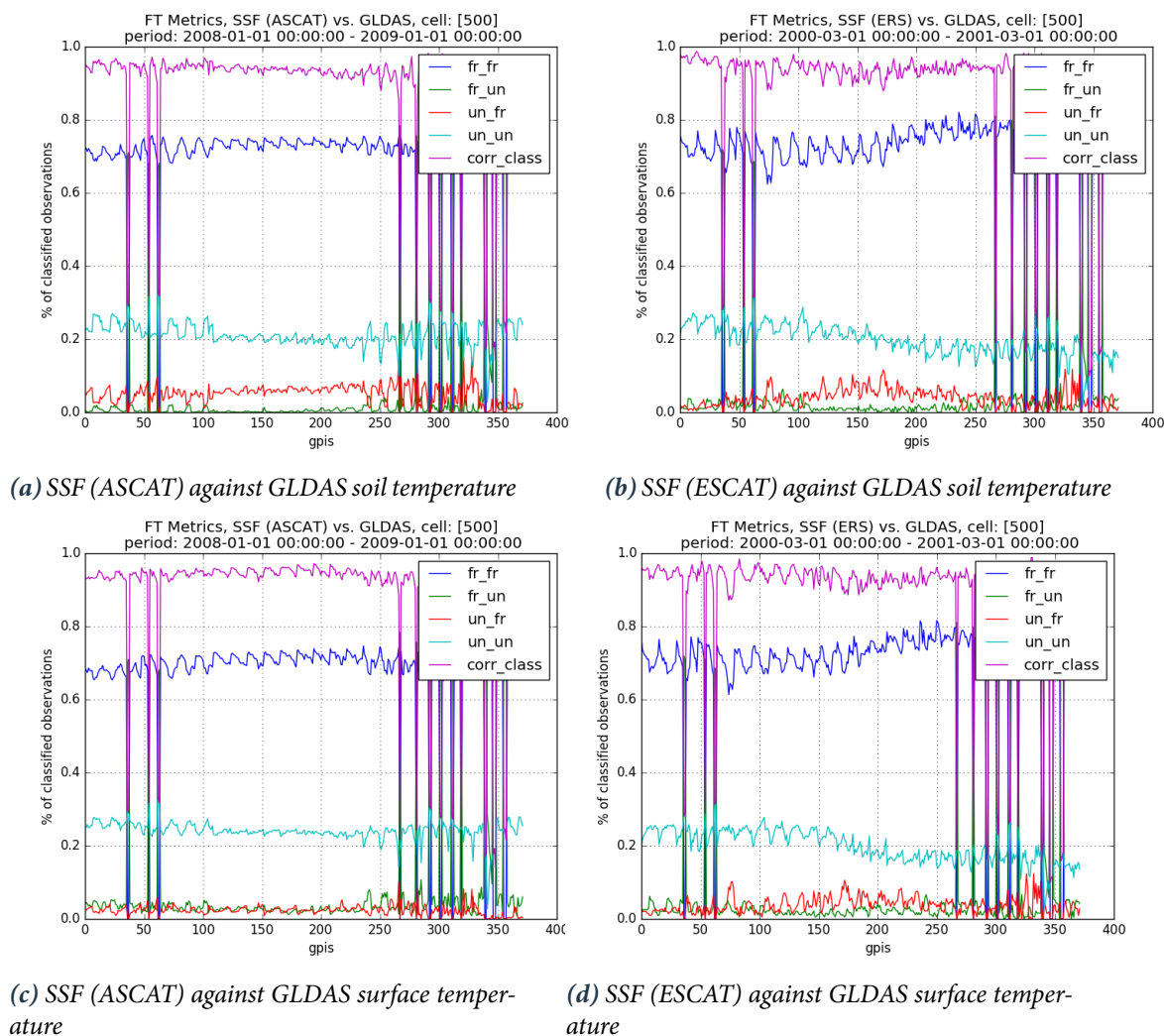


Figure 6.9: Validation of SSF against soil and surface temperature from the GLDAS for a region in polar Tundra climate (northern Canada; cell 500).

The curves show the percentage of classified observations for the following classes: frozen/frozen (blue), unfrozen/unfrozen (cyan), frozen/unfrozen (green), unfrozen/frozen (red), and correctly classified observations (frozen/frozen and unfrozen/unfrozen; purple).

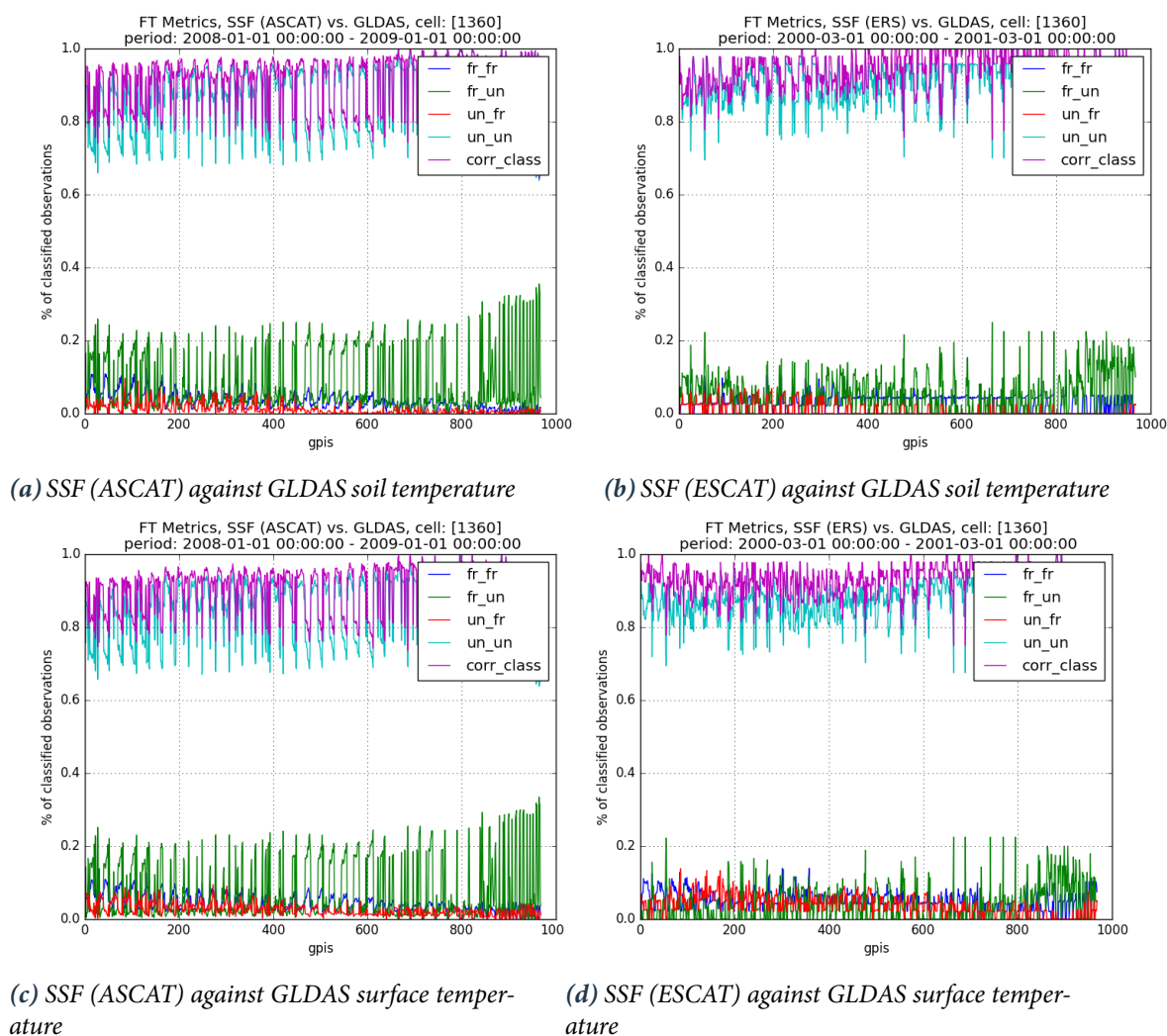


Figure 6.10: Validation of SSF against soil and surface temperature from the GLDAS for a region in polar Tundra climate (northern Canada; cell 1360).

The curves show the percentage of classified observations for the following classes: frozen/frozen (blue), unfrozen/unfrozen (cyan), frozen/unfrozen (green), unfrozen/frozen (red), and correctly classified observations (frozen/frozen and unfrozen/unfrozen; purple).

6.3.1 Validation of Seasonal Results

The validation of the SSF against GLDAS temperature data, which has been done globally for continuous date ranges, has been split into seasonal validations in order to see if there are differences in the SSF performance between different seasons. The following seasons were validated:

- TZ1: transition day between winter and summer ± 30 days
- TZ2: transition day between summer and winter ± 30 days
- summer: time between TZ2 and TZ1
- winter: time between TZ1 and TZ2

Since the transition days are different for every grid point, the four seasons have to be defined for each grid point respectively. In addition to the four seasons, the results of a whole year are displayed.

SSF	GLDAS	Color
Frozen	Frozen	Blue
Frozen	Unfrozen	Red
Unfrozen	Unfrozen	Yellow
Unfrozen	Frozen	Green

Table 6.3: Possible validation outcomes and the colors used in Figure 6.14-Figure 6.11

Figure 6.11-Figure 6.16 show the results for the six regions described in Section 5.2. Table 6.3 lists the colors used in these figures. The SSF determination works best in winter and summer, when there is usually no variation in the surface states over a longer time period. In the transition zones, state changes can happen frequently, predominantly influenced by the illumination of the sun and the temperature changes between day and night. However, as shown by the figures, the percentage of incorrectly classified observations never rises above 30%; in most regions, there are less than 20% incorrect classifications in the transition zones.

Generally, the regions that are located at higher latitudes show good classification results in all seasons. At lower latitudes, there are incorrect classifications not only in the transition zones but also in winter. In cell 1362, which is located in Norway and influenced by the Gulf Stream, the soil is not permanently frozen during winter. Thawing and refreezing periods alternate depending on the weather situation.

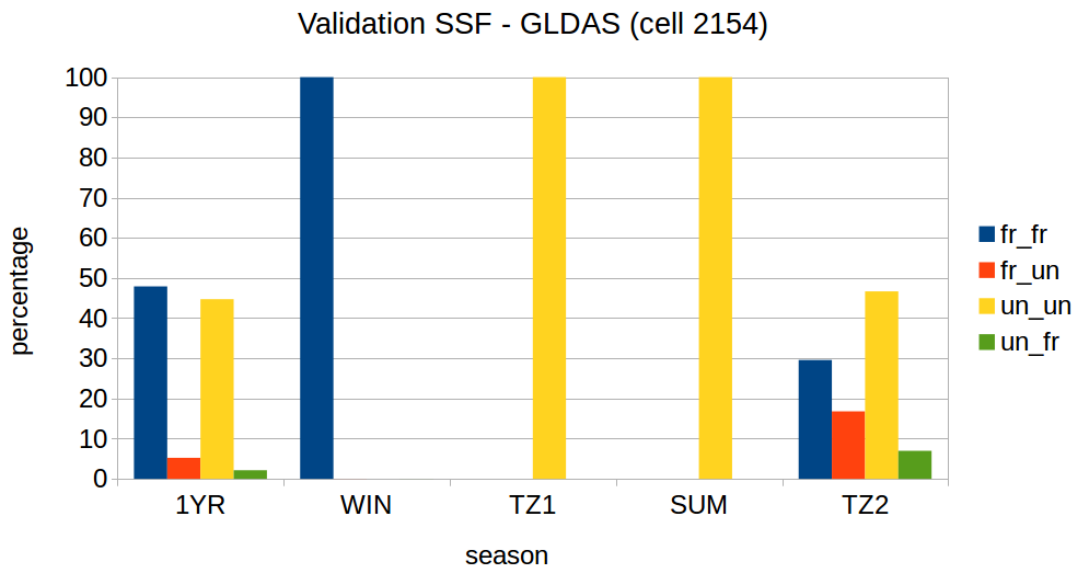


Figure 6.11: Results of the validation of ESCAT SSF and GLDAS, divided into seasons. Cell 2154 is located in Russia, in cold climate. The area is dominated by deciduous needleleaf forest.

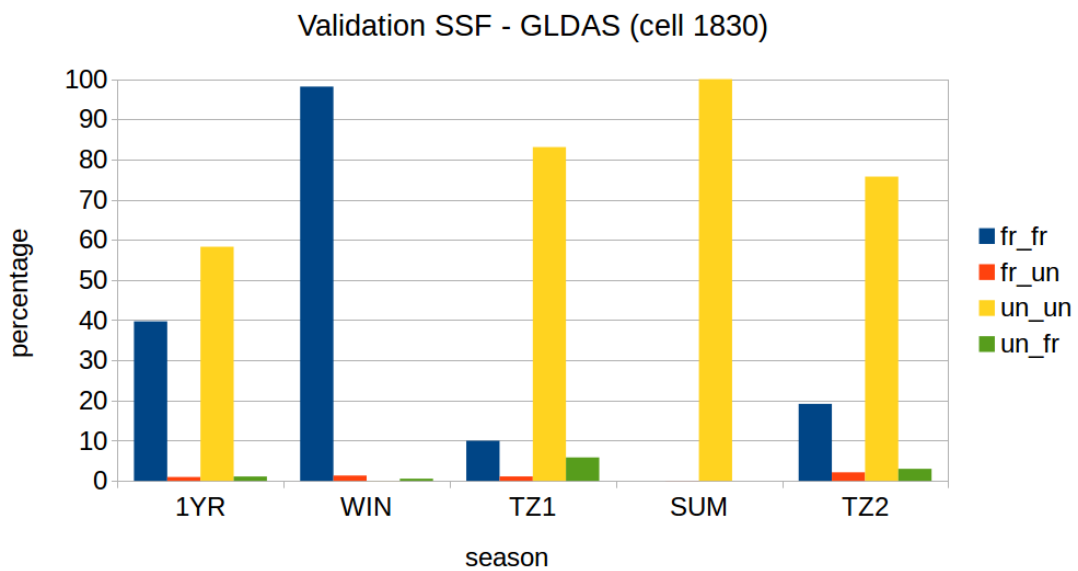


Figure 6.12: Results of the validation of ESCAT SSF and GLDAS, divided into seasons. Cell 1830 is situated in Russia in an area in cold climate, covered with permanent wetlands.

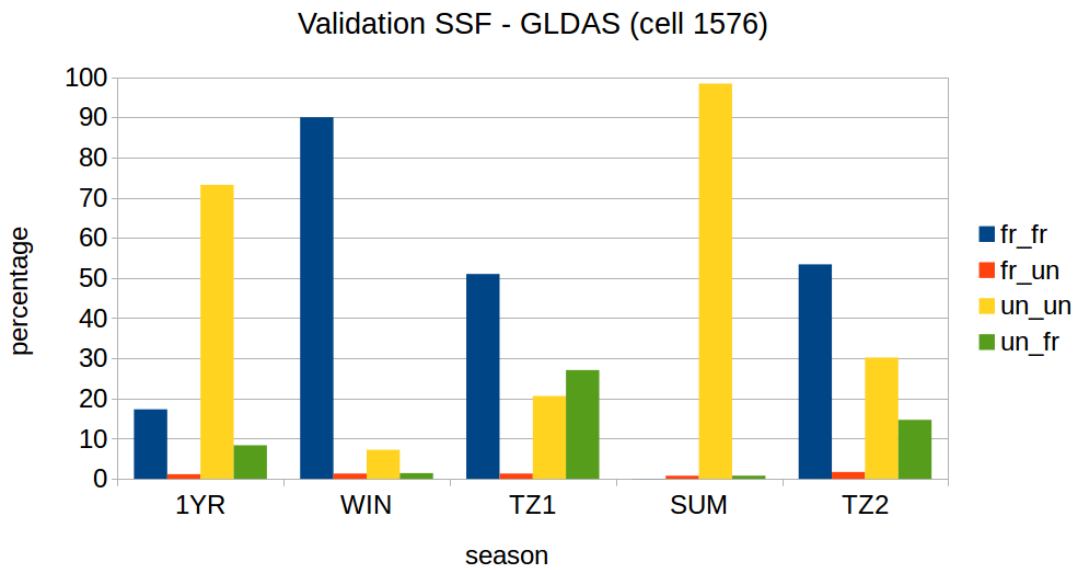


Figure 6.13: Results of the validation of ESCAT SSF and GLDAS, divided into seasons. Cell 1576 is located in south-west Russia at the boarder to Ukraine. The climate is continental. The predominant land cover type are croplands.

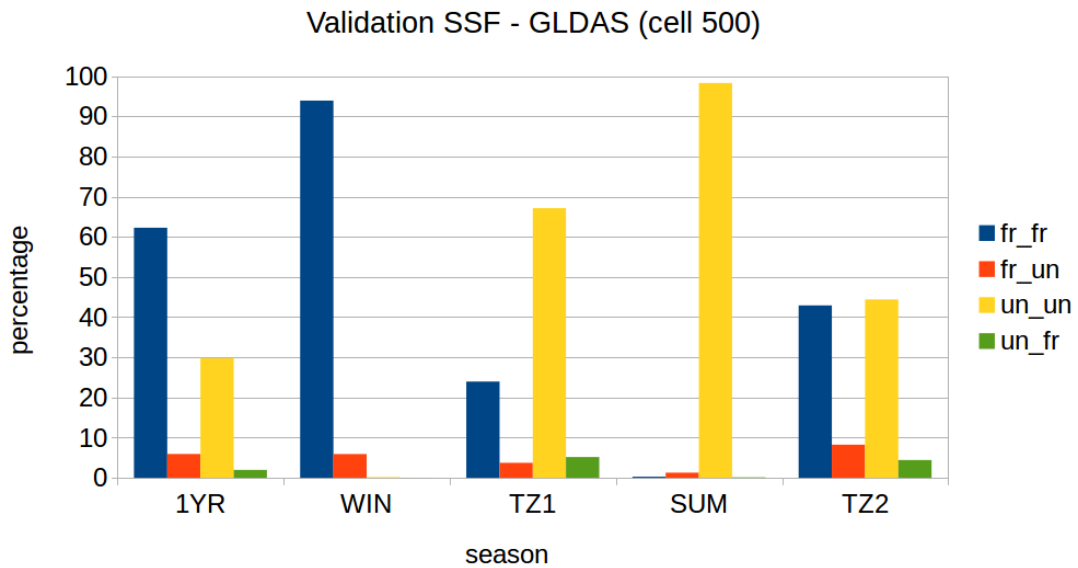


Figure 6.14: Results of the validation of ESCAT SSF and GLDAS, divided into seasons. Cell 500 is situated in northern Canada, in polar Tundra climate. The region is covered by grasslands.

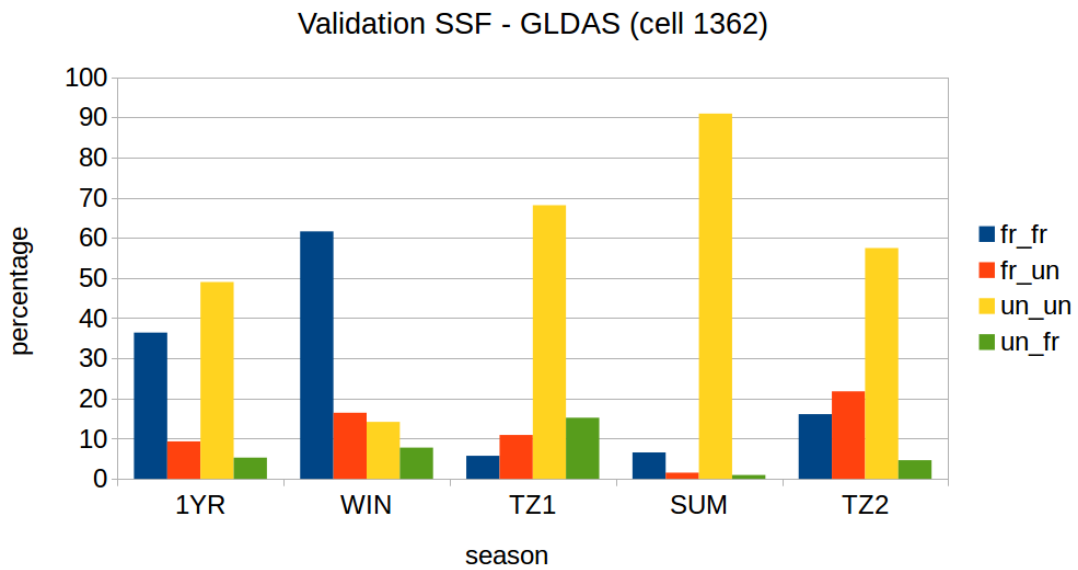


Figure 6.15: Results of the validation of ESCAT SSF and GLDAS, divided into seasons. Cell 1362 is located in Norway. The climate is cold and the land cover is heterogenous, including grasslands and, in some parts, snow and ice.

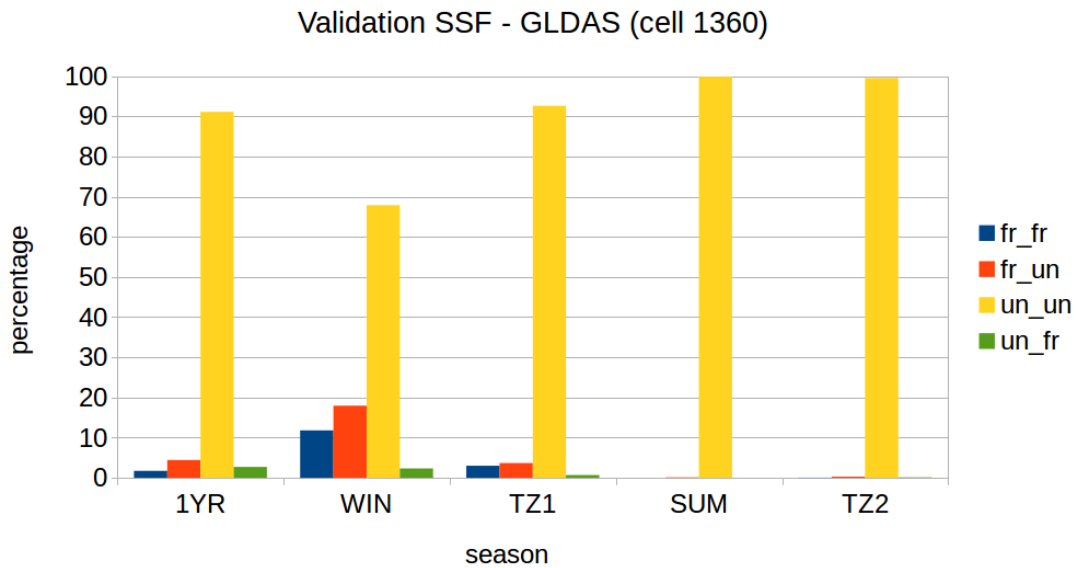


Figure 6.16: Results of the validation of ESCAT SSF and GLDAS, divided into seasons. Cell 1360 is situated in Europe, in temperate climate influenced by the Gulf Stream. The land cover in this region is heterogenous; it includes mixed forests, croplands, and urban areas.

Chapter 7

Conclusion

The Remote Sensing research group at TU Wien has developed methods to retrieve global soil moisture and freeze/thaw states of the Earth's surface from backscatter measurements obtained from active microwave remote sensing missions. The algorithm for the retrieval of the surface state was originally developed for ASCAT data, covering the period from 2007 to 2013. Since geoscientific studies require data from different periods, it's desirable to have long time series available.

The goal of this thesis was to investigate if the ASCAT surface state algorithm can also be applied on ESCAT data in order to obtain prolonged freeze/thaw time series. Due to technical problems of the gyroscopes and the tape recorder on-board ERS-2, the available amount of data is limited from 2001 on. Since the algorithm requires a certain amount of observations under different conditions in order to derive a surface state, the data availability was the largest factor of uncertainty when starting the work on the algorithm adaptation.

First of all, the SSF algorithm was started with ESCAT data without any modifications of the implementation of the algorithm. The result were incorrect freeze/thaw parameters and consequently incorrect surface state flags. After some modifications concerning mainly the handling and formatting of the input data, the algorithm was started again, producing satisfying outcomes.

Different climate and land cover regions were selected to compare the ESCAT surface state flags with those retrieved from ASCAT backscatter data. The overall outcome shows very satisfying results, contradicting the expectation that the low data availability might prevent the successful SSF determination from ESCAT data.

Furthermore, the ESCAT surface state flags were validated against soil and surface temperature data from the GLDAS and in-situ networks, as well as against arctic freeze/thaw soil state from the NSIDC. All validations show very good coherence between the datasets.

The division of the validation into different periods, namely summer, winter, and the two transition periods between summer and winter and winter and summer, respectively, shows that the SSF determination works best in summer and winter when the freeze/thaw conditions are not as complex as in spring and fall, when the Earth's surface is exposed to multiple thawing and refreezing events in short time intervals. However, the performance of the algorithm is still sufficiently high in the transition periods.

The transition periods are defined as the period ± 30 days around the transition day. In some regions, especially at lower latitudes or close to the sea, this definition might not be suitable. As shown for example in Figure 5.8, winter is not everywhere a season of permanent frozen conditions. Especially in this region, a quite large number of unfrozen states is classified during winter, which suggests re-defining the transition periods. Considering this in the algorithm might deliver improved results for the surface state flag.

Processing flags calculated during the SSF determination process confirm the good performance of the algorithm for both ASCAT and ESCAT backscatter data, although there are some areas where no ESCAT SSF can be determined due to the lack of backscatter measurements in these regions.

Building on the successful adaptation of the SSF algorithm for ESCAT data, the research on the algorithm shall be further continued. An assessment of the reliability of the computed SSF values could be valuable for different applications, by providing a confidence flag for each surface state flag. SSF values in summer and winter will be given higher reliability values than SSF values in the transition periods.

The SSF algorithm is based on ERA-Interim model temperature data. Since a model can never fully represent the true natural conditions, it would be very interesting to replace the model data with suitable land surface temperature observations, which might be available in the near future.

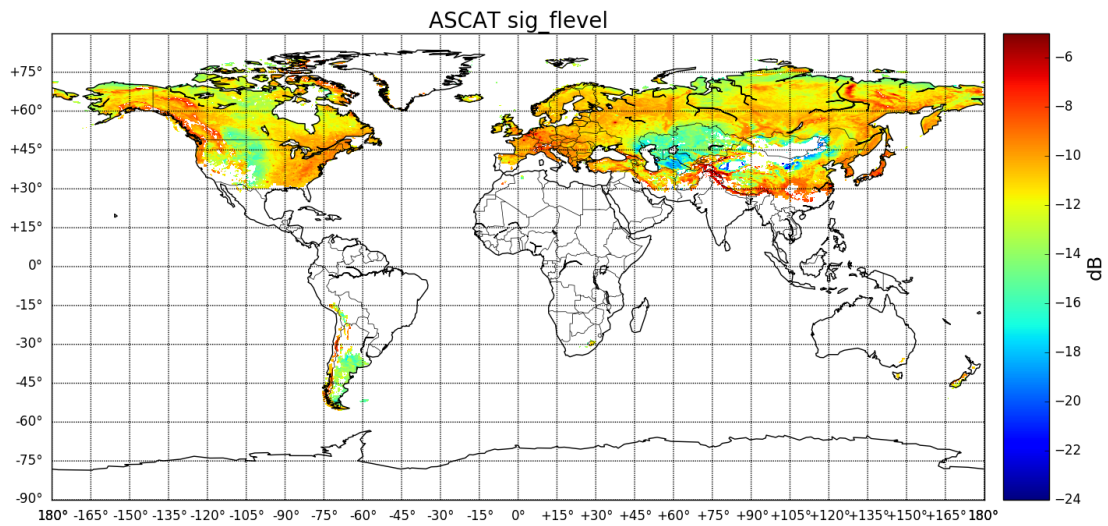
Thanks to this successful adaptation, the surface state time series can be extended to the end of the twentieth century. Since the freeze/thaw states of the Earth's surface are becoming more and more important for the understanding of our environment and the counteraction against climate change, this time series extension provides very important data for numerous research areas.

Appendix A

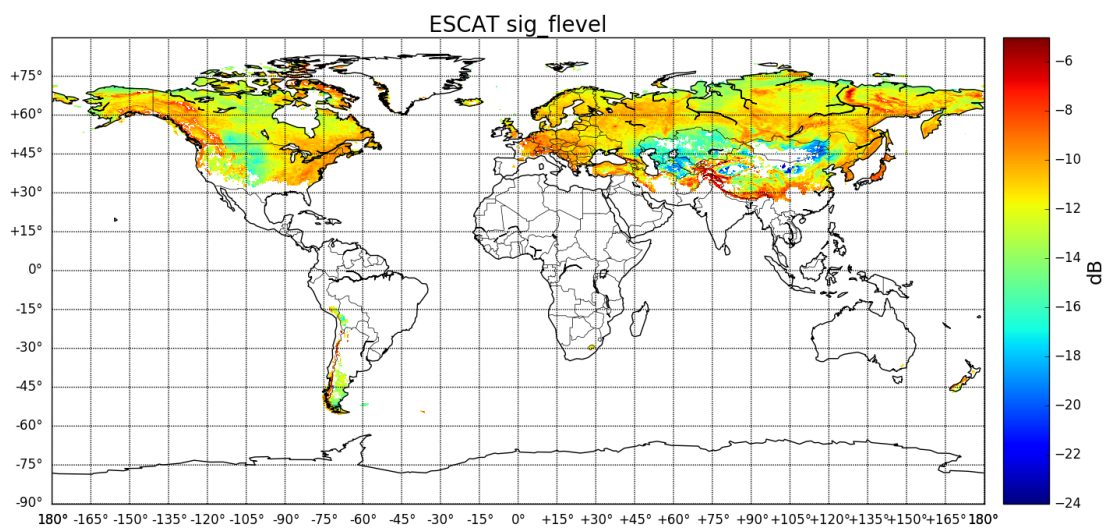
Additional Figures

A.1 Freeze/Thaw Parameters

Figure [A.1](#)-Figure [A.5](#) show images complementing Section [4.2](#).

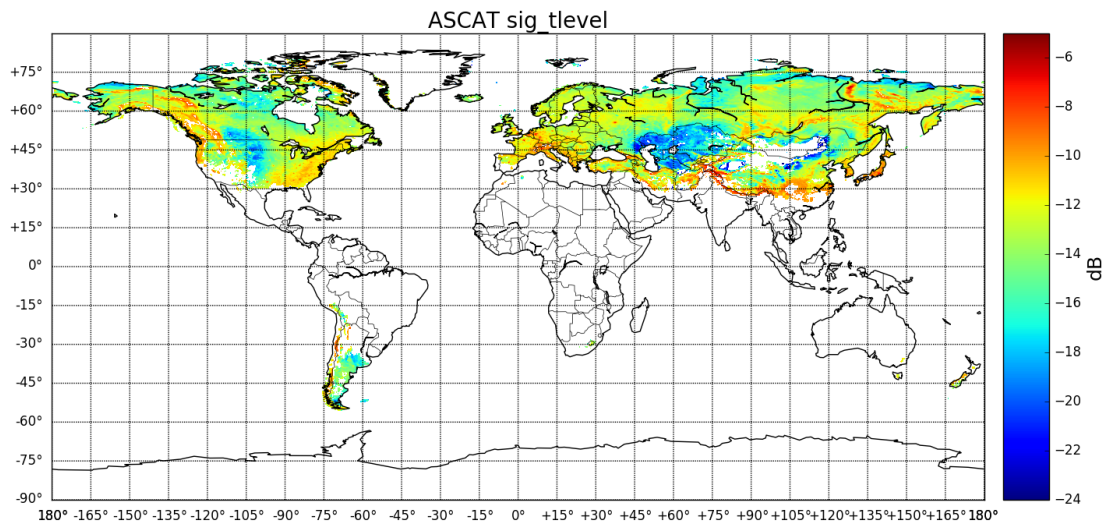


(a) ASCAT —Freeze/thaw threshold

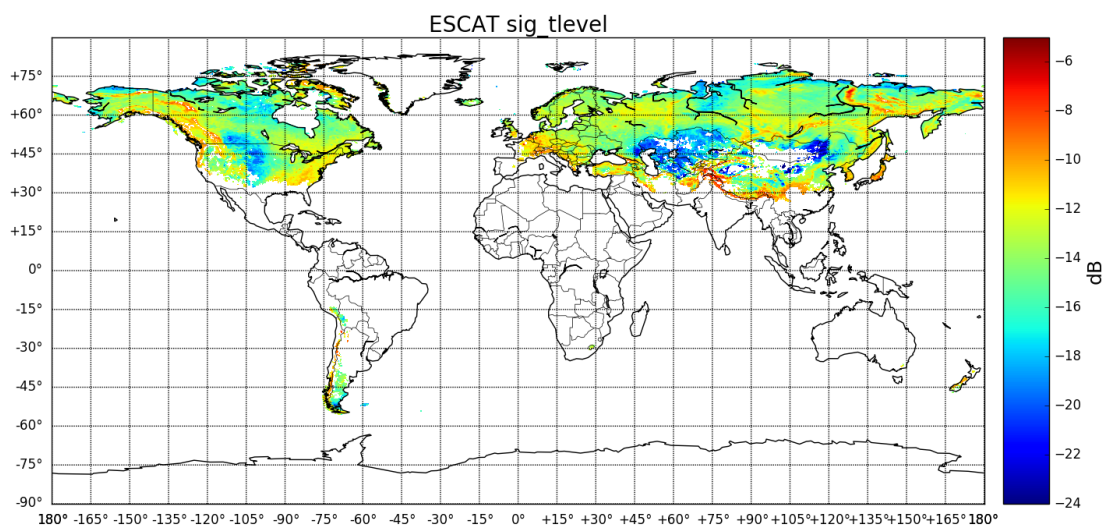


(b) ESCAT —Freeze/thaw threshold

Figure A.1: Freeze/thaw threshold derived from ASCAT and ESCAT backscatter data.

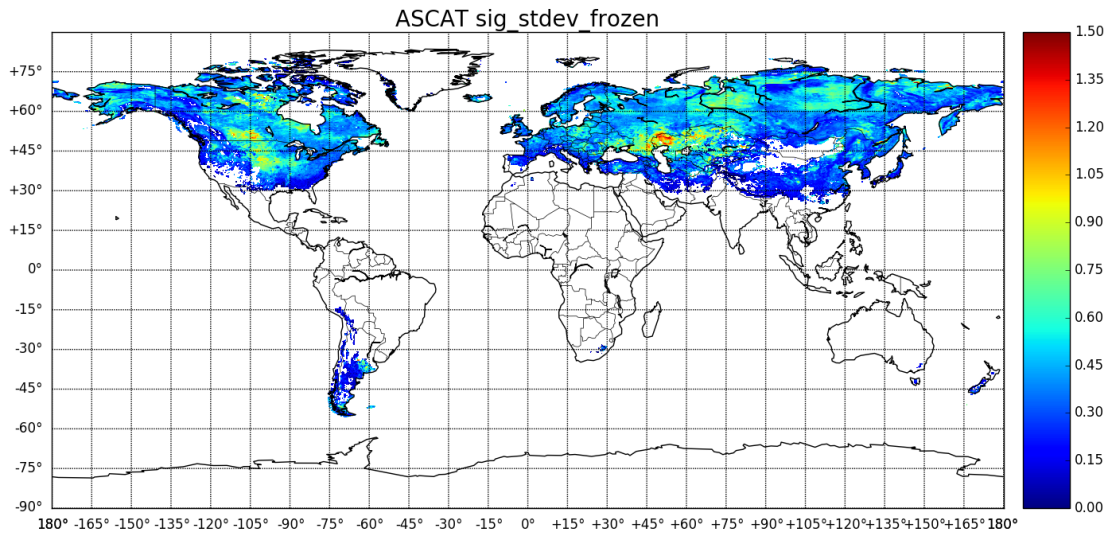


(a) ASCAT — Snowmelt/water level

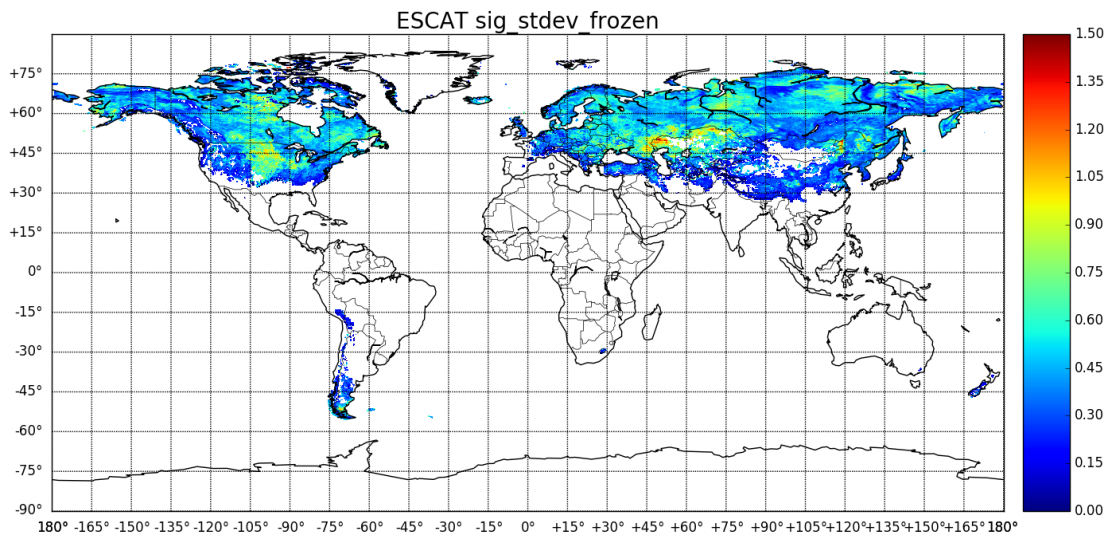


(b) ESCAT — Snowmelt/water level

Figure A.2: Snowmelt/water level derived from ASCAT and ESCAT backscatter data.

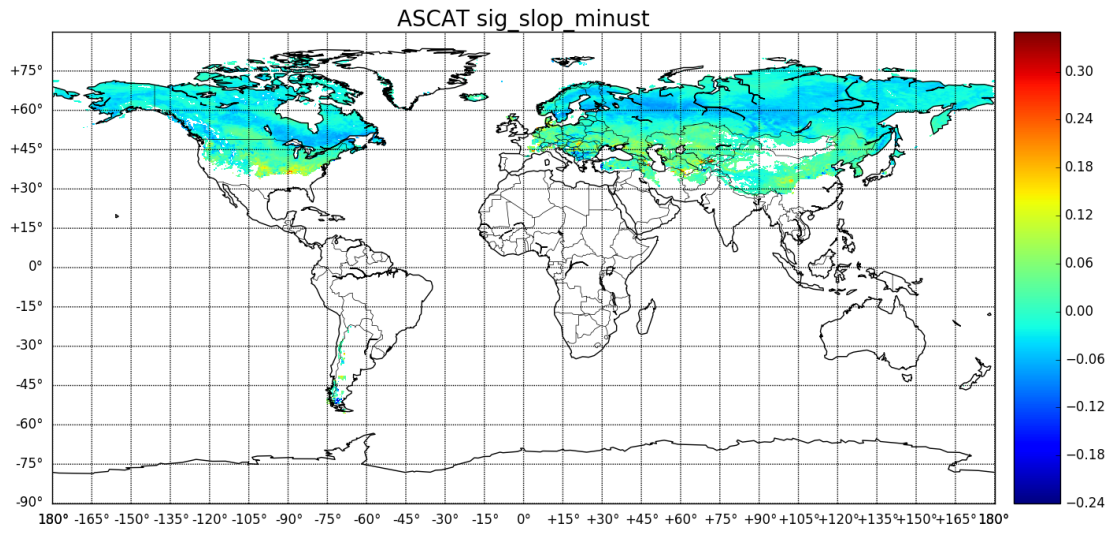


(a) ASCAT — Standard deviation during frozen period

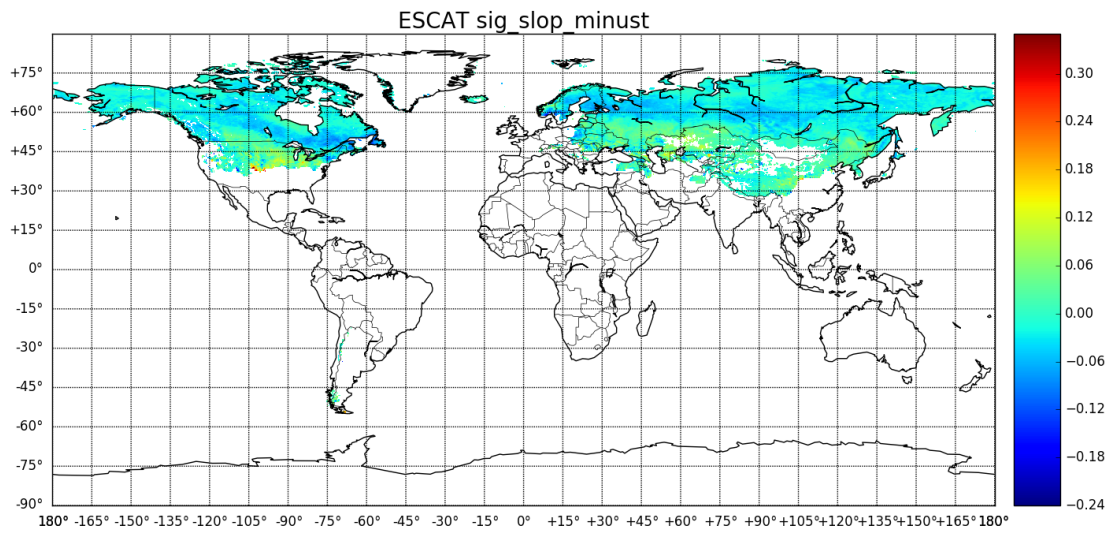


(b) ESCAT — Standard deviation during frozen period

Figure A.3: Standard deviation during frozen period derived from ASCAT and ESCAT backscatter data.

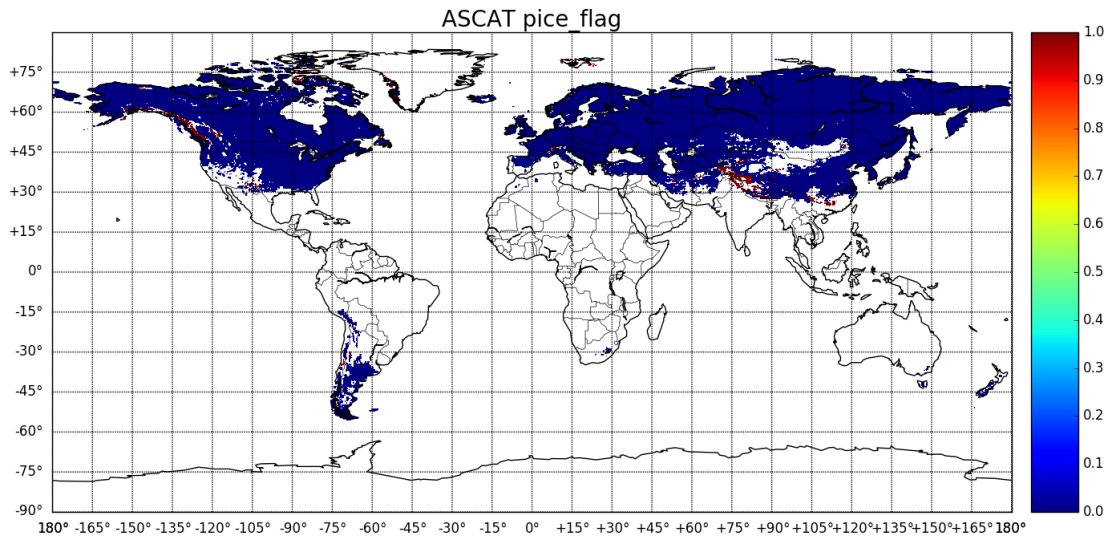


(a) ASCAT — Steepness of linear regression during frozen period

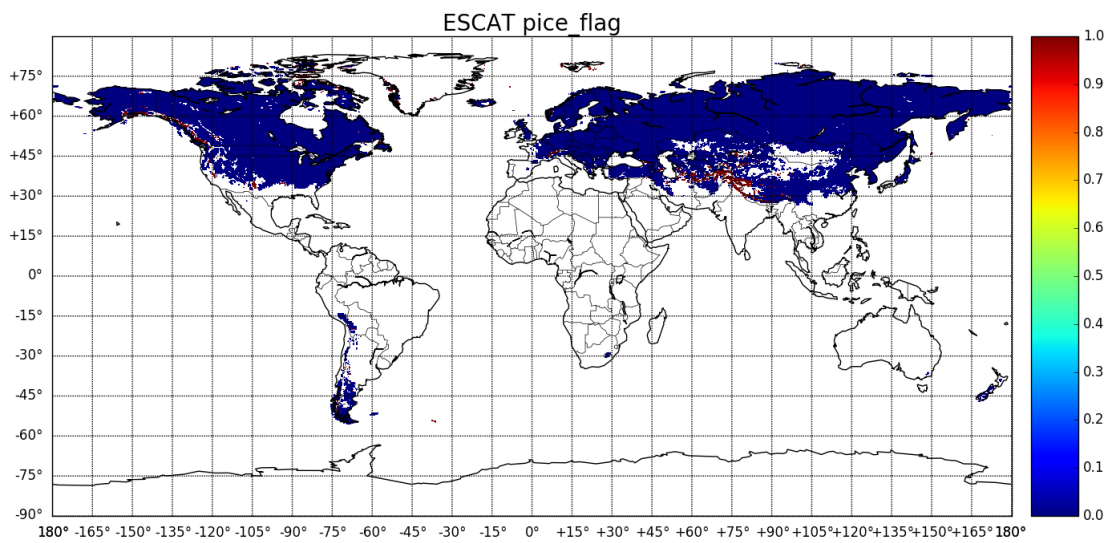


(b) ESCAT — Steepness of linear regression during frozen period

Figure A.4: Steepness of linear regression during frozen period derived from ASCAT and ESCAT backscatter data.



(a) ASCAT —Permanent ice flag



(b) ESCAT —Permanent ice flag

Figure A.5: Permanent ice flag derived from ASCAT and ESCAT backscatter data.

A.2 Surface State Flags in Different Climatic Regions

Figure A.6-Figure A.9 show additional SSF results, complementing Section 4.3.

A.2.1 SSF determination in cold climate (mixed land cover)

Figure A.6a shows the location of cell 1398 on a MODIS land cover map. The land cover in this cell consists of evergreen needleleaf forest, open shrublands, and woody savannas. According to the Koeppen-Geiger climate map, cell 1398 is dominated by cold climate without a dry season.

A.2.2 SSF determination in cold climate (woody savannas)

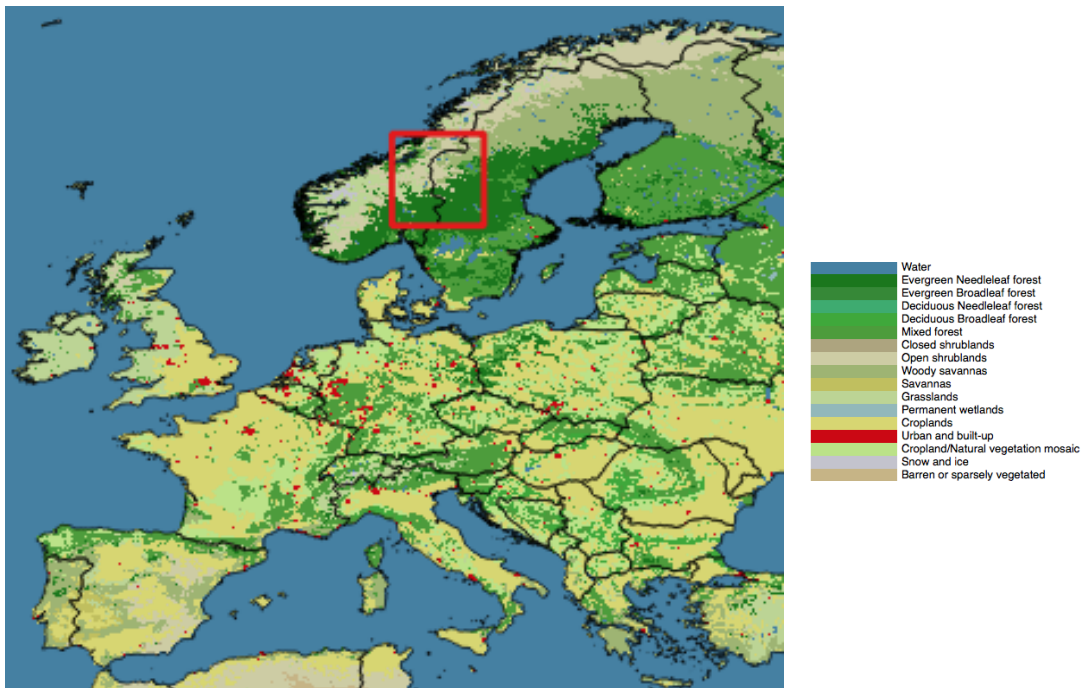
Cell 1507 is located in northern Finland, in a region dominated by woody savannas. Small parts of the cell are covered with open shrublands (see Figure A.7a). The climate is cold without a dry season, the summers are cold.

A.2.3 SSF determination in cold climate (shrublands)

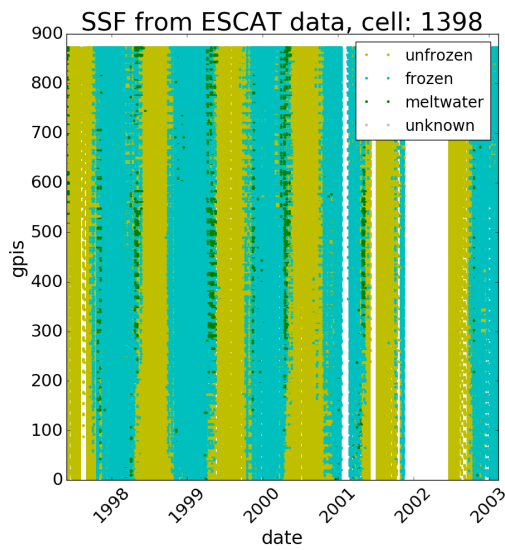
Figure A.8a shows the location of cell 1903 on a MODIS land cover map. The predominant land cover type in this region are open shrublands; the climate is cold without a dry season and with cold summers.

A.2.4 SSF determination in polar Tundra climate climate (shrublands)

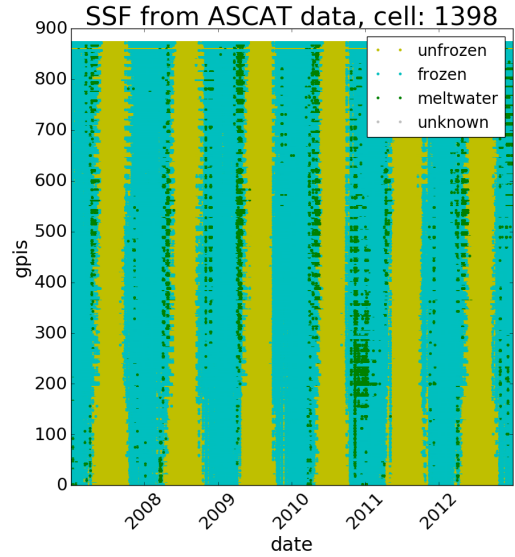
Cell 1904 is located 5° north of cell 1903. It is dominated by the same land cover type (open shrublands, see Figure A.9a). The climate is classified as polar Tundra climate.



(a) Location of cell 1398

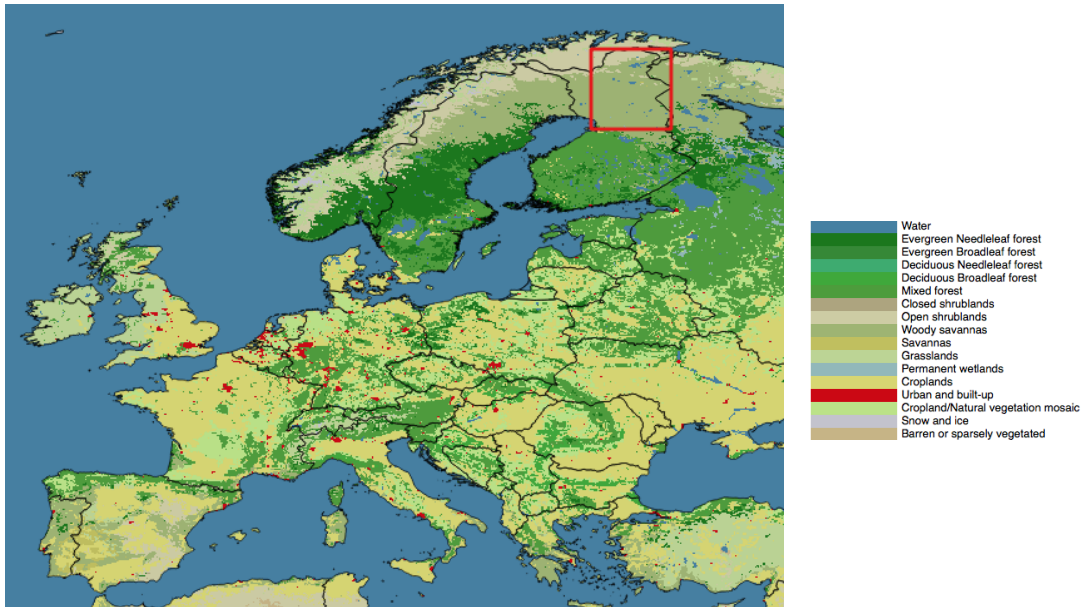


(b) SSF from ESCAT data

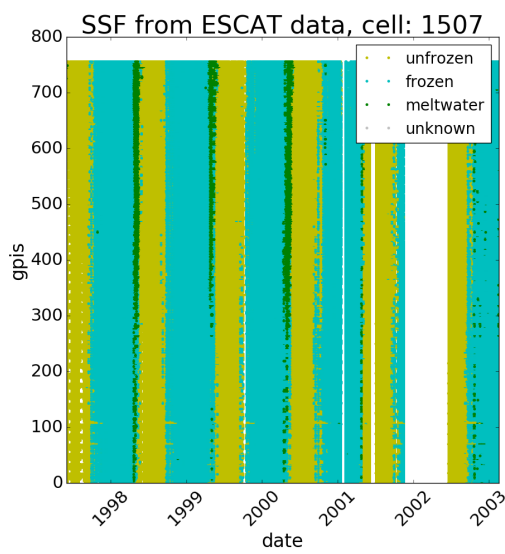


(c) SSF from ASCAT data

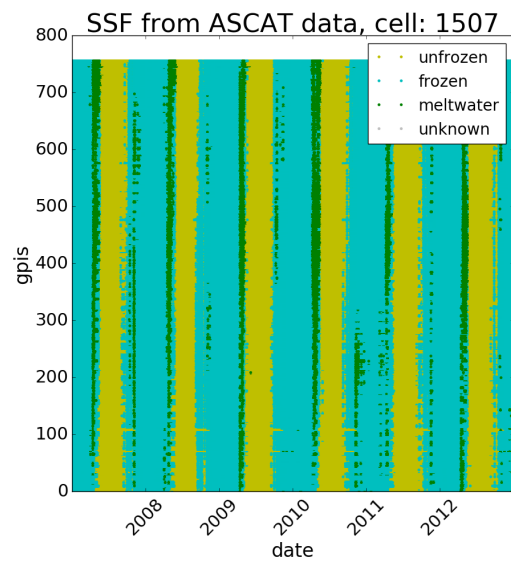
Figure A.6: SSF time series plot for cell 1398, determined from ESCAT (b) and ASCAT (c) backscatter values.



(a) Location of cell 1507

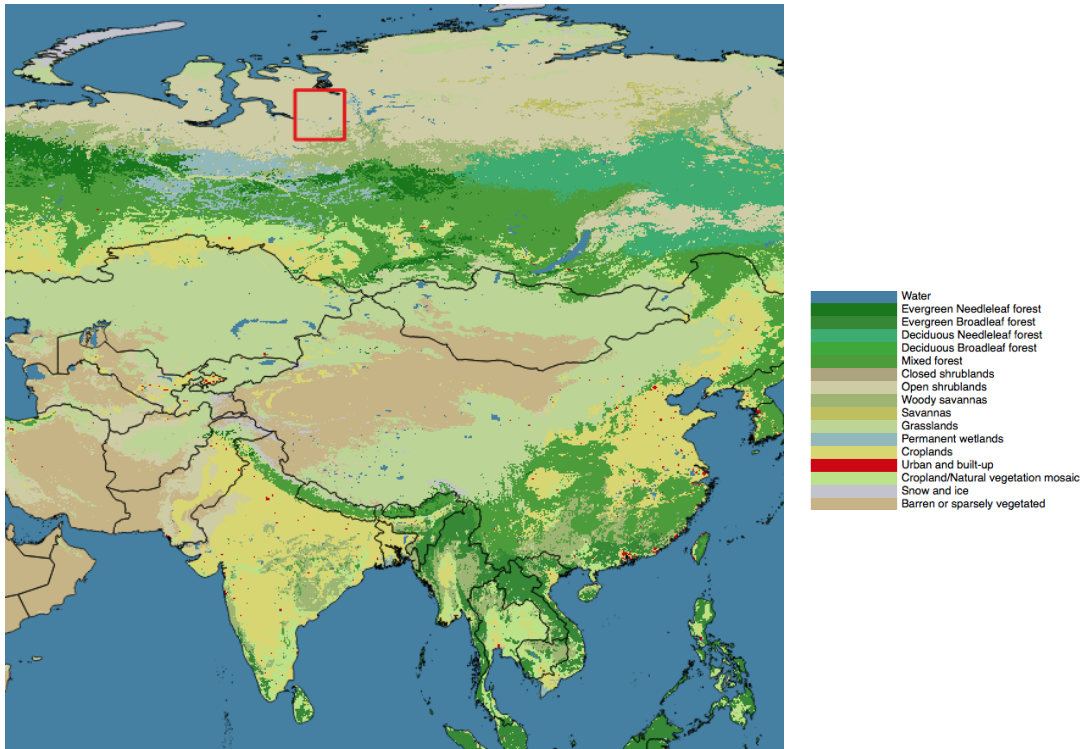


(b) SSF from ESCAT data

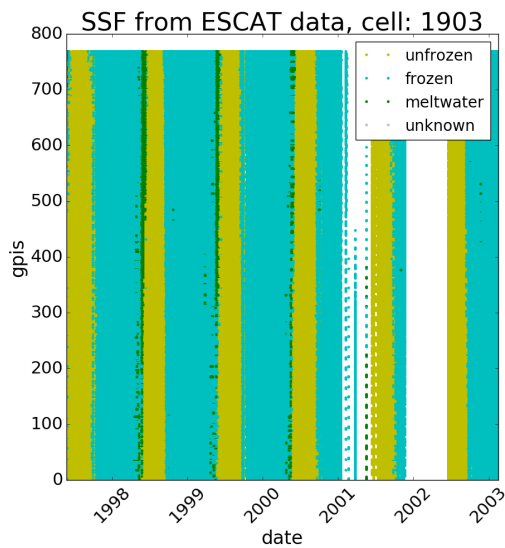


(c) SSF from ASCAT data

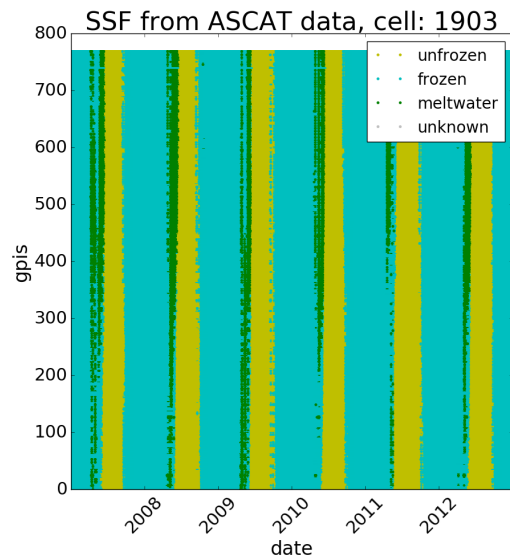
Figure A.7: SSF time series plot for cell 1507, determined from ESCAT (b) and ASCAT (c) backscatter values.



(a) Location of cell 1903

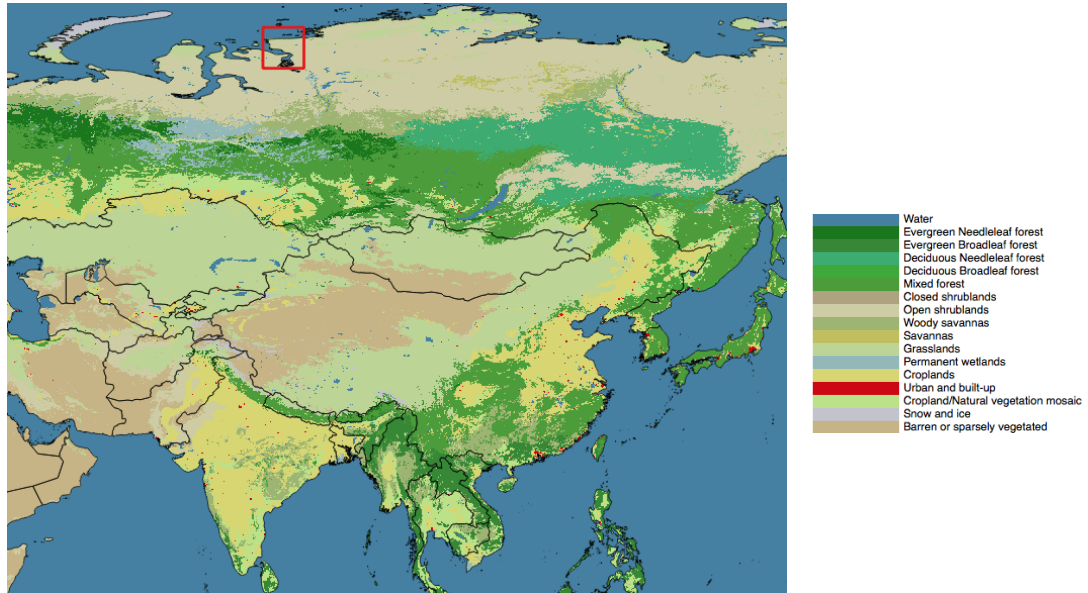


(b) SSF from ESCAT data

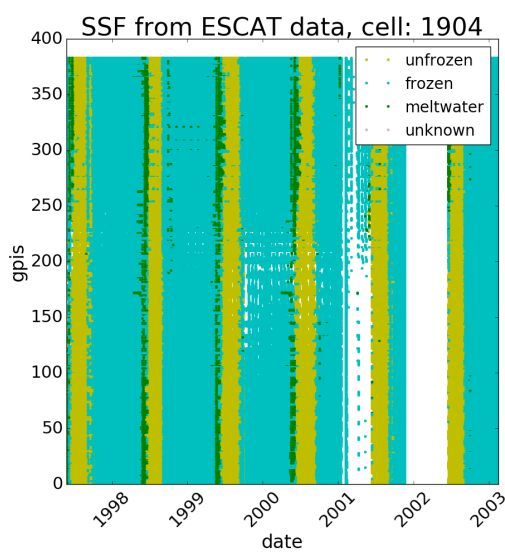


(c) SSF from ASCAT data

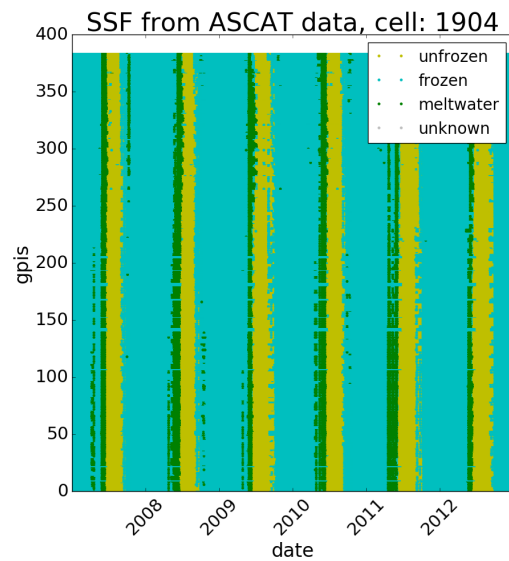
Figure A.8: SSF time series plot for cell 1903, determined from ESCAT (b) and ASCAT (c) backscatter values.



(a) Location of cell 1904



(b) SSF from ESCAT data



(c) SSF from ASCAT data

Figure A.9: SSF time series plot for cell 1904, determined from ESCAT (b) and ASCAT (c) backscatter values.

Bibliography

- Bartalis, Z. (2009), Spaceborne scatterometers for change detection over land., Ph.D. thesis, Vienna University of Technology, Austria. ix, 9
- Caesar, J., L. Alexander, and R. Vose (2006), Large-scale changes in observed daily maximum and minimum temperatures: Creation and analysis of a new gridded data set, *Journal of Geophysical Research: Atmospheres*, **111**(D5). 30
- Channan, S., K. Collins, and W. Emanuel (2014), Global mosaics of the standard MODIS land cover type data, *University of Maryland and the Pacific Northwest National Laboratory, College Park, Maryland, USA*. xi, 30, 32
- Crapolicchio, R., G. D. Chiara, A. Elyouncha, P. Lecomte, X. Neyt, A. Paciucci, and M. Talone (2012), ERS-2 Scatterometer: Mission Performances and Current Reprocessing Achievements, *IEEE Transactions on Geoscience and Remote Sensing*, **50**(7), p. 2427–2448, doi:10.1109/TGRS.2011.2179808. 8
- De Chiara, G., R. Crapolicchio, and P. Lecomte (2007), ERS-1/2 Scatterometer new products: mission reprocessing and data quality improvement, in *2nd Space for Hydrology Workshop, Geneva, Switzerland*, Citeseer. ix, 10
- Figa-Saldaña, J., J. J. Wilson, E. Attema, R. Gelsthorpe, M. Drinkwater, and A. Stoffelen (2002), The advanced scatterometer (ASCAT) on the meteorological operational (MetOp) platform: A follow on for European wind scatterometers, *Canadian Journal of Remote Sensing*, **28**(3), p. 404–412. 11
- Kimball, J., K. McDonald, A. Keyser, S. Frolking, and S. Running (2001), Application of the NASA scatterometer (NSCAT) for determining the daily frozen and nonfrozen landscape of Alaska, *Remote Sensing of Environment*, **75**(1), p. 113–126. 1
- Naeimi, V. (2009), *Model improvements and error characterization for global ERS and METOP scatterometer soil moisture data*, na. 23

- Naeimi, V., C. Paulik, A. Bartsch, W. Wagner, R. Kidd, S.-E. Park, K. Elger, and J. Boike (2012), ASCAT Surface State Flag (SSF): Extracting information on surface freeze/thaw conditions from backscatter data using an empirical threshold-analysis algorithm, *Geoscience and Remote Sensing, IEEE Transactions on*, **50**(7), p. 2566–2582. [ix](#), [11](#), [17](#), [22](#), [23](#), [24](#), [25](#)
- Peel, M. C., B. L. Finlayson, and T. A. McMahon (2007), Updated world map of the Köppen-Geiger climate classification, *Hydrology and Earth System Sciences Discussions Discussions*, **4**(2), p. 439–473. [ix](#), [xi](#), [30](#), [31](#)
- Poli, P., D. Dee, P. Berrisford, and J.-N. Thépaut (2010), Overview of satellite data assimilation in the ERA-Interim reanalysis, in *Proceedings of 2010 EUMETSAT Meteorological Satellite Conference*, p. 1–8. [11](#)
- Rango, A. (1993), II. Snow hydrology processes and remote sensing, *Hydrological Processes*, **7**(2), p. 121–138. [7](#)
- Rodell, M., P. Houser, U. e. a. Jambor, J. Gottschalck, K. Mitchell, C. Meng, K. Arsenault, B. Cosgrove, J. Radakovich, M. Bosilovich, et al. (2004), The global land data assimilation system, *Bulletin of the American Meteorological Society*, **85**(3), p. 381–394. [48](#)
- Toomay, J., and P. J. Hannen (2004), *Radar Principles for the NonSpecialist*, SciTech Publishing. [5](#)
- Ulaby, F. T., R. K. Moore, and A. K. Fung (1981), *Microwave Remote Sensing: Microwave remote sensing fundamentals and radiometry*, vol. 1, Addison-Wesley Publishing Company, Advanced Book Program/World Science Division. [3](#)
- Ulaby, F. T., R. K. Moore, and A. K. Fung (1982), *Microwave remote sensing: active and passive. Vol. 2, Radar remote sensing and surface scattering and emission theory*, Addison-Wesley. [4](#)
- Zhang, T., and R. Armstrong (2003 updated 2005), *Arctic Soil Freeze/Thaw Status from SMMR and SSM/I, Version 2*, National Snow and Ice Data Center/World Data Center for Glaciology. Digital Media., Boulder, CO. [46](#)